# Development of a Novel Peptide Based Probe for Tumour Imaging

Department of Physics and Nanotechnology

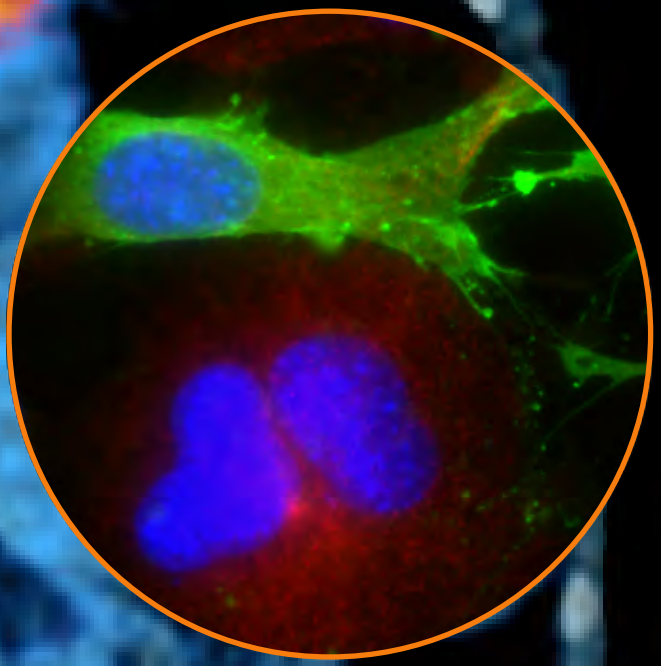

*Tue Bennike*

*M.Sc. Thesis, 2010 - 2011*

AALBORG UNIVERSITY

AALBORG UNIVERSITY

Department of Physics and Nanotechnology

http://www.nano.aau.dk/

**Title:**

Development of a Novel Peptide Based Probe for Tumour Imaging

**Titel (DK):**

Udvikling af et Nyt Peptid Baseret Probe til Billeddannelse af Tumorer

**Master Thesis Period:**

9-10$^{th}$ semester of Nanobiotechnology
1$^{st}$ of September 2010 - 7$^{th}$ of June 2011

**Author:**

Tue Bennike

**Supervisors:**

Peter Fojan
Allan Stensballe

**Print run:** 7

**Report page count:** 68

**Appendix page count:** 7

**Total page count:** 92

**Front page picture:** An edited positron emission tomography / X-ray computer tomography (PET/CT) image of a patient carrying a tumour [1], with a 63x fluorescence microscope image of the NR6wtEGFR cell line, the latter a result of this work. Staining of anti-human EGFR and EGFRvIII antibody cocktail (green), anti-mouse α-tubulin (red) and hoechst 33342 (DNA) (blue).

# Abstract

In the diagnosis and therapy of cancer, radioactive compounds are often applied. The awareness of altered receptor expression associated with many types of cancer, has permitted the development of receptor targeting by utilising radioactively labelled peptides with selective receptor affinity. The epidermal growth factor receptor (EGFR) is involved in cellular growth and differentiation. Although EGFR is not tumour specific, it is frequently overexpressed in many types of cancers, and overexpression of EGFR is correlated with poor relapse free and survival rates. Therefore represents the EGFR a significant target for cancer diagnosis and therapy, and for the above given reasons was selected as target in this project.

The natural ligand for the EGFR, the epidermal growth factor (EGF), has strong mitogenic activity, which makes it a poor choice as an EGFR targeting drug. Therefore was GE11, a peptide analogue of EGF, selected to investigate the feasibility of an EGFR targeting drug.

GE11 was synthesised by solid phase peptide synthesis, however, labelling with the fluorophore fluorescein (as free acid) was unsuccessful. GE11 was, however, successfully labelled with 5(6)carboxyfluorescein. The correct sequence and weight of the labelled GE11 was verified by mass spectrometry techniques. Purification of the product was troublesome, and signs of peptide degradation were detected.

The synthesis protocol was optimised and GE11 with lysine inserted at the N-terminus was labelled with 5(6)carboxyfluorescein and obtained at a higher yield. The fluorescent drug was tested *in vitro* using four different variants of the Swiss 3T3 murine fibroblast cell line, NR6. NR6 lacks expression of endogenous EGFR, and has previously been stably transfected with cDNA encoding the full length human EGFR or the EGFRvIII mutant. Thus, the lines express either physiological levels of EGFR, over-expresses EGFR or expresses the truncated, cancer specific and constitutively active EGFRvIII.

The expression of the receptors was partly verified by immunofluorescence, using two different antibodies, and analysed with fluorescence microscopy and fluorescence confocal laser scanning microscopy. The cell lines were incubated in medium containing the synthesised fluorescently labelled drug, and the internalisation of the cells was analysed by fluorescence microscopy. However, the targeting ability was found to be poor, as the highest intensity was found with the physiological EGFR expression cell line and the EGFRvIII expression cell line. These findings were confirmed by flow cytometry analysis. However, the flow cytometry data also revealed, unlike the fluorescence microscopy, that the lowest intensity was seen in the EGFRvIII expressing cell line.

Lysine-GE11 with the chelating agent DOTA attached to the N-terminus was also synthesised and purified, to allow the drug to be tested *in vivo* using a PET/CT scanner. The ability of the drug to form complexes with stable gallium and fluorescent europium were verified. However, as the affinity of the fluorescent peptide for EGFR was low and due to project time limitations, the metal DOTA-Lysine-GE11 complex was not tested *in vivo*.

In conclusion, it was in this project found that the affinity of lysine-GE11 for the EGFR was poor, most likely due to the added lysine amino acid. Future projects could investigate GE11 or other peptides e.g. with affinity for the cancer-specific EFGRvIII receptor, to continue the development of affinity drugs for the diagnostics and therapy of cancer.

# Dansk Resume

Til diagnosticering og behandling af kræft bliver radioaktive stoffer ofte anvendt. Opdagelsen af ændret receptor udtrykkelse i forbindelse med mange typer af kræft, har muliggjort udviklingen af receptor-målrettede stoffer ved at bruge radioaktivt mærkede peptider med selektiv receptor affinitet. Den epidermale vækstfaktor receptor (EGFR) er involveret i cellevækst og differentiering. Selvom EGFR ikke er tumor specifik, er den ofte overudtrykt i mange former for kræft, og overekspressionen af EGFR korrelerer med dårlig tilbagefald- og overlevelsesrate. Derfor udgør EGFR et potentielt mål for kræft diagnose og terapi, og for de ovennævnte anførte grunde blev receptoren valgt som mål i dette projekt.

Det naturlige ligand for EGFR, den epidermal vækstfaktor (EGF), har stærk mitogenisk aktivitet, hvilket gør den til et dårligt valg i EGFR målrettet medicin. Derfor blev GE11, et EGF peptid analog, udvalgt til at undersøge muligheden for et EGFR målrettet affinitets peptid.

GE11 blev syntetiseret med fast fase peptid syntese og forgæves forsøgt fluorescens mærket med fluoroforen fluorescein (som fri syre). GE11 blev efterfølgende mærket med 5(6)carboxyfluorescein. Den rigtige vægt og aminosyre rækkefølge af mærket GE11 blev eftervist med massespektrometri teknikker. Forsøg på at oprense produktet voldt imidlertid problemer, og der blev påvist tegn på nedbrydningen af peptidet.

Protokollen til syntesen blev optimeret, GE11 med lysin indsat i N-terminalen blev syntetiseret med et højere udbytte, og lysin-GE11 blev mærket med 5(6)carboxyfluorescein. Det fluorescerende stof blev afprøvet *in vitro* med fire forskellige varianter af den schweiziske 3T3 murine fibroblast cellelinje, NR6. NR6 har ingen endogen EGFR udtrykkelse, og er blevet stabilt transfekteret med cDNA, kodende for den fulde humane-EGFR eller mutanten EGFRvIII. Linjerne udtrykker derved enten fysiologiske niveauer af EGFR, over-udtrykker EGFR eller udtrykker den afkortede, kræft specifikke og konstitutivt aktive EGFRvIII.

Udtrykkelsen af receptorerne blev delvist bekræftet med immunfluorescens, med to forskellige antistoffer, og analyseres med fluorescens mikroskopi og fluorescens konfokal laser skannende mikroskopi. Cellelinjer blev inkuberet i medium, indeholdende det syntetiserede fluorescens-mærkede stof, og internaliseringen af stoffet blev analyseret ved fluorescens mikroskopi. Affiniteten var imidlertid dårlig, da cellelinjerne med højeste intensitet blev fundet til at være de EGFRvIII- og fysiologiske EGFR udtrykkende. Disse resultater blev bekræftet af flow-cytometri analyse. Flow-cytometri analysen viste imidlertid også, i modsætning til fluorescens mikroskopi, at den laveste intensitet var af den EGFRvIII udtrykkende cellelinje.

Lysin-GE11 med det kelatdannende DOTA bundet til N-terminalen blev syntetiseret og oprenset, for at teste peptidet *in vivo* ved hjælp af PET/CT-scannere. Stoffets evne til at danne komplekser med stabile gallium og fluorescerende europium blev verificeret, men da affiniteten af det fluorescerende peptid for EGFR var lav, og på grund af begrænset tid i projektet, blev metal DOTA-Lysin-GE11 komplekset ikke testet *in vivo*.

Det blev konkluderet, at den dårligt affinitet af lysin-GE11 for EGFR sandsynligvis skyldes den ekstra aminosyre lysin. Fremtidige projekter kunne undersøge GE11, eller andre peptider f.eks med affinitet for den kræft-specifikke EFGRvIII receptor, for at fortsætte udvikling af affinitets lægemidler til diagnostik og behandling af kræft.

# Preface

This report was conducted in the 9$^{th}$ and 10$^{th}$ semester periods of Nanobiotechnology at the Department of Physics and Nanotechnology; Aalborg University, during 1$^{st}$ of September 2010 to 7$^{th}$ of June 2011. The project was prepared and carried out with supervision from Aalborg hospital.

References in this report are denoted by [number] and are sorted by appearances in the bibliography. In the text, a reference that is placed before a full stop refers to that specific sentence. References that are placed after a full stop refers to the previous subsection. References to figures and tables are denoted (x.y), (chapter-number,figurenumber). The report features a CD containing the high resolution laboratory-results and the report in PDF.

Experimental work was carried out at Aalborg University (Departments of Physics and Nanotechnology, of Biotechnology, Chemistry and Environmental Engineering and of Health Science and Technology), and at Aalborg Hospital (Department of Clinical Immunology).

I would like to thank *Rune Wiik Andersen* (M.Sc.) and *Søren Naaby Hansen* (Senior researcher, Aalborg hospital) for their help in the planning of the project. Thanks to *Poul Larsen* (Post doc, Aalborg University) for help conducting fluorescence confocal laser scanning microscopy, *Anne Elbæk* (Biomedical laboratory technician, Aalborg Hospital) for help conducting fluorescence activated cell sorting and *Meg Duroux* (Associate Professor, Aalborg University) for introduction to fluorescence microscopy and mammalian cell maintenance.
Finally, a special thanks to *Svend Borup Jensen* (Head of radiochemistry, Aalborg Hospital), for his large interest and involvement throughout all stages of the project.

Tue Bennike / date

# Abbreviations

| | |
|---|---|
| AA | Amino acid |
| ACN | Acetonitrile |
| bp | Base pair |
| BSA | Bovine serum albumin |
| cf | 5(6)carboxyfluorescein |
| cf_GE11 | GE11 with cf- conjugated to the amino N-terminus of tyrosine |
| cf_K_GE11 | GE11 with cf-lysine- conjugated to the amino N-terminus of tyrosine |
| CLSM | Confocal laser scanning microscopy |
| DCM | Dichloromethane |
| DHB | 2,5-dihydroxy benzoic acid |
| DMEM/high | Dulbecco's modified Eagle's medium with 4.5 g/L glucose |
| DIC | Differential interference contrast |
| DIPEA | N,N-Diisopropylethylamine |
| DMF | N,N-Dimethylformamide |
| DMSO | Dimethyl sulfoxide |
| DOTA | 1,4,7,10-tetraazacyclododecane-1,4,7,10-tetraacetic acid |
| DTPA | Diethylenetriaminepentaacetic acid |
| EDT | Ethane-1,2-dithiol |
| EDTA | Ethylenediaminetetraacetic acid |
| EGF | Epidermal growth factor |
| EGFR | Epidermal growth factor receptor |
| EGFRvIII | EGFR type III deletion mutant (Δ2-7 EGFR) |
| ESI | Electrospray ionisation |
| FBS | Fetal bovine serum |
| ff | Fluorescein, free acid |
| FITC | Fluorescein isothiocyanate |
| Fmoc | 9-fluorenylmethyl chloroformate |
| FSC | Forward scatter |
| FWHM | Full width at half maximum |
| GE11 | Peptide with sequence N-term YHWYGYTPQNVI C-term |
| HBTU | O-benzotriazole-N,N,N,N-tetramethyl-uronium-hexafluoro-phosphate |
| HOBt | 1-Hydroxybenzotriazole |
| LC | Liquid chromatography |
| MALDI-TOF | Matrix-assisted laser desorption/ionization - time of flight |
| MS | Mass spectrometry |
| NET | Neuroendocrine tumour |
| OS | Overall survival rate |
| PBS | Phosphate buffered saline |
| p.d.u. | Procedure defined unit |
| PET/CT | Positron emission tomography / X-ray computer tomography |
| PVDF | Polyvinylidede difluoride |
| RFS | Relapse free survival rate |
| RIPA | Radioimmunoprecipitation assay |
| RP-HPLC | Reverse phase - high performance liquid chromatography |
| RV | Reaction vessel |
| SPECT | Single-photon emission computed tomography |
| SPPS | Solid phase peptide synthesis |
| SSC | Side scatter |
| TFA | Trifluoroacetic acid |
| TIS | Triisopropylsilane |
| Wang Resin | 4-benzyloxybenzyl alcohol resin |

# Contents

# 1 Introduction

Cancer remains one of the most devastating diseases with more than 10 million new cases each year world wide, which is expected to have increased by 20% by 2020 [2]. However, due to a better understanding of cancer, and improved diagnostics equipment and treatment strategies, the mortality is decreasing [2]. In today's cancer treatment strategies, radiotherapy is often successfully applied for diagnostics and therapy. The increasing awareness of altered receptor expression associated with many types of cancer, has permitted the development of oncogenic receptor targeting strategies. This is utilised in radioimmunotherapy, which is used in the diagnosis and treatment of specific cancer types today, where ligands with affinity for cancer associated receptors are used. Recent progress in radioactive receptor ligands have shown that ligands can be both specific and sensitive, to an extend where it is possible to detect the presence and abundance of various tumours as well as target tumour proliferation. Radioactive labelling of peptides or other biological molecules, such as antibodies with high affinity for overexpressed cell surface receptors, is for that reason of immense interest, and is believed to become a standardised part of the cancer treatment of tomorrow. [3–8]
In nuclear medicine, the two major molecular imaging techniques used are positron emission tomography (PET) and single photon emission computed tomography (SPECT) [9]. Radiolabelled peptides are of increasing interest in nuclear medicine, especially in the field of peptides labelled with positron emitters, as resolution and sensitivity are better with PET scanners than SPECT scanners [9]. Especially the increased sensitivity in PET, i.e. the ability to detect and record a higher percentage of the emitted events, which is higher by a magnitude of two to three orders, is an important advantage [3, 9].

An example of peptide-mediated radiotherapy is the diagnosis and treatment of patients with neuroendocrine tumours (NETs). The NETs differ from most other malign tumours by being slow growing, thus chemotherapy has little anti-tumour effect, but the NETs still spread by metastasis. Labelling of somatostatin peptide analogues with $^{68}$Ga, $^{90}$Y, $^{111}$In or $^{177}$Lu, using the metal chelator DOTA, has let to radiopharmaceuticals (radioactively labelled affinity ligands) with affinity for overexpressed somatostatin targets on the NET cells, amongst others $^{68}$Ga-DOTA-TOC, $^{90}$Y-DOTA-TOC, $^{111}$In-DOTA-octreotate and $^{177}$Lu-DOTA-TATE. [3, 6]

In a similar way, a novel labelled peptide analogue can be designed, a promising target being the epidermal growth factor receptor (EGFR). Elevated levels and mutations of EGFR have been identified as common components amongst numerous types of cancer. Due to its negative impact on the overall- and relapse free survival rate, EGFR has been used as a cancer marker for poor prognosis in a number of years. Although EGFR is not tumour specific, it is frequently overexpressed in many types of cancers, thus represents a significant target for cancer diagnostics and therapy. [10–12]

## 1.1 Affinity Ligands in the Diagnosis of Cancer

An affinity ligand for the diagnosis of cancer, such as the positron emitting $^{68}$Ga-DOTA-TOC used in the diagnosis of NETs, consists of a targeting vector molecule with affinity for a cancer target, coupled to a labelling part (Fig. 1.1). For targeting vectors, commonly antibodies or peptides are used, and the cancer target can e.g. be an overexpressed cell surface receptor. The development of targeting vectors tends to move in the direction from antibodies and antibody fragments toward smaller molecular tracers, such as peptide analogues to the natural receptor hormones. The smaller molecules have desirable pharmacokinetic properties such as higher target-to-background ratios, faster blood clearance, readily diffusibility, low immunogenicity, and in many cases the affinity of the peptides for the targeted receptor is significantly greater than that of the monovalent antibody fragment. [13, 14]

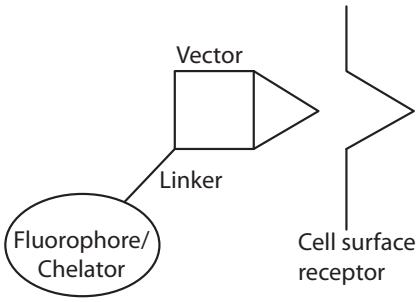


**Figure 1.1:** *Schematic drawing of an affinity ligand with affinity for a cancer target, in this case a cell surface receptor. By complexing different radionuclides with the chelator, the affinity ligand can either be used for diagnostics or therapy. Another option is to attach a fluorophore to the vector. [7]*

There are two classes of ligand analogues which are used in cell surface receptor binding, agonists and antagonists. An agonist mimics the natural ligand (hormone) and induces the normal reaction of the receptor, as binding of the natural hormone would. The differences to the natural ligand can e.g. be a changed *in vivo* half-life or a changed affinity of the ligand analogue for the receptor. An advantage of agonists is the possibility of internalisation of the drug into the targeted cells, if the targeted receptor has this ability, which allows for intracellular targeting and makes it possible to achieve a high intracellular concentration of the drug. An antagonist also binds to the receptor but does not induce a receptor response. However, by occupying the binding site, or a part of it, an antagonist can function as an inhibitor, which e.g. is utilised in the treatment and prevention of breast cancer where the antagonists tamoxifen and raloxifene are used to block an estrogen parthway essential for the tumour growth. The affinity of the ligand for the receptor can also be designed arbitrary high as the function of the receptor does not need to be conserved. [15, 16]

A much used technique to determine high affinity peptide candidates for target-

ing vectors is phage libraries. A library of possible peptide vectors are screened against the chosen cancer target. Promising peptide candidates are identified and produced, and the affinity of the vector toward the target is verified. [13, 17]

In some cases, the use of a linker between the targeting vector and the label can be advantageous. The linker can consist of amino acids (AAs) or an alkyl spacer to mention some, and is used to influence some property of the affinity ligand, e.g. the affinity for the target, the biodistribution, pharmacokinetic properties or *in vivo* lifetime. The linker can also facilitate conjugation to other molecules, be used in the purification steps during production or used in the labelling protocols. [18]

An example of the use of a linker is the attachment of the peptide ligand analogue GE11 to liposomes, using a polyethylene glycol linker. The linker was used to minimize sterical interference of the liposomes, when binding to the EGFR target on the surface of the cells. [19]

### 1.1.1 Combination of Affinity Ligands and Fluorophores

A fluorescently labelled affinity ligand allows for detection of the tracer by fluorescence microscopy, flow cytometry, fluorescence confocal laser scanning microscopy (CLSM) etc. Cell samples or studies on isolated receptors can be used to verify the affinity of the affinity ligand toward the target *in vitro*. Another option is to test a tissue sample from a patient for the cancer target. By exciting the fluorophore, cells or areas with high affinity ligand concentration can be detected/depicted. [20]

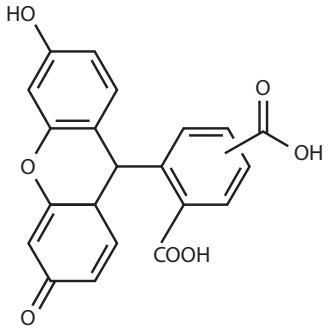


**Figure 1.2:** *Structure of 5(6)carboxyfluorescein. Modified from [21]*

Fluorescein derivatives are often used fluorophores for the labelling of peptides, because of the favourable fluorescence properties and relatively low costs. Amongst the many derivatives, carboxyfluorescein (Fig. 1.2) is much used for the production of hydrolytically stable fluorescent peptides and protein conjugates [22]. The labelling of peptides with carboxyfluorescein can be done using solid phase peptide synthesis as a step in the synthesis, as only one reactive carboxyl group is present under these conditions. A possible drawback of carboxyfluorescein is the need for activation prior to coupling. Often activated fluorescein derivatives are used such as FITC or carboxyfluorescein-N-succinimidyl ester, however, these are rather expen-

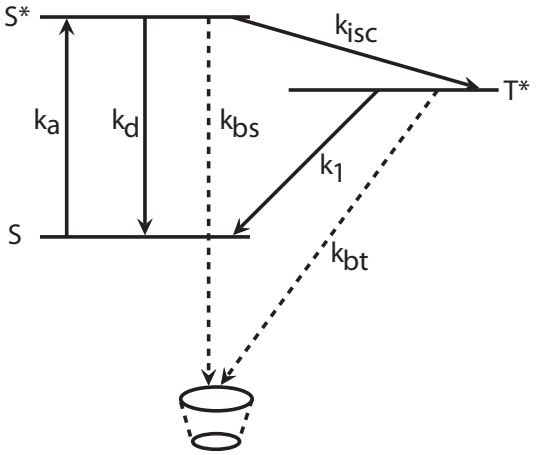


**Figure 1.3:** *Simplified Jablonski energy diagram. The fluorophore absorb photon energy ($k_a$), is excitet to the exited energy state $S^*$ and returns to the ground state S, by a fluorescent or non-fluorescent pathway (internal conversion) ($k_d$), or undergoes intersystem crossing ($k_{isc}$) to an excited triplet state $T^*$. From $T^*$ the system may relax into S with emitted phosphorescence ($k_1$). Photobleaching can take place from $S^*$ ($k_{bs}$) or $T^*$ ($k_{bt}$), and renderers the molecule unable to emit. [23]*

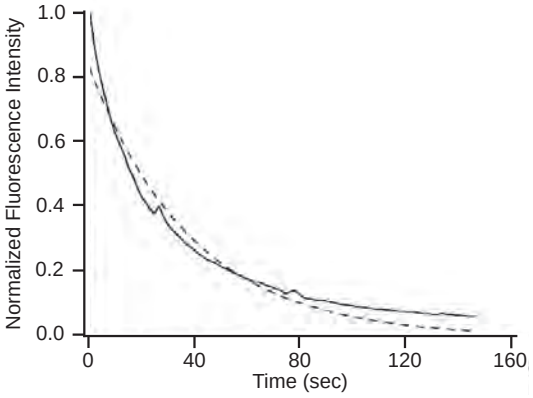


**Figure 1.4:** *Photobleaching of fluorescein in a fluorescence microscope. The broken line is an exponential fit. A 100 W Hg lamp was used with excitation 450-490 nm, 0.7 s integration and a 63x oil objective. 9 µm diameter fluorescein coated spheres was used, yielding a fluorescein concentration of approx 10 mM in PBS, pH 7.6. [23]*

sive compared to 5(6)carboxyfluorescein (cf). [22]

A potential issue with fluorescein and its derivatives is photobleaching, the relatively high loss of fluorophore from each excitation and emission cycle, which can be an issue when conducting fluorescence microscopy and similar techniques (Fig. 1.4). Upon excitation, when the molecule is in the excitet state $T^*$ or $S^*$, photobleaching may occur. The effect is cumulative over time in an exponential decay and is proportional to the intensity of the excitation (Fig. 1.3). [23]

### 1.1.2 Combination of Affinity Ligands and Chelating Agents

A chelating agent conjugated to the vector instead of a fluorophore, enables different metals to be complexed with the otherwise same affinity ligand. However, the possible release of the metal from the chelate has to be taken into account, so a fitting chelator for the given metal must be chosen. Today, the two most used chelators in radiotherapy are 1,4,7,10-Tetraazacyclodo-decane-1,4,7,10-tetraacetic acid (DOTA) (Fig. 1.5) and diethylenetriaminepentaacetic acid (DTPA) (Fig. 1.6) [24]. Of the two, DOTA complexes are the more thermo-dynamically- and kinetically stable [24]. In general, complexes of Y(III) and lanthanide(III) ions in DOTA have exceptional kinetic inertness to metal ion release, making DOTA the attractive choice of the two [25]. Therefore, lanthanide(III) complexes of DOTA and its derivatives are being used in many areas of medical chemistry, where binding of

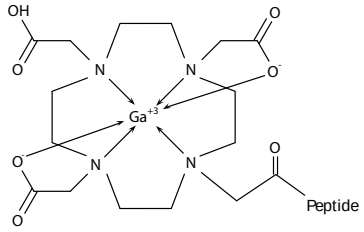


**Figure 1.5:** *DOTA chelated with $^{68}$Ga, conjugated to a peptide. [27]*

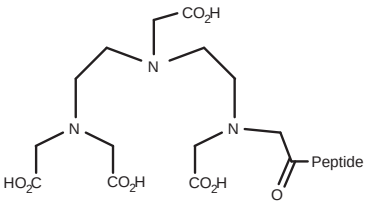


**Figure 1.6:** *Structure of DTPA, conjugated to a peptide. [28]*

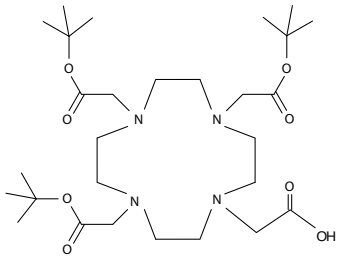


**Figure 1.7:** *DOTA-tris (t-Bu ester), suitable for SPPS. [24]*

radioactive isotopes are used as carriers in nuclear medicine [26]. A drawback of DOTA complexes is the requirement for heating in the chelation reaction to aid the formation of the complex. This is not needed when using the less stable DTPA complexes which can form at room temperature, but DTPA has a higher degree of metal ion release [24, 25]. Generally, peptides are stable to heating, so for peptide labelling applications DOTA is preferred. [24, 25]

As DOTA is a tetra acid there exist four possible sites of conjugation. Fortunately, a range of DOTA derivatives are available, one suitable for SPPS being ester tri-*t*-butyl protected DOTA (Fig. 1.7). [24]

### Chelator Mediated $^{68}$Ga Labelling

The positron emitter $^{68}$Ga ($T_{1/2}$ = 68 min) stands out amongst many other radionuclides for PET diagnosis, because it is generator produced from $^{68}$Ge ($T_{1/2}$ = 271 days) eliminating the need for an onside cyclotron. [6, 29, 30]. More, the 68-min half-life of $^{68}$Ga matches the pharmacokinetics of many peptides and other small molecules in terms of localisation at the target and fast blood clearance [5]. Combined with the high percentage of positron decays ($^{68}$Ga decays by 89% positron emission of max 1.92 MeV and 11% orbital electron capture [5]), makes the radionuclide suitable to PET receptor regulation study [5]. Finally, the coordination chemistry of Ga(III) is defined by coordination number six making DOTA a feasible ligand for binding [5, 31]. In DOTA, gallium is coordinated to the nitrogen atoms, and to two of the oxygen (Fig. 1.5). [31, 32]

As a consequence of the above, $^{68}$Ga is being used in PET/CT diagnostics of NETs with DOTA.

### Chelator Mediated Europium(III) Labelling

By forming a complex with a metal having applicable fluorescence properties, a fluorescent affinity ligand can be made of the otherwise almost identical radioactively labelled affinity ligand. The advantages over labelling with e.g. fluorescein, are that the difference between the fluorescent- and radioactively labelled affinity ligand is minimised so the affinity for the target can be presumed conserved, and

only one version of the affinity ligand needs to be synthesised. By having an atom with a high fluorescence lifetime, time-gated fluorescence techniques can be used, which possibly eliminate a high degree of the autofluorescence which otherwise can be problematic e.g. when examining tissue slides with fluorescence. In the case of luminescent probes, the number of water molecules directly coordinated to the fluorescent ion should be kept as low as possible to avoid quenching effects of the proximal O-H oscillators [26].

Europium is a metal with a narrow atom-like emission spectra utilised in the lightning and display areas, e.g. as the red component in television projection tubes [33]. As europium is emitting in the visual range, a luminescent probe could be constructed by attaching an europium complex to a bioactive molecule. As the europium(III) ion forms stable complexes with DOTA-like ligands, it seems feasible that an europium(III) DOTA complex can be used as a fluorescent label on an affinity ligand. The europium(III) ion forms a complex with DOTA with coordination number seven in a similar way as gallium(III) [26, 27]. In the DOTA complex, Europium(III) is protected from the quenching by water and is fluorescent. Upon excitation of a Eu(III)-DOTA-peptide at 340 nm, emission was found at 615 nm using time-resolved luminescence with a delay time of up to 400 $\mu$s [34]. The rate limiting step in the formation of the Europium(III) do3ap (DOTA-like) complex (Fig. 1.8), was found to be the deprotonation of the nitrogen atoms and the simultaneous translocation of the metal ion inside the DOTA cavity. A decrease in solution acidity from pH 2.5-3 to pH 5.5 accelerated the complex formation from days to minutes, and the same effect was observed for pH range 2.5 to 4.6. [35]

## 1.2 State of the Art

Many conventional chemotherapeutic agents, such as anthracyclines, alkylating agents and antimicrotubules, can cause toxic side effects and have low specificity for the tumour cells [36]. As a consequence, new means of cancer diagnostics and therapy are continuously being investigated. In 2004, the USA National Cancer Institute committed $144 million, to the improvement of cancer patient survival with the focus on six areas: (1) detection of molecular changes responsible for disease pathogenesis. (2) disease diagnosis and imaging. (3) drug delivery and therapy. (4) multifunctional systems for combined therapeutic and diagnostic applications. (5) vehicles to report the *in vivo* efficacy of a therapeutic agent. (6) nanoscale enabling technologies. [14]. Peptides and antibody fragments are being developed to overcome some of the shortcomings of antibodies for cancer cell targeting, and the strategy has been used experimentally to deliver toxins and radioactive molecules selectively to tumours. A large number of peptides with affinity for cell surface targets have been isolated, and several of these ligands are now under clinical trials. An example is Cilengitide, the cyclic RGD peptide which as of 2007 was under phase II clinical evaluation for the treatment of several tumours, including prostate can-

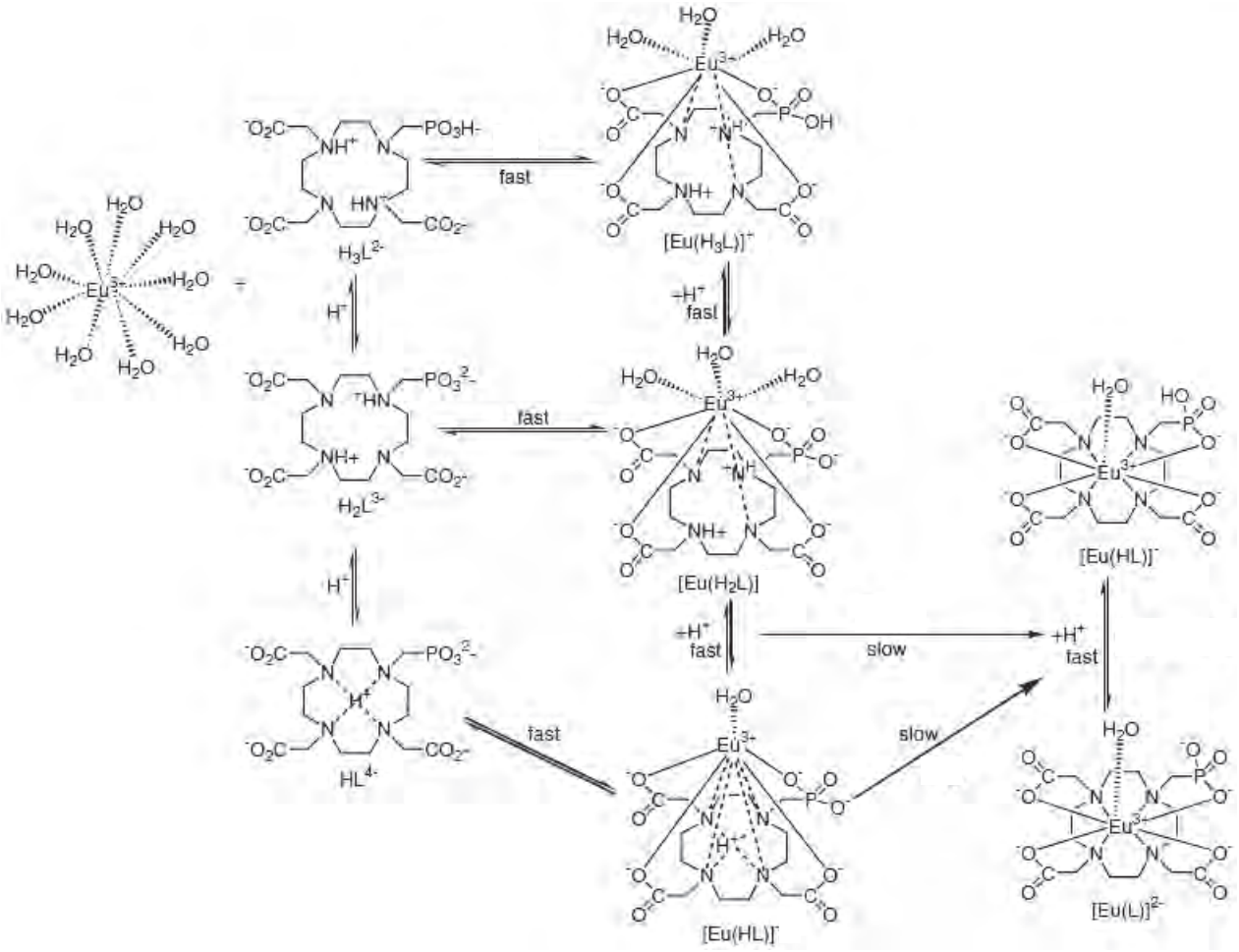


**Figure 1.8:** *A proposed reaction mechanism for the formation of the Eu(III) DOTA-like $H_5$do3ap complex in water. NB: sites of the protonations are tentative. Modified from [35]*

cer and recurrent Glioblastoma multiforme. [2, 14] Another peptide, GE11, which binds to the EGFR overexpressed by many tumours has also been reported, along with the peptide p160 which has shown to bind to several types of human cancer cells, but the target of which is yet to be determined. [36]

Nanocarriers, coated with imaging agents and targeting ligands are also being investigated. Advantages are control-release of the drug when the particle is bound to the cells and the possibility of gene-therapy. Nanocarriers include polymer conjugates, polymeric nanoparticles, lipid-based carriers such as liposomes and micelles, carbon nanotubes, and gold nanoparticles, including nanoshells and nanocages. As of 2007, at least 12 polymer-drug conjugates had entered Phase I and II clinical trials, especially within the field of targeting blood vessels in tumours. [2]

## 1.3 Positron Emission Tomography Scanner

The usability of radio labelled ligands in tumour imaging, relies on the method of detection. The recent implementation of high-resolution imaging molecular technology in health care is believed by many to potentially lead to a revolutionary paradigm shift [9]. In nuclear medicine, the two major molecular imaging techniques used are PET and single photon emission computed tomography (SPECT) [9]. Radiolabelled affinity ligands are of increasing interest in nuclear medicine, especially in the field of peptides labelled with positron emitters, due to that resolution and sensitivity are better with PET scanners than SPECT scanners [9]. Especially the increased sensitivity in PET, i.e. the ability to detect and record a higher percentage of the emitted events which is higher by a magnitude of two to three orders, is an important advantage [9]. The PET scan has proven its usefulness in the diagnosis of patients with NETs, using a radioactive metal labelled affinity ligand [3].

For cancer diagnosis the PET scanner is usually combined with a X-ray computer tomography (PET/CT) scanner . The two 3D images produced are combined to show the PET image of the tumour, in relation to the internal organs depicted by the CT scanner [7, 9]. $^{68}$Ga-DOTA-TOC is today used for accurate tumour diagnosis of NETs with PET/CT scanners. Besides detection and imaging of the tumour, the data can be used to estimate patient dosimetry, which can be a difficult task and possibly limits the usage of radioimmunotherapy [5, 37].

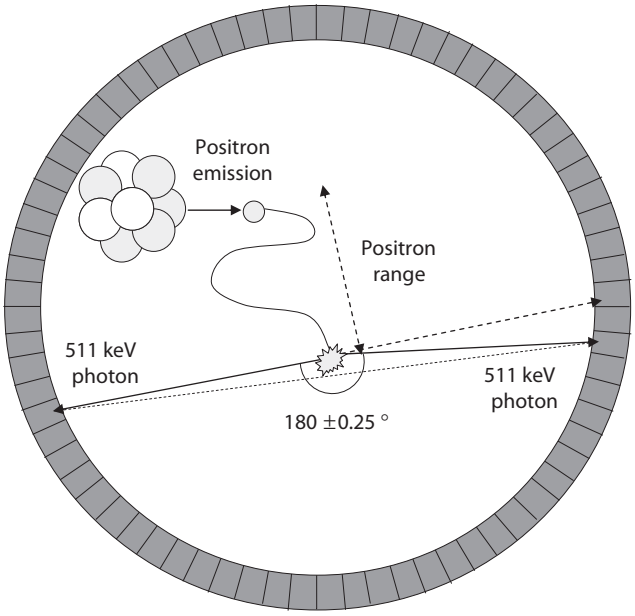


**Figure 1.9:** *Schematic drawing of a PET scanner with the emission of a positron from a nuclide and subsequent annihilation. The positron range and non-collinearity of the two annihilation photons, resulting in a positional inaccuracy in PET are illustrated. The line of response is the photon paths from the annihilation to the detectors. Positron range and angles are to a great extent exaggerated. [9]*

The subject to be analysed is injected with a positron emitting radionuclide and placed in the field of view of the PET detectors, which are placed round the subject (Fig. 1.9). The radionuclide decays, resulting in the emission of a positron. The emitted positron looses kinetic energy through several Coulomb-interactions with electrons. As the positron reaches thermal energies, it interacts with a nearby electron in an annihilation reaction, resulting in two 511 keV photons travelling in almost opposite directions. The two photons are then detected by the surrounding detectors, using the coincidence-detection method. When two almost opposite signals are detected within a few nanoseconds, the signals are assumed to be coincident and originate from the same annihilation. The signal is recorded and the origin of the decay along the line of response can be calculated. [7, 9]

The average distance between the point of emission and annihilation is denoted the positron range, and is isotope specific. The photon non-collinearity arises from the non-zero net momentum of the emitted positron and the annihilation electron. This results in a deviation from the 180° difference between the trajectories of the two emitted photons. The distribution of angles is Gaussian and is around 0.25° full width at half maximum (FWHM), and the scanner must be configured accordingly to allow for this. The resulting FWHM blurring of the image is also dependent on the detector separation, i.e. the ring diameter, and can be described by the relation:

$$FWHM \approx \left(0.25^\circ \cdot \frac{\pi}{180^\circ}\right) \frac{D}{2}, \tag{1.1}$$

where $D$ is the ring diameter of the PET scanner. For a typical whole body scanner D is 70 to 80 cm which results in a 1.54 to 1.76 mm FWHM blurring. [9]

Photon attenuation attends to the probability that the annihilation photons interact with tissue and other material before reaching the detector. The interactions can be photoelectric or Compton scattering (inelastic). However, for photon energies around 511 keV, photoelectric interactions are neglectable. The probability that a photon survives (is not attenuated) can be expressed by the relation:

$$P_L = \exp\left[-\int_L \mu(\vec{x})\, d\vec{x}\right], \tag{1.2}$$

where $P_L$ is the survival probability. The parameter $\mu$ is referred to as the linear attenuation coefficient an energy- and tissue dependent measure of the photon attenuation, $\vec{x}$ is the line of response along which the integration runs and $L$ is the path length. In PET, $L$ represents the entire line of response, along which the emitted photons travel to both the detectors, as in contrast to SPECT where only one signal is detected at a time. Therefore, in PET attenuation is independent of the photons point of origin along the line of response, which makes the data handling easier.

## 1.4 The EGFR as a Cancer Target

As mentioned, the EGFR is believed by many to be a potential target for nuclear medicine in diagnosis and therapy. Growth factors belong to a family of cell secreted polypeptides, which plays a key role in the regulation of cell growth and proliferation. Upon binding to a cell surface receptor the effect of the growth factor is mediated. A series of intracellular signalling events is triggered, leading to changes in the transcription level. In this way growth factors relay information provided by the surrounding environment. The effect of a given growth factor is restricted in time and is cell type specific. [10]

One of the first growth factors to be discovered was the epidermal growth factor (EGF), which was found by Stanley Cohen (Nobel prize in physiology and medicine, 1986) [12]. In the mid-seventies a plasma membrane spanning receptor which bound EGF was identified and named the EGFR. Upon EGF binding cellular proliferation and/or differentiation are stimulated [38]. The EGFR has besides EGF several known natural ligands and is one of the closely related receptor tyrosine kinases in the ErbB subfamily. [10]

| Cancer type | Association with RFS | Assiciation with OS |
|---|---|---|
| Ovarian | 80% (n=5) | 67% (n=9) |
| Head and neck | 75% (n=8) | 82% (n=11) |
| Cervical | 75% (n=4) | 71% (n=7) |
| Bladder | 60% (n=5) | 63% (n=11) |
| Non-small-cell lung cancer | 20% (n=10) | 10% (n=10) |
| Colorectal | N/A | 67% (n=3) |
| Breast | N/A | 55% (n=11) |
| Gastric | N/A | 50% (n=6) |
| Endometrial | N/A | 40% (n=5) |

**Table 1.1:** *Frequency of studi es (n) showing association between increased EGFR levels and relapse-free survival (RFS) and overall survival (OS). Only general conclusions should be made from the study as it has not been standardised with respect to patient population and assays used to determine tumour EGFR levels. However, the study indicates a correlation between RFS, OS and EGFR positive tumours. [11]*

Due to its impact on cellular growth and proliferation, elevated levels and mutations of EGFR have been identified as common components amongst numerous cancer types [10–12]. Furthermore, several studies have shown that the overall survival rates and relapse-free survival rates drops dramatically for EGFR positive tumours when comparing to EGFR negative (Table 1.1) [12, 39]. Therefore, EGFR has been used as a cancer marker for poor prognosis in a number of years, and EGFR blocking antibodies has been found to slow the progress of EGFR positive xenografts tumours. an affinity ligand specific for the EGFR is therefore of immense interest. However, EGFR is expressed on the surface of the majority of normal cells

| Cancer type | EGFRvIII expression |
|---|---|
| Low grade gliomas | 86% |
| Medullablastomas | 86% |
| Breast carcinomas | 78% |
| Ovarian carcinomas | 73% |
| Paediatric gliomas | 66% |
| High grade gliomas | 57% |
| Non-small-cell lung | 16% |
| Prostate cancer | * |

**Table 1.2:** *EGFRvIII association with various cancer types. *In prostate cancer the expression depends progressively on the cells gradual transformation from normal to malignant cells. [10]*

so the use of EGFR targeting may be limited by the uptake in organs with high endogenous wild type EGFR expression [40]. The affinity of the ligand to the receptor should therefore be optimised for targeting EGFR overexpressing cells as much as possible.

Besides EGFR amplification, mutated versions of EGFR are often seen in human tumours. Another option is therefore to target a mutated version of the receptor, the most commonly observed being the type III mutant EGFR (EGFRvIII), also known as Δ2-7 EGFR [12, 39, 41]. EGFRvIII is a naturally occurring truncated EGFR, lacking a large part of the extracellular part, which includes most of the ligand binding site. So far, EGFRvIII has only been detected in human tumours (Table 1.2) [10, 41]. More, several studies indicate a correlation between EGFRvIII expression and the tumourigenicity of the tumour cells *in vitro* and *in vivo*. Expression of EGFRvIII has shown to change characteristics of fibroblast cells, including poor adherence, spindle shaped morphology, disordered growth pattern and a lack of density enhanced growth inhibition. The cells exhibited anchorage-independent growth and formed tumours when inserted in athymic mice. Non-tomourogenic murine haematopoietic cells were shown to transform into a tumourogenic phenotype upon EGFRvIII transfection. Finally, a clinical study showed correlation between positive EGFRvIII expression and a lower mean survival time. The enhanced tumourgenicity seemed to be most pronounced *in vivo* systems, indicating that unknown factors are interacting with the EGFRvIII, which are not present *in vitro* systems. [12, 39, 41]

### 1.4.1 The EGFR- and EGFR Mutant Subtype vIII Gene

The human EGFR gene is located on chromosome 7p11-13. It consists of 28 exons spanning nearly 200 kbps of DNA, encoding the 170 kDa full-length EGFR (Fig. 1.10) [10, 12, 38, 42].

Exon 1-14 codes the extracellular-, exon 15-17 the transmembrane- and exon

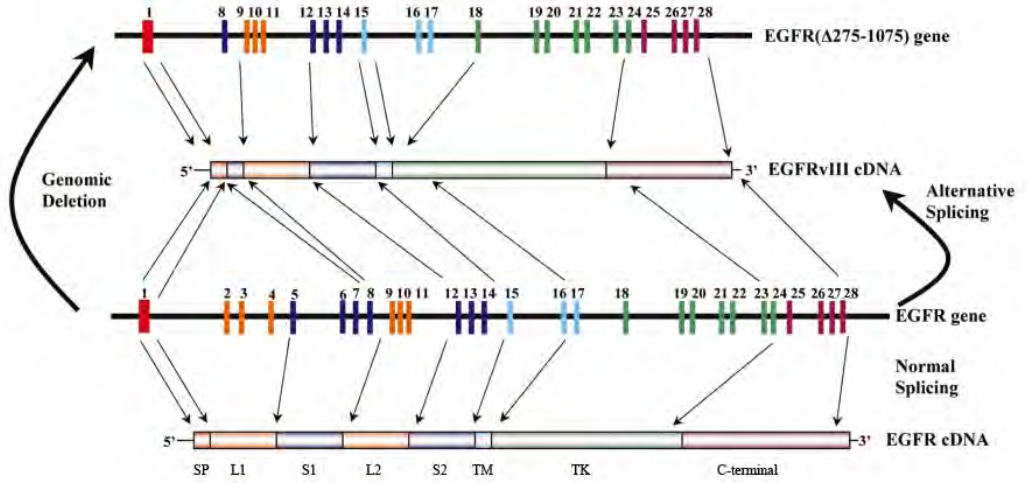


**Figure 1.10:** *Representation of the EGFR gene and two ways of forming the truncated EGFRvIII, genomic deletion and alternative splicing. The red box codes the signal peptide, orange boxes L1 and L2 domains, dark blue S1 and S2 domains, light blue the transmembrane domain, green the tyrosine kinease domain and purple the C-terminal domain. Modified from [10]*

18-28 the intracellular domain including the tyrosine kinase domain. The extracellular domain can be further divided into four sub domains; L1 exon 1-4, S1 exon 5-8, L2 exon 9-11 and S2 exon 12-14. The 5' part of exon 15-17 codes for the transmembrane domain and the remaining, the highly charged stop-transfer region named the juxtamembrane region. Exons 18-28 codes for the intracellular domain where 18-24 codes the tyrosine kinase domain. [42]

As mentioned, EGFRvIII is a truncated version of EGFR resulting from the deletion of exons 2-7. It contains the entire exon 1 followed by base 3 of exon 8 and the remaining EGFR gene in frame, with the formation of the new codon GGT (Gly) at the splicing junction (Fig. 1.11). The EGFRvIII gene/transcript is often found in tumours which also has amplified normal EGFR genes, and the mutant arises presumingly during the amplification process, which is likely to be the consequence of a genomic deletion event. [10] However, EGFRvIII has also been detected in some tumours without EGFR amplification [10], so in some cases the joining of exon 1 to exon 8 and resulting EGFRvIII is believed to arise from alternative splicing of the mRNA [12].

### 1.4.2 Protein Structure of the EGFR and EGFRvIII

The mature EGFR is a single polypeptide chain of 170 kDa, 1186 AAs N-glycosylated at 12 potential sites, which constitute an extracellular domain, a single transmembrane domain and an intracellular domain consisting of a juxtamembrane domain, a protein kinase domain and a carboxy-terminal domain. [10, 12]

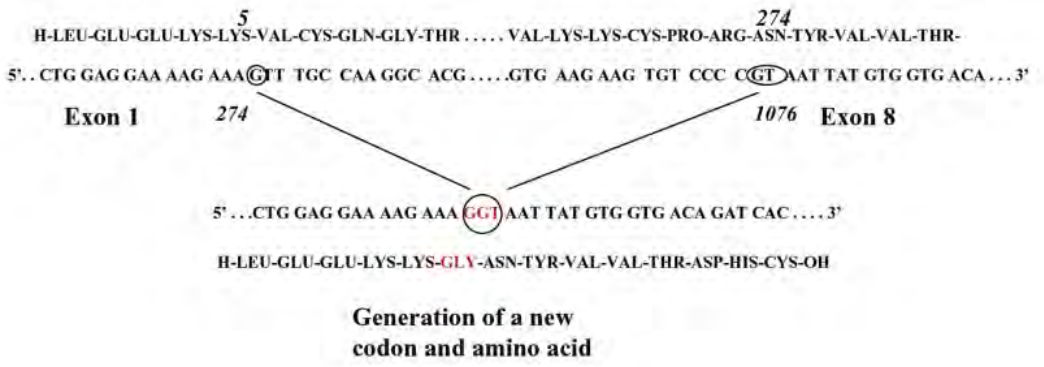


**Figure 1.11:** *The cDNA and AA sequences of EGFRvIII. The deletion of bases 275-1075 (801 bps) is shown with the resulting unique GGT (Gly) codon Numbers indicate the bases and AA residues adjacent to the deleted area. [10]*

### Extracellular Domain

The extracellular domain, consisting of 621 AAs, can be divided into four domains; L1, S1, L2 and S2 (Fig. 1.10). Domain L1 and L2 are right-handed β-helices and form the ligand binding pocket. EGF binds on either side of the receptor, unlike other similar receptors where the binding is done in the middle [43]. Domain S1 and S2 are cystein rich which form approximately 22 disulfide bonds. [10, 38]

In the case of EGFRvIII, AAs 6-273 are lacking from the extracellular domain, resulting in a total of 145 kDa. As the deletion does not include the signal peptide, the EGFRvIII is properly inserted into the membrane. However, it lacks the entire L1 domain except AA residues 1-5, and two thirds of the S1 domain which results in a large portion of the binding pocket is missing (Fig. 1.12). The result of the deletion is a structure which is similar to the conformational changes induced by ligands in the wild type EGFR, thus the receptor is permanently active (Fig. 1.12). [10]

### Intracellular Domain

The intracellular part consists of 542 AAs. The region between the transmembrane domain and the tyrosine kinase domain, the juxtamembrane region, is involved in the regulation of receptor sensitisation and downregulation. There are three serine-threonine phosphorylation sites present in the region; Thr-654, Thr-669 and Ser-671. Thr-654 is phosphorylated by protein kinase C which has an inhibitory effect on the kinase activity and the binding of high affinity ligands to the EGFR. The intrinsic tyrosine kinase domain of the receptor is constituted by AAs 690-954, and is capable of phosphorylating several cytoplasmic proteins as well as the receptor itself. Autophosphorylation of specific tyrosine residues creates binding sites for several proteins involved in signal transduction. AA 974-1021 has a regulatory function and are involved in the receptor internalisation.

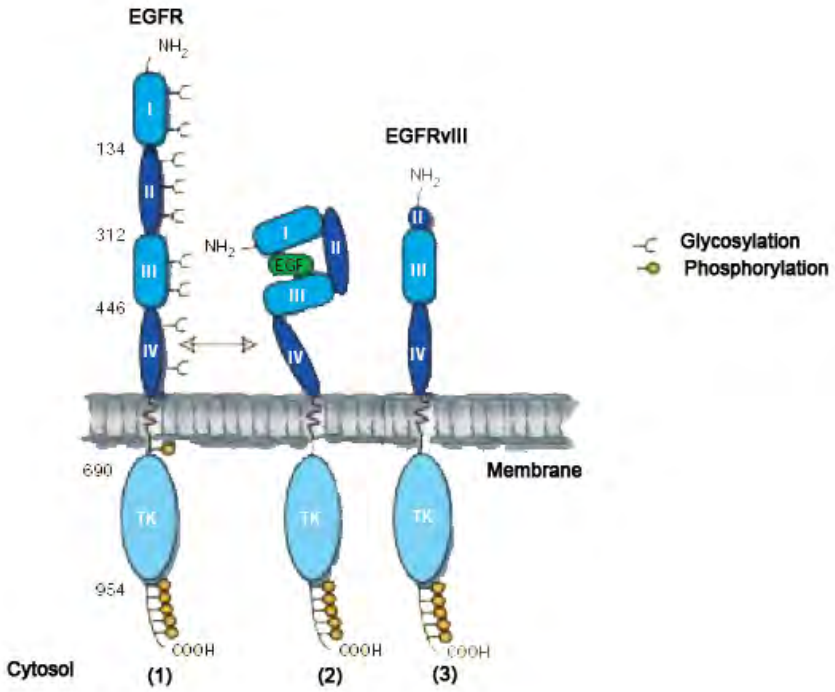


**Figure 1.12:** *Schematic representation of (1) EGFR, (2) EGFR with EGF bound and (3) EGFRvIII. TK is the tyrosine kinase. The four extracellular subdomains I=L1, II=S1, III=L2 and IV=S2 are illustrated. Upon ligand binding to L1 and L2, the receptor changes conformation. EGFRvIII is lacking L1 and two thirds of S1, and us unable to bind any known naturally occurring ligands. Modified from [44]*

EGFRvIII has the same intracellular primary and secondary structure, as EGFR but several differences in the activity of the tyrosine kinease and autophosphorylation sites have been identified. [10, 38]

### 1.4.3 Activation, Dimerization and Downregulation

The EGFRs are normally diffusely distributed on the surface of the cell. Ligand binding by e.g. EGF causes a conformational change in the receptor, leading to an increased affinity for other EGFR receptors, and dimerisation occurs (Fig. 1.13). Instead of acting like glue between the two chains, EGF appears to mold the receptor into the proper shape for dimerisation. The dimerisation can be homogeneous with another EGFR, or it can be heterogeneous with other members of the EGFR family. The dimerisation increases the catalytic activity of the intrinsic tyrosine kinases of the receptors, which leads to receptor autophosphorylation of several intracellular C-terminal tyrosine residues. The autophosphorylation residues represents specific binding sites for cytoplasmic proteins, involved in signal transduction. In this way,

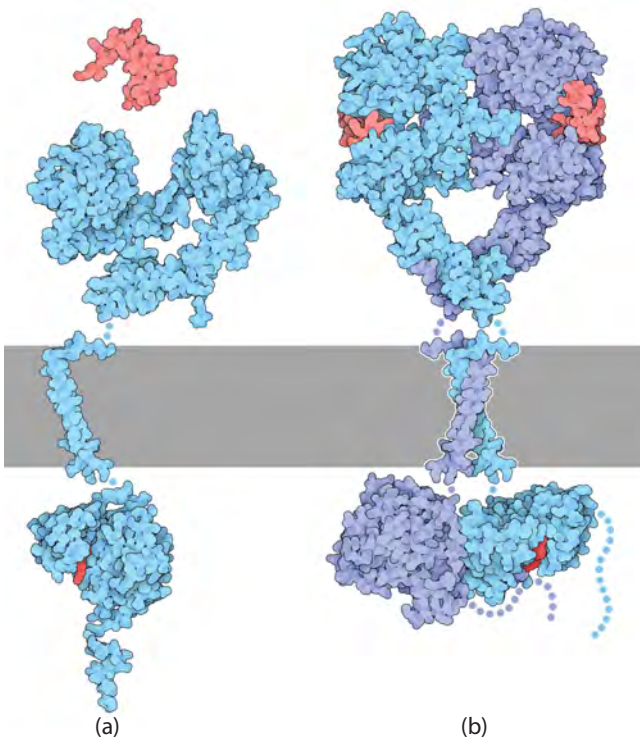


**Figure 1.13:** *EGF (red) activated dimerisation of two EGFR (blue) spanning a membrane (gray). Also some intracellular phosphorylation sites are illustrated (red). (a) The structure of EGFR and EGF prior to binding. (b) The ligand induced dimerisation of the two receptors and bound ligands. [43]*

DNA synthesis and cell proliferation is induced and the information delivered by the growth factor is mediated. [10, 12, 38, 41]

The termination of EGF-induced signalling is a tightly regulated process, where the receptor is internalised in endosomes and for the most part degraded in lysosomes (Fig. 1.14). Studies indicate that the autophosphorylation results in a more open conformation, exposing the internalisation- and lysosomal targeting motifs, thereby triggering receptor downregulation [10]. Ubiquitin ligase plays a key role in the termination, and binds to the EGFR. The appended ubiquitins recruit adaptors that contain an ubiquitin-interacting motif which targets the internalised receptors to lysosomes for degradation (Fig. 1.14). De-ubiquitylating emzymes might interrupt the process and send the receptor to the default recycling pathway and back to the surface instead of degradation by lysosomes. However, the EGFR is for the most part degraded after internalisation. Besides the EGF induced internalisation, there is a basal rate of internalisation. [10, 12, 38, 41]

EGFRvIII lacks the dimerisation arm and an essential part of the EGF binding pocket, and does not bind any known ligands. However, studies have shown that EGFRvIII undergoes dimerization with EGFR comparable to ligand induced EGFR dimerization, so the deletion may result in a structure which mimics the conforma-

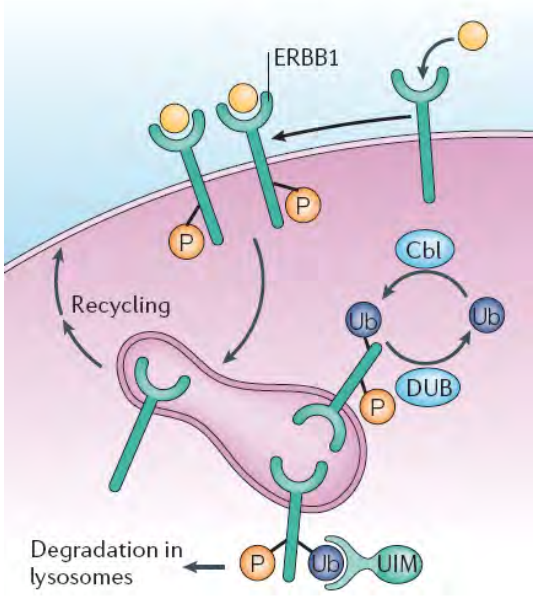


**Figure 1.14:** *Ligand binding to ERbB1 (EGFR) and subsequent receptor dimerisation with a nearby receptor and internalisation by endosomes. In the endosomes the receptor may undergoe ubiquitylation, Ub, by Cbl ubiquitin ligase. The appended ubiquitins then recruit adaptors that contain a ubiquitin-interacting motif UIM which targets the internalised receptors to lysosomes for degradation. De-ubiquitylating emzymes, DUBs might interrupt the process and sent the receptor to the default recycling pathway. Modified from [45]*

tional change induced by ligand binding in EGFR [10]. Despite the lack of ligand binding, EGFRvIII is continuously phosphorylated and able to activate downstream signalling pathways. The major binding autophosphorylation sites in EGFRvIII are Tyr-1068, Tyr-1148 and Tyr-1173, and mutations in any of these sites inhibits the tumourigenesis characteristics of EGFRvIII. During autophosphorylation, EGFRvIII is not down-regulated to the same extend as EGFR, which may be due to the more open conformation never being reached, and the internalisation- and lysosomal targeting motifs therefore are less accessible. EGFRvIII can be ubiquitinated, internalised and degraded, suggesting that EGFRvIII can enter the degradation pathway of EGFR, but the rate is significantly lower that that of unstimulated EGFR [41]. EGFRvIII binds the ubiquitin ligase Cbl, but the receptor fails to become effectively ubiqitinylated. Therefore, the small fraction of internalised EGFRvIII is for the most part not delivered to the lysosomes but recycled [41]. This combined with the lower degree of internalisation are two factors which can explain the increased lifetime of EGFRvIII. [10, 41]

### 1.4.4 Epidermal Growth Factor

One of the natural EGFR ligands is the EGF. The human EGF gene is located on chromosome 4, and consists of 24 exons separated by large non-coding regions. The pre-mRNA transcript is approximately 110 Kbp. After splicing and export from the nucleus, approximately 4.8 Kbp mRNA remains, coding for a 1207 AA EGF precursor. The EGF precursor contains a hydrophobic domain, assumed to be required for anchoring to the membrane. This is consistent with that EGF is synthesised as an integral plasma membrane protein, and can signal adjacent cells by direct contact. Cleavage by an extracellular protease releases the soluble form of EGF. [15, 38]

The mature human EGF is a 6045 Da, 53 AA residue single chain polypeptide (Fig. 1.16). In addition, the mature human EGF is very stable, is found in most body fluids especially in milk and appears to be non-glycosylated. Human EGF contains three intramolecular disulfide bonds, which are required for proper tertiary structure. [38] The AA sequence for mature human EGF constitutes residues 971-1023 of the EGF precursor (Fig. 1.15) [46, P01133]. The three disulfide bonds are marked by dotted lines and AAs important for the biological activity are described in more detail below [38, 47].

```
      1          11         21         31         41         51
N-term NSDSECPLSH DGYCLHDGVC MYIEALDKYA CNCVVGYIGE RCQYRDLKWW ELR C-term
     |--------------|              |---------|
                |------------------|
```

**Figure 1.15:** *AA sequence of EGF. (residues 971-1023 of the EGF precursor [46, P01133]*

The crystal structure of human EGF (residues 6-53) was obtained from *RCSB Protein Data Bank* [43, 1JL9] (Fig. 1.17). The three disulfide bonds are characteristic for EGF and related peptides, and are essential for biological activity. The third loop, defined by $Cys^{33}$ and $Cys^{42}$ contains the most conserved region in the EGF-like family. In the loop, five AAs are constantly conserved: the two Cys which define the loop, the $Gly^{39}$ presumed to be conserved for energetic reasons, and $Tyr^{37}$ and $Arg^{41}$. [38, 47]

Numerous groups have investigated the importance of the different residues using site directed mutagenesis. $Arg^{41}$ seems to be directly involved in the binding to the receptor [38, 47]. Due to the proximity to $Arg^{41}$, $Tyr^{13}$ also influences the binding [38]. $Ile^{23}$ also appears to have a central role in the binding to EGFR. It is exposed on the surface of EGF and seems to bind to a hydrophobic pocket on the receptor [48]. $Tyr^{29}$ and $Leu^{47}$ also proved essential for the biological activity, unlike $Tyr^{37}$ which proved to be structurally important [38]. Finally, the hydrophobic residues in the $\beta$ sheet, constituted by residues 19-31 are also believed to be involved in the ligand-receptor interaction [38].

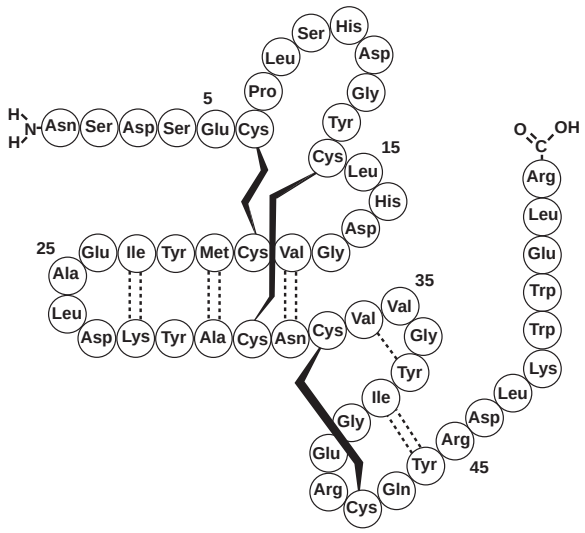


**Figure 1.16:** *Schematic representation of the secondary structure of human EGF. Disulfide bonds are indicated by solid lines and hydrogen bonds within the peptide backbone by dashed lines. NMR has shown that residues 49-53 are without rigid structure characteristics. [38]*

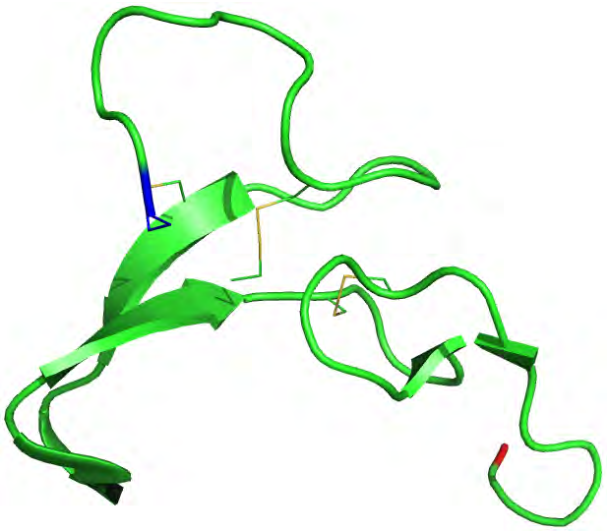

**Figure 1.17:** *Crystal structure of human EGF, AA residues 6-53. The β sheets are marked as arrows, disulfide bonds as lines, and first and last AA as blue and red respectively. Image processed with PyMol, PDB file from [43, 1JL9]*

### 1.4.5 The EGFR Peptide-Ligand Analogue GE11

If the natural ligand to the EGFR receptor, EGF was used in an affinity ligand, growth and cell differentiation would be induced upon a treatment as EGF, has strong mitogenic and neoangiogenic activity. This makes it a poor choice as a possible vector in an affinity ligand targeting EGFR overexpression. Another option is to use a peptide ligand analogue, and several have been identified for both EGFR and EGFRvIII [17, 20, 49]. The affinity of the peptide for the EGFR or EGFRvIII target should be conserved even after the peptide has been conjugated to different groups, to ensure the usability of the peptide.

A novel peptide ligand with affinity for the EGFR, was identified by phage display peptide library [17]. The peptide has the AA sequence N-term YHWYGYTPQNVI C-term, and was designated GE11. By using competitive binding, it was demonstrated that GE11 bound specifically to EGFR. The binding was inhibited by the presence of EGF, which indicates that the binding site of GE11 and EGF are partly overlapping. GE11 was shown to have much lower mitogenic activity than EGF or many other known peptide ligand analogues, and induced a 10% growth increase compared to 50% for EGF. By conjugating FITC to the N-terminus of GE11, the fluorescent labelled GE11 was shown to be internalised preferentially into EGFR overexpressing SMMC-7721 cells. The internalisation could be inhibited by a high concentration of unlabelled GE11 peptide or hEGF. The peptide was also conjugated to a polyethylenimine vector with the AA linker $(GGGGS)_3$ at the C-terminus of GE11, and was shown to be capable of mediating target-specific gene

delivery *in vivo* to mice bearing subcutaneous EGFR overexpressing SMMC-7721 tumours. [17] In another study, Cy5.5 was conjugated to the N-terminus of GE11 and subsequently conjugated to lipids. By using the fluorescence signal from Cy5.5, it was demonstrated that GE11 could be used in EGFR targeting liposomes *in vivo* using a xenograft in a mouse model [19].

## 1.5 Strategy

The peptide EGFR ligand analogue GE11 has been studied *in vitro* on cells overexpressing the EGFR, and *in vivo* in a mouse model using fluorescence. It has been modified at the N- and C- terminus in several ways and still retained affinity for the EGFR. However, the diagnosis potential to detect EGFR overexpressing tumours in PET/CT scanners using a $^{68}$Ga-DOTA modification remains uninvestigated. As EGFR is commonly overexpressed in many types of cancers, and correlates with a poor survival rate, the radio pharmaceutical could be used to diagnose a broad range of cancers and follow the development, as well as assess patient prognosis. Even though the EGFR is not tumour specific, like the EGFRvIII, overexpression of this receptor is more commonly observed in tumours, compared to EGFRvIII, signifying EGFR overexpression as a promising target in cancer diagnostics. Therefore, radiopharmaceyticals targeting EGFR overexpression is of great interests [10].

The aim of this project is defined: To produce an affinity ligand using the peptide ligand analogue GE11 with affinity for EGFR, and evaluate the targeting ability (Fig. 1.18). GE11 will be synthesised by SPPS and verified by mass spectrometry (MS), and if necessary purified by reversed phase high performance liquid chromatography (RP-HPLC). As the labelling part of the affinity ligand, both fluorescent- and chelator mediated approaches are chosen.

The fluorophore will be conjugated to GE11 to allow for detection using fluorescence spectroscopy, flow cytometry, fluorescence microscopy and fluorescence CLSM. The amino N-terminus have previously been modified with a fluorophore. Therefore, was it chosen as the target for peptide modifications in this project [17]. The peptide will be tested *in vitro* using a variant of the Swiss 3T3 murine fibroblast cell line, NR6. NR6 lacks expression of endogenous EGFR, and has been stably transfected with cDNA encoding the full length human EGFR or the EGFRvIII mutant. Therefore, the cell lines are expressing either physiological levels of EGFR, over-expressing EGFR, or expressing the truncated and constitutively active EGFRvIII (NR6wtEGFR, NR6W, and NR6M, respectively). The expression and lack of EGFR and EGFRvIII, will be verified by two different antibodies, a EGFR/EGFRvIII cocktail which recognises both EGFR and EGFRvIII, and Mab 806 which recognises EGFRvIII and about 10% of overexpressed EGFR [40]. Finally western blotting and MS driven expression verification will be used.

The chelating agent will later be conjugated to the N-terminus of GE11. $^{68}$Ga is used in PET centers today and forms stable complexes with DOTA, therefore

DOTA is chosen as the chelating agent. To verify that complexes can be formed with $^{68}$Ga and the novel DOTA-GE11 peptide, stable gallium will be complexed with DOTA, which subsequently will be analysed by MS. The design allows for a feasible transformation of the diagnostic drug to a therapeutic, by forming complexes with different radionuclides, such as $^{90}$Y. Europium will also be complexed with the DOTA-peptide to investigate if europium fluorescence could serve as a second way of fluorescently labelling the DOTA-GE11 peptide, and the successful complex formation will be monitored by fluorescence spectroscopy.

Finally, if the affinity of the fluorescently labelled peptide for the EGFR can be verified, DOTA-GE11 will be labelled with $^{68}$Ga and tested in a mouse model, using a xenograft tumour with the NR6 cell lines. The affinity will be verified by a PET/CT scanner, and the activity of the internal organs measured. In this way, the *in vivo* targeting ability of the novel labelled affinity ligand can be investigated, and the potential assessed.

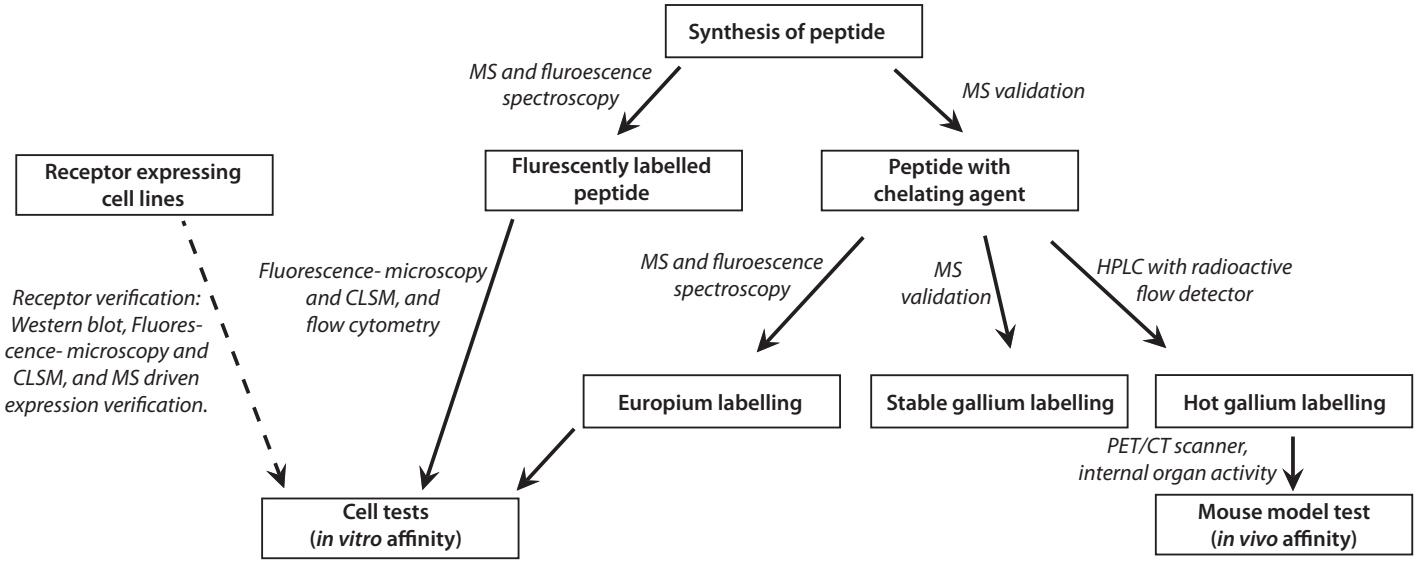


**Figure 1.18:** *Flow chart of the strategy to be employed in this project, and the techniques used to verify the steps.*

# 2 Methods

All chemicals were of analytical grade and used without further purification. Material specifications can be found in Appendix A, and Milli-Q water was used as $H_2O$.

## 2.1 Synthesis and Purification of GE11 Derivatives

The three peptides used in this project, were synthesised using a standard solid phase peptide synthesis strategy with Fmoc chemistry on an Activo-P11 solid phase peptide synthesiser. The three peptides GE11 (N-term YHWYGYTPQNVI C-term), K_GE11 (GE11 with lysine attached to the N-terminus of tyrosine) and DOTA_K_GE11 (K_GE11 with the metal chelator DOTA attached to the N-terminus of lysine) were synthesised with theoretical yields of 0.20, 0.10 and 0.10 mmol respectively. Ile preloaded Wang resin was utilised and 2.5 molar equivalent AA to resin bound Ile was used, in accordance with the protocol. GE11 was synthesised using the standard protocols defined by the system with DMF as solvent. The protocols for the synthesis of K_GE11 and DOTA_K_GE11, were optimised by increasing the coupling time from the standard 20 min to 60 min (Table 2.1), along with employing a double coupling protocol for chosen AAs (Table 2.2), where another portion of the same activated AA was added to the reaction vessel (RV) after the first coupling was completed.

| **Procedure** | **Addition** | **Time** | **Cycles GE11** | **Cycles K_GE11** |
|---|---|---|---|---|
| Swelling | 2.0 mL DMF<br>2.0 mL DMF | 15 min<br>60 min | **1** | **1** |
| Deprotection | 2.0 mL 25% piperidine in DMF<br>2.0 mL 25% piperidine in DMF | 3 min<br>12 min | **11** | **17** |
| Washing X 5 | 2.0 mL DMF 5 times | 1 min X 5 | | |
| Activation of AA | 0.5 mL 0.48 M HBTU/HOBt in DMF<br>0.5 mL 1.0 M DIPEA in DMF | 12 min<br>1 min | | |
| Coupling | Activated- and deprotected AA | 20* / 60 min | | |
| Washing X 5 | 2.0 mL DMF 5 times | 1 min X 5 | | |
| Deprotection | 2.0 mL 25% piperidine in DMF<br>2.0 mL 25% piperidine in DMF | 3 min<br>12 min | **1** | **1** |
| Final washing X 5 | 2.0 mL DMF 5 times | 1 min X 5 | | |
| Final washing X 4 | 2.0 mL DCM 4 times | 1 min X 4 | | |

**Table 2.1:** *SPPS protocol used in the synthesis of GE11*, K_GE11 and DOTA_K_GE11 with DMF as solvent. In the double coupling steps of K_GE11 and DOTA_K_GE11 the deprotection step was emitted for the second coupling (dashed line).*

| Coupling # | AA | Coupling Protocol | Coupling # | AA | Coupling Protocol |
|---|---|---|---|---|---|
| - | Ile | Precoupled | 7 | Gly | single |
| 1 | Val | single | 8 | Tyr | single |
| 2 | Asn | single | 9 | Trp | double |
| 3 | Gln | single | 10 | His | double |
| 4 | Pro | single | 11 | Tyr | double |
| 5 | Thr | double | 12 | Lys | double |
| 6 | Tyr | single | | | |

**Table 2.2:** *Coupling protocols used in the SPPS of cf_K_GE11 and DOTA_K_GE11. In the synthesis of GE11 the single coupling protocol was used for all AAs.*

### 2.1.1 Fluorescent Labelling of GE11 Derivatives

The fluorescent labelling of GE11 and K_GE11 was performed using an Activotec RV shaker at 180° rotation/mixing step, with DMF as solvent. A threefold molar excess of fluorophore to the theoretical peptide yield was used, and the standard SPPS protocol from the Activo-P11 was employed with a modified coupling time [22, 50].

#### Solid Phase Fluorescent Labelling of GE11 and K_GE11

The fluorophore was activated in 0.5 mL 0.48 M HBTU/HOBt in DMF, and mixed with 1:1 (v/v) 1.0 M DIPEA in DMF just prior to coupling in the RV. GE11 and fluorescein as free acid (ff) was coupled for 2 h. K_GE11 and cf was coupled for 24 h, the product here forth denoted cf_K_GE11. After six 2 mL DMF washes of cf_K_GE11 a final deprotection step with 2 mL 25% piperidine in DMF was performed to aviod product carrying additional cf molecules [22, 50]. Finally, the products were washed five times with DMF, three times with DCM and dried in vacuum for 20 min prior to TFA-mediated cleavage.

#### Liquid phase Fluorescent Labelling of GE11

Liquid phase fluorescent labelling was used to label GE11 with ff and subsequently with cf. GE11 was dissolved in 0.5 mL DMF and swelled in the RV for 15 min. The fluorophore was dissolved in 0.5 mL 0.48 M HBTU/HOBt in DMF, and 1:1 (v/v) 1.0 M DIPEA in DMF was added just prior to coupling in the RV. The coupling was allowed to proceed for 4 h. The reaction was stopped and purified by diethyl ether precipitation.

### 2.1.2 Conjugation of K_GE11 and DOTA

K_GE11 and DOTA-tris (t-Bu ester) were conjugated in the Activo-P11 synthesiser as an AA coupling step, prior to the final washing steps (Table 2.1). A threefold molar excess of activated DOTA-tris (t-Bu ester) to resin-bound Ile was added to the RV and coupled with K_GE11, for a total of 4 h [24]. After 2 h, an additional

0.5 mL 1.0 M DIPEA in DMF was added to the RV and the reaction was allowed to proceed for another 2 h. The product was dried in a low vacuum for 20 min, and cleaved by TFA.

### 2.1.3 Cleavage of GE11 Derivatives and Wang Resin

The GE11 and derivatives were cleaved from the resin and remaining protection groups removed, using an Activotec at 180° rotation/mixing step. For GE11 and cf_K_GE11, 2 mL TFA:TIS:$H_2O$:EDT (v/v) (92.5: 2.5: 2.5: 2.5) was added to the RV, mixed for 2 h in the Activotec and the solution was collected. For DOTA_K_-GE11, 2 mL TFA:TIS:H2O (v/v) (95: 2.5: 2.5) was added to the RV, mixed for 4 h in the Activotec and the solution was collected [24]. The RV was rinsed with 2 mL TFA which also was collected, and the product was diethyl ether precipitated.

### 2.1.4 Precipitation of GE11 Derivatives

Diethyl ether at -18 °C was added to the collected product and centrifuged at 3,000 g at 4 °C for 10 min. The solvent was disposed of and the procedure repeated twice. The product was dried in a low vacuum overnight, and the dry product was stored at -18 °C.

### 2.1.5 RP-HPLC analysis and Purification of GE11 Derivatives

The synthesis product was analysed and purified by RP-HPLC, on a Dionex Gemini-NX C18 5 $\mu$ (10.00 x 250 mm, 110 Å) reverse-phase column (*Phenomenex*).

For analytical runs, a few corns of peptide was dissolved in 0.1% TFA in $H_2O$ which was sonicated at 100 W for 10 min. The column was loaded with 2 mL of the solution, and an analytic linear gradient was run at a flow rate of 1 mL/min (Table 2.3). For all measurements, an absorption spectrum of the eluent was recorded at 214 nm to detect the peptide bond [51], 280 nm to detect tryptophan [52] and 437 nm to detect fluorescein [53, 54]. Fractions were selected for MS analysis, and based on the chromatogram, a multistep purity profile was prepared. For RP-HPLC purification of cf_GE11, a solution of 30%ACN, 2% DMSO and 0.1% TFA in $H_2O$ was saturated with the peptide and sonicated for 10 min at 100 W. For RP-HPLC purification of DOTA_K_GE11, a solution of 0.1% TFA in $H_2O$ was saturated with the peptide and sonicated for 10 min at 100 W. The column was loaded with 2 mL of the solution and the protocol loaded (Table 2.3), with a flowrate of 2 mL/min. The collected fractions were freeze dried in an ALPHA 2-4 LD plus, and the dry product was stored at -18 °C.

*Analytical*

| **Time** | **100% ACN** | **0.1% TFA in $H_2O$** |
|---|---|---|
| 0 min | 2% | 98% |
| 60 min | 60% | 40% |

*Purification cf_GE11*

| **Time** | **100% ACN** | **0.1% TFA in $H_2O$** |
|---|---|---|
| 0 min | 35% | 65% |
| 1 min | 42% | 58% |
| 31 min | 47% | 53% |
| 32 min | 80% | 20% |

*Purification DOTA_K_GE11*

| **Time** | **100% ACN** | **0.1% TFA in $H_2O$** |
|---|---|---|
| 0 min | 2% | 98% |
| 1 min | 20% | 80% |
| 46 min | 35% | 65% |
| 47 min | 80% | 20% |

**Table 2.3:** *Gradients used in the RP-HPLC. The the sample was injected and allowed to bind to the column for 5 min, prior to the program. The gradient used for purification was designed from the analytical analysis.*

## 2.2 Metal Complex Formation with DOTA_K_GE11

Based on the protocols being used at Aalborg Hospital (Denmark), the formation of the complex with DOTA_K_GE11 and europium/gallium was studied.

For $GaCl_3$ experiments, a 82% 0.2 M acetic acid in $H_2O$ and 18% sodium acetate solution buffer was prepared with pH 3.89 (was to be within $4 \pm 0.2$). 965 $\mu$L buffer was heated to 40, 60, 80 or 95 °C in a heating block with 300 RPM shaking. 25 $\mu$L 12.2 $\mu$M (1 mg/mL) DOTA_K_GE11 in buffer and 10 $\mu$L 14.6 $\mu$M $GaCl_3$ in buffer was added. The reaction was allowed to proceed for 8 min, after which the tubes were placed in an icebath. As references, DOTA_K_GE11 and $GaCl_3$ in acetic acid and sodium acetate solution buffer were run concurrently. The samples were analysed by MALDI-TOF MS.

For the $EuCl_3$ experiments, $H_2O$ pH 5.87 was used instead of buffer throughout the experiment. 965 $\mu$L $H_2O$ was heated to 40, 60, 80 or 95 °C in a heating block with 300 RPM shaking. 25 $\mu$L 12.2 $\mu$M (1 mg/mL) DOTA_K_GE11 in $H_2O$ and 10 $\mu$L 14.6 $\mu$M $EuCl_3$ in $H_2O$ was added. The reaction was allowed to proceed for 8 min, after which the tubes were placed on ice. As references DOTA_K_GE11 in $H_2O$ and $EuCl_3$ in $H_2O$ were run concurrently. The samples were analysed by MALDI-TOF MS and fluorescence spectroscopy. Also a fluorescence time study was performed with europium, where 965 $\mu$L $H_2O$ was heated to 25 °C or 40 °C in the fluorescence spectrometer. 25 $\mu$L 12.2 $\mu$M (1 mg/mL) DOTA_K_GE11 in $H_2O$ and 10 $\mu$L 14.6 $\mu$M $EuCl_3$ in $H_2O$ was added and fluorescence emission measurements were started every 5 min, with a 90 sec scan time, with the temperature maintained throughout the experiment.

## 2.3 Fluorescence Spectroscopy

Fluorescence spectroscopy measurements were performed with a Fluorescence Spectrophotometer in a precision cell made of quartz suprasil (type 101-QS) with a 10 mm light path.

### 2.3.1 Verification of cf_K_GE11 Fluorescence

Solutions of cf and cf_K_GE11 were prepared to a concentration of 5.0 $\mu$M in $H_2O$ [17], and the samples were kept in the dark when possible. A water spectrum was recorded for all measurements, pH 5.87.

From the provider of cf (*SIGMA-ALDRICH*), cf $\lambda_{exc}$ = 492 nm and $\lambda_{emi}$ = 517 nm. First an emission scan was obtained with $\lambda_{exc}$ = 492 nm to determine the maximum emission. Subsequently, an excitation scan was obtained monitoring emission at the before determined maximum emission. Finally, an emission scan was obtained using the determined excitation with maximum emission. Instrument parameters are given below (Table 2.4).

| Parameter | cf experiments | Europium experiments |
|---|---|---|
| Emission scan range | [500 - 700] nm | [500 - 700] nm |
| Excitation scan range | [400 - 500] nm | N/A |
| Step size | 0.5 nm | 0.5 nm |
| Integration | 0.2 s | 0.2 s |
| Averages | 5 | 1 |

**Table 2.4:** *Instrument parameters used in the fluorescence spectroscopy analysis of cf_K_GE11 and the Eu-DOTA_K_GE11 complex.*

### 2.3.2 Eu-DOTA_K_GE11 Fluorescence

Fluorescence emission scans were performed on the $EuCl_3$ and DOTA_K_GE11 solution in $H_2O$. An emission scan was obtained with $\lambda_{exc}$ = 340 nm and subsequently at $\lambda_{ext}$ = 270 nm.

## 2.4 Cultivation of Cells

Four murine cell lines were utilised in the project: NR6, NR6wtEGFR, NR6W and NR6M. NR6W overexpresses human EGFR, NR6wtEGFR has an expression consistent to what is seen on normal human fibroblast cells, NR6M overexpresses the EGFR type III mutant and NR6 has no expression of the EGFR. The variants were constructed by transfecting NR6, a variant of the Swiss 3T3 murine fibroblast cell line lacking expression of endogenous EGFR, with cDNA encoding the full length human EGFR (NR6wtEGFR and NR6W) or the EGFR type III mutant (NR6M). [55, 56]

All cell lines were maintained in Dulbeccos's modified Eagle's medium with a high (4.5 g/L) glucose content (DMIM/high), supplemented with 10% fetal bovine serum (FBS), 2 mM L-glutamine, 200 U/mL penicillin, 200 $\mu$g/mL streptomycin and 20 $\mu$g/mL gentamicin. Cells were grown in T75 bottles until about 80% confluency at which point they were sub cultivated. A 1:1 (v/v) solution of 0.25% trypsin and 0.02% EDTA in PBS was used to loosen the adherent cells. The cells were kept in a humidified chamber with 5% $CO_2$ at 37 °C for up to 10 passages [39], and counted using a haemocytometer and trypan-blue. Initially, a frozen stock of each cell line was constructed, using fresh medium, modified to 30% FBS and 7.5% DMSO. The cells were kept in cryotubes at -135 °C.

The doubling times of the cell lines were determined, by evaluating the number of cells :

$$\begin{aligned} N(t) &= N_0(t) * \exp^{kt} \\ \ln N(t) &= kt + \ln N_0(t) \end{aligned} \tag{2.1}$$

N and $N_0$ is the number of cells at time t and initially, and k is the growth rate. The doubling time is then found as ln2/k.

## 2.5 Verification of EGFR and EGFRvIII Expression

### 2.5.1 Cell Lysate Preparation

Cells were seeded in 6 well plates, and allowed to grow to about 80% confluency. Radioimmunoprecipitation assay (RIPA) buffer was prepared (20 mM Tris-HCl pH 8, 137 mM NaCl, 2 mM $Na_2EDTA$, 10% glycerol, 1% Triton X-100, 0.25% Na-deoxycholate and a protease inhibitor cocktail tablet with $H_2O$ as solvent). The medium was aspirated from the cells, and the cells were washed twice with PBS buffer. The cells were lysed by adding 1 mL 4 °C RIPA buffer per well, and incubating the cells at 4 °C for 5 min. A cell scraper was used to remove and lyse remaining adherent cells, and the cell lysate was transferred to a tube on ice and stored at -80 °C. Prior to usage, the lysate was centrifuged at 8,000 g for 10 min at 4 °C to pellet the cell debris, soluble proteins were left in the solution.

### 2.5.2 Western Blotting

Immunoblotting was performed using standard western blot protocols, with anti-human EGFR and EGFRvIII antibody cocktail to detect receptor expression and anti-mouse α-tubulin antibody as a positive control. Proteins in the cell lysate were separated by size using a 12% SDS-PAGE gel, with the prestained protein ladders SM1859 and SM0671. Prior to blotting two pieces of filter paper and two fiber pads were equilibrated in transfer buffer (192 mM glycine in $H_2O$ and 25 mM Tris-base in $H_2O$) for 20 min and a polyvinylidede difluoride (PVDF) membrane was activated in methanol for 10 min. The transfer sandwich was assembled, and con-

tact between the SDS-PAGE and the PVDF membrane was assured by rolling a tube over the membrane and the gel. Transfer took place at 350 mA (and approximately 150 V) for 3 h in transfer buffer with stirring and cooling elements. After blotting, the membrane was blocked in blocking buffer (1% (w/v) skimmed milk powder in basic buffer (20 mM Tris-HCl in $H_2O$ pH 7.5, 150 mM NaCl in $H_2O$ and 0.05% (v/v) Tween-20 in $H_2O$)) for 1 h, and the SDS-PAGE was stained with Coomassie Brilliant Blue. The PVDF membrane was then probed overnight with the primary antibodies at 4 °C; anti-human EGFR and EGFRvIII mouse antibody cocktail (1:1000 v/v in blocking buffer) and anti-mouse α-Tubulin mouse antibody (1:7000 (v/v) in blocking buffer). The membrane was washed three times for 15, 30, and 30 min respectively in washing buffer (0.1% (v/v) Triton X-100 in basic buffer) before incubation with Alexa fluor 488 goat anti-mouse as the secondary antibody (1:1000 v/v in blocking buffer) for 2 h in the dark. After repeating the washing step in the dark the proteins were visualized using a Typhoon Fluorescence scanner with emission filter 526 SP.

### 2.5.3 In-Gel Tryptic Digest

After western blot and staining, spots were selected for in-gel digest on the 12% SDS-PAGE gel separation of the cell lysate. Also a control piece of gel was cut from a region of the gel without any visible staining as a negative control, and processed in parallel with the sample. The gel pieces were washed twice with 100 $\mu$L 0.1 M $NH_4HCO_3$ in $H_2O$ 1:1 (v/v) ACN for 5 min each, and then dehydrated in ACN for 5 min, which was removed. The gel pieces were reduced in 10 mM dithiotreitiol in $H_2O$ / 0.1 M $NH_4HCO_3$ in $H_2O$ by swelling for 45 min at 56 °C in a heating block. The tubes were cooled to room temperature and the liquid was aspirated. The proteins were alkylated by covering the gel pieces with 55 mM iodoacetic acid in 0.1 M $NH_4HCO_3$ in $H_2O$, and the tube was incubated for 30 min at room temperature in the dark. The gel particles were washed twice with 100 $\mu$L 0.1 M $NH_4HCO_3$ in $H_2O$ 1:1 (v/v) ACN for 5 min each, and were dehydrated in ACN for 5 min. The ACN was aspirated and the gel pieces were rehydrated by covering them in 4 °C digestion buffer (50 mM $NH_4HCO_3$ in $H_2O$ pH 8.0 and 12.5 ng/$\mu$L trypsin). The tubes were incubated in an icebath for 45 min, after which the supernatant was replaced with 50 mM $NH_4HCO_3$ in $H_2O$ pH 8.0 without trypsin, and left overnight at 37 °C. After overnight digestion, the supernatant was recovered and saved in a 0.5 mL low binding Eppendorf tubes. To extract proteins, the gel pieces were covered with 5% formic acid in $H_2O$ and incubated for 15 min, followed by addition of 1:1 (v/v) ACN and 15 min incubation. The supernatant was added to the low binding Eppendorf tube, and the extraction step was repeated. The extracted solutions were dried to a volume of 1-2 $\mu$L in a vacuum centrifuge. The tryptic peptides were redissolved in 10-30 $\mu$L 5% formic acid in $H_2O$, and transferred to the LC-ESI MS/MS system for analysis, or stored at -80 °C.

### 2.5.4 Immunostaining

The cells were grown as monolayers in glass chamber slides until they were about 80% confluent. They were washed briefly with PBS twice and fixed by adding 4% neutral buffered formaldehyde in PBS to a depth of 2-3 mm in the chambers for 15 min at room temperature, where after the cells were washed three times with PBS for 5 minutes each. The cells were permeabilised by adding ice-cold methanol to a depth of 3-5 mm to each chamber, and incubation for 10 minutes at -18 °C. After permeabilisation the cells were rinsed in PBS for 5 minutes and blocked with 3% bovine serum albumin (BSA) 0.3% Triton X-100 in PBS for 1 h at room temperature. The blocking solution was aspirated and the primary antibody solution was added (1:100 (v/v) anti-human EGFR and EGFRvIII mouse antibody cocktail- and 1:500 (v/v) anti-mouse α-Tubulin rabbit antibody in 0.3% Triton X-100 in PBS) and the cells were incubated overnight at 4 °C. The cells were then rinsed in PBS three times for 5 minutes each and incubated with the secondary antibody solution (1:200 (v/v) Alexa fluor 488 goat anti-mouse antibody and Alexa fluor 647 goat anti-rabbit antibody in 0.3% Triton X-100 in PBS) for 2 h at room temperature in the dark. The secondary antibody solution was aspirated and the cells were washed three times with PBS, 5 minutes each. For DNA staining, 100 $\mu$L 1 mg/mL Hoechst 33342 diluted 1:100 in PBS was added to the cells and incubated for 15 min at room temperature. After rinsing three times with PBS for 5 minutes each, the cells were mounted with Dakocytomation fluorescent mounting medium and a cover glass. The slides were sealed with nail polisher and the cells were analysed by fluorescence microscopy and fluorescence confocal laser scanning microscopy.

## 2.6 Targeting and Internalisation of cf_K_GE11 *in vitro*

The uptake of cf_K_GE11 was studied using adherent cells in chamber slides and cells in solution for flow cytometry.

### 2.6.1 Chamber Slides Preparation

The cells were grown as monolayers in glass chamber slides until $\sim$ 80% confluent, at which point the medium was aspirated and fresh medium with 5 $\mu$M cf_K_GE11 was added. As a negative control, cells were grown concurrently in medium without cf_K_GE11. The cells were grown in the dark overnight [17], after which the cells were washed briefly in PBS twice and fixed by adding 4% neutral buffered formaldehyde in PBS for 15 min. The cells were washed in PBS three times for 5 min each, after which the DNA was stained by adding 100 $\mu$L 1 mg/mL Hoechst 33342 diluted 1:100 in PBS to the chamber slides. The cells were incubated for 15 minutes in the dark at room temperature, and washed three times with PBS for 5 minutes each. The cells were mounted by adding a drop of Dakocytomation fluorescent mounting medium and a cover glass was added to the chamber slides. The

slides were sealed with nail polisher, and the cells were analysed by fluorescence microscopy and fluorescence confocal laser scanning microscopy (CLSM).

### 2.6.2 Flow Cytometry Preparation

The cells grown as monolayers in 6 well incubation boxes until $\sim$ 80% confluent, at which point the medium was aspirated and fresh medium with 5 $\mu$M cf_K_GE11 was added. As a negative control, cells were grown concurrently in medium without cf_K_GE11. The cells were grown in the dark overnight [17], after which the cells were washed briefly in PBS twice. The cells were then detached from the wells by adding either 1:1 (v/v) 0.25% trypsin and 0.02% EDTA, or 2 mM EDTA in PBS solution. The cells were transferred to a flow cytometry tube, medium without cf_K_GE11 was added, and the cell suspension was centrifuged at 500 g for 5 min. The supernatant was disposed and PBS was added for washing. The tube was vortexed until the cells were in solution again and the tube was centrifuged at 500 g for 5 min, the PBS was disposed. The washing procedure was repeated twice after which 400 $\mu$L 1.35% formaldehyde in PBS was added to the cells and the tube was vortexed. The cells were kept at 4 °C overnight and analysed with a FACSanto flow cytometry using a FITC filter. Based on the forward scatter (FSC), which correlates with the cell volume, and side scatter (SSC) which depends on the inner complexity of the cell, the intact cells were selected and the fluorescence evaluated.

## 2.7 Fluorescence Imaging

Fluorescence- microscopy and CLSM was used to analyse the chamber slides stained with antibodies (Section 2.5.4) and cf_K_GE11 (Section 2.6.1).

### 2.7.1 Fluorescence Microscopy

The cells in the sealed chamber slides were examined with an Axiovert 200M inverted microscope with excitation at 650 nm ($Exc_{650}$) and emission at 680 ($Emi_{680}$) for Cy5 / Alexa 647, $Exc_{488}$ and $Exc_{530}$ for FITC / Alexa 488, and $Exc_{350}$ and $Exc_{461}$ for Hoechst 33342. A 63x oil objective was used and the images were recorded in an as similar way as possible to ensure comparability between the samples.

### 2.7.2 Fluorescence Confocal Laser Scanning Microscopy

The cells in the sealed chamber slides were examined with a LSM510 meta confocal laser scanning microscope. No filter was present for Hoechst 33342, so only Cy5 (anti-mouse $\alpha$-tubulin) and FITC (anti-human EGFR and EGFRvIII, and cf_K_GE11) could be analysed.

## 2.8 Mass Spectrometry

MS was used to investigate the synthesised products, the in-gel tryptic peptides and the formation of the metal complex.

### 2.8.1 MALDI-TOF MS

Delayed extraction MALDI mass spectra was recorded on a Bruker Reflex 3 reflector TOF-MS, equipped with a nitrogen laser ($\lambda$ = 337 nm). Positive ion reflector mode was used in all experiments.

The sample was mixed 1:1 (v/v) with 3 g/L DHB in 1 vol ACN and 2 vol 0.1% TFA in $H_2O$. 1 $\mu$L of the mixture was placed on a sample support and left to dry (dried droplet method) and loaded into the mass spectrometer. Mass calibration was performed prior to all analysis on a peptide mixture of angiotensin II, bombesin, adrenocorticotropic hormone and somatostatin.

When necessary to increase the sample concentration and remove salts, the samples were purified using an Empore high performance extraction disk (Pk/20 2215). A needle with an internal steel wire was used to extract a C18 nanocolumn from a 47 mm disk, and the nanocolumn was mounted in a GeLoader tip. The column was equilibrated with 15 $\mu$L 5% formic acid in $H_2O$ using a piston. 15 $\mu$L sample was loaded onto the column and washed with 15 $\mu$L 5% formic acid in $H_2O$. The sample was eluted onto the sample support with 1 $\mu$L 3 g/L DHB in 2 vol ACN and 1 vol 0.1% TFA in $H_2O$, dried and loaded into the mass spectrometer. The data was analysed in *Mmass* [57, 58] supplemented with data from GPMAW v9.02 [59].

### 2.8.2 ESI MS/MS

ESI MS/MS spectra was recorded on a a hybrid QTOF mass spectrometer. A few corns of the sample was dissolved in 5% formic acid and 2 $\mu$L was loaded into an ESI loading tip, and by using a piston the sample was sprayed into the apparatus. The MS spectrum was saved, the correct precursor ion chosen and fragmented by collision induced dissociation by increasing the collision cell energy 0-35 eV, yielding a tandem MS spectrum with peptide fragments where different series could be identified (Fig. 2.1). The data was analysed in *Mmass* [57, 58] supplemented with data from GPMAW v9.02 [59].

### 2.8.3 LC-ESI MS/MS

Automated LC-ESI MS/MS was performed using an Ultimate nano-HPLC system mounted with a vented-column system on a hybrid QTOF mass spectrometer. An in-house packed reverse phase C18 column was loaded with the sample, with a flow rate of 3 $\mu$L/min and subsequently eluted at 175 nL/min. A 35 min 5-40% ACN in 0.6% acetic acid in $H_2O$ gradient was used, and the mass spectrometer was setup in data dependent mode, to automatically switch between MS and MS/MS acqui-

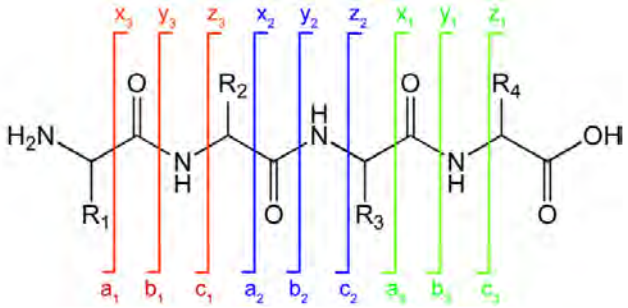


**Figure 2.1:** *MS/MS peptide fragmentation pattern. [60]*

sition, selecting the three most abundant ions. The resulting MS/MS spectra were deconvoluted, deisotoped and the resulting peptide mass lists were used in database searches. Protein homologues were identified using an in-house Mascot database search engine, using the NCBI and SwissProt databases. The search parameters chosen were: Taxonomy: Homo sapiens, fixed modification: carboxymethyl and variable: oxidation. Max miss cleavage was set to two, peptide- and MS error tolerance to $\pm$0,1 Da and peptide charges 2+, 3+ and 4+. A decoy database search was performed to access the validity of the result.

# 3 Results

## 3.1 Synthesis and Purification of GE11 Derivatives

The synthesis of cf_GE11, cf_K_GE11 and DOTA_K_GE11 was performed using an Activo-P11 synthesiser, and the products were evaluated with RP-HPLC and MS techniques. Absorption at 214 nm resulted in signal saturation, so this data was only used in the collection process and is not presented. All masses are given as monoisotopic, calculated using GPMAW v9.02 [59] and MS spectra analysed in mMass 3.10.0 [57, 58].

### 3.1.1 Synthesis of cf_GE11

The synthesis and obtained results of GE11 are described in Appendix B. Several attempts were made to label the peptide with ff, first using solid- and then liquid phase labelling protocols, but MALDI-TOF MS concluded that the labellings with ff was unsuccessful.

The labelling of GE11 was then performed with the isomeric mixture 5(6)carboxyfluorescein (cf), and the successful labelling was verified by MS, but unlabelled product was also detected. However, after purification of the labelled product with several diethyl ether precipitations and RP-HPLC, impurities were still found by MS with the peptide along with signs of peptide degradation (data in Appendix B), so a second synthesis was conducted.

### 3.1.2 Synthesis of cf_K_GE11 and DOTA_K_GE11

For the second synthesis, lysine was added to the N-terminus of the GE11 sequence (denoted K_GE11). K_GE11 was then fluorescently labelled with cf, the product henceforth denoted cf_K_GE11. Also a K_GE11 peptide with the chelating agent DOTA conjugated to the N-terminus was synthesised, henceforth denoted DOTA_K_GE11. A theoretical yield of 0.10 mmol of both peptides were synthesised.

RP-HPLC analysis was conducted on the synthesis products of cf_K_GE11 (Fig. 3.1) and DOTA_K_GE11, and analysed by MS. The MALDI-TOF MS spectra

| GE11 Derivative | Ionisation | $m/z_{calc}$ | $m/z_{measured}$ | Deviation m/z |
|---|---|---|---|---|
| cf_K_GE11 | $Na^+$ | 2048.9 | 2048.7 | -0.2 |
| cf_K_GE11 | $H^+$ | 2026.9 | 2026.7 | -0.2 |
| cf_K_GE11 | $2H^{2+}$ | 1013.94 | 1013.93 | -0.01 |
| cf_K_GE11 | $3H^{3+}$ | 676.29 | 676.29 | 0.00 |

**Table 3.1:** *Table of m/z used throughout this Section, containing the calculated and measured m/z for the analysis of cf_K_GE11. ESI MS masses are given with two decimal precision, MALDI-TOF MS with one. Masses are calculated in GPMAW [59].*

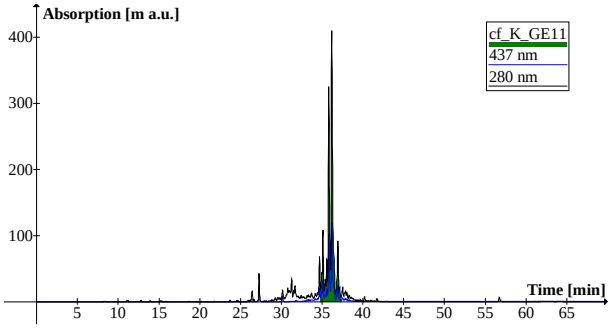


**Figure 3.1:** *RP-HPLC chromatogram of the synthesis product cf_K_GE11 with the analytical program, 100% ACN as gradient and 0.1% TFA in $H_2O$ as solvent. The marked fraction (∼ 70%) was analysed by MS (Fig. 3.2).*

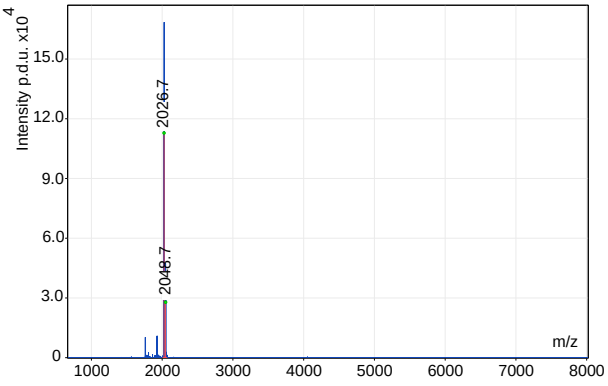


**Figure 3.2:** *MALDI-TOF spectrum of cf_K_GE11 RP-HPLC fraction (Fig. 3.1). Single charged peaks at m/z 2026.7 and 2048.7, corresponding well to [cf_K_GE11 + H / Na]$^+$ = m/z 2026.9 / 2048.9 respectively.*

of cf_K_GE11 eluent at retention times 34.8 - 37.3 min (Fig. 3.2) contained single charged peaks at m/z 2026.7 and 2048.7, corresponding well to the $H^+$ and $Na^+$ ionised of cf_K_GE11, respectively (Table 3.1). The fraction constitutes ∼70% of the sample detected at 280 nm. To further assess the purity of cf_K_GE11, ESI MS/MS was conducted on the synthesis product (Fig. 3.3). A double charged peak is detected at m/z 1013.93 and a triple charged peak at m/z 676.29, corresponding well to the $2H^{+2}$ and $3H^{+3}$ ionised cf_K_GE11 respectively (Table 3.1). To validate the sequence of cf_K_GE11, ESI MS/MS analysis with CID was performed by choosing the double charged ion at m/z 1013.9 as precursor (Fig. 3.4). Peptide sequences were identified corresponding well to overlapping parts of the a, b and y' peptide fragmentation series of cf_K_GE11 (described in Methods, Section 2.8), along with several internal fragments (Table 3.5).

The eluent from the RP-HPLC analysis of DOTA_K_GE11 (Fig. 3.6) at retention time 29.3 - 31.0 min was analysed by MALDI-TOF MS (Fig. 3.8), and single charged peaks were detected at m/z 2055.3 and 2077.3 corresponding well

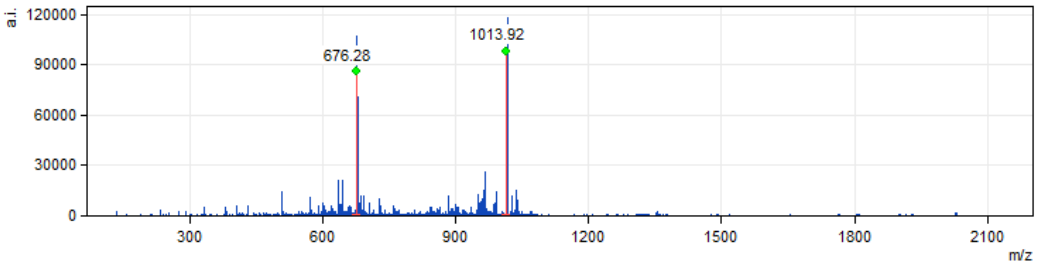


**Figure 3.3:** *ESI MS of the crude cf_K_GE11 synthesis product. Double charged peak at m/z 1013.93 and triple charged peak at m/z 676.29, corresponding well to [cf_K_GE11 + 2H / 3H]$^{+2/3}$ = m/z 1013.94 / 676.30 respectively.*

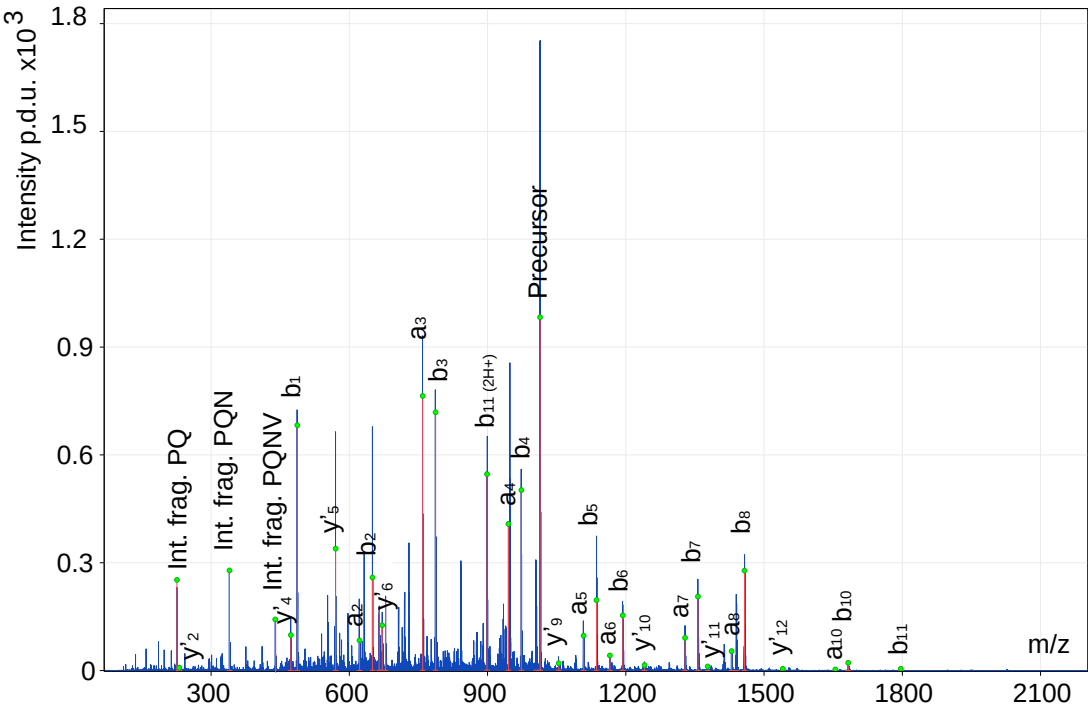


**Figure 3.4:** *ESI MS/MS on c_K_GE11, with precursor ion m/z 1013.9 and the collision cell energy was raised 0-35 eV. Masses corresponding well to overlapping parts of the a, b and y' series of cf_K_GE11 were identified (Table B.2).*

| | | *a Series* | | *b Series* | |
|---|---|---|---|---|---|
| **Peptide** | **#** | **Meas. m/z** | **Deviation m/z** | **Meas. m/z** | **Deviation m/z** |
| cfK | 1 | | 487.15 | 0 | |
| cfKY | 2 | 622.20 | -0.02 | 650.20 | -0.01 |
| cfKYH | 3 | 759.25 | -0.03 | 787.25 | -0.02 |
| cfKYHW | 4 | 945.35 | -0.01 | 973.35 | 0 |
| cfKYHWY | 5 | 1108.42 | 0 | 1136.41 | -0.01 |
| cfKYHWYG | 6 | 1165.45 | 0.01 | 1193.45 | 0.01 |
| cfKYHWYGY | 7 | 1328.48 | -0.04 | 1356.45 | -0.05 |
| cfKYHWYGYT | 8 | 1429.55 | 0 | 1457.55 | 0 |
| cfKYHWYGYTPQ | 10 | 1654.65 | -0.01 | 1682.65 | -0.01 |
| cfKYHWYGYTPQN | 11 | | | 1796.65 | -0.05 |

| | | *y Series* | | *Other* | | |
|---|---|---|---|---|---|---|
| **Peptide** | **#** | **Meas. m/z** | **Deviation m/z** | **Peptide** | **Meas. m/z** | **Deviation m/z** |
| VI | 2 | 231.19 | 0.02 | PQ | 226.10 | -0.02 |
| QNVI | 4 | 473.16 | -0.11 | PQN | 340.15 | 0.01 |
| PQNVI | 5 | 570.30 | -0.03 | PQNV | 439.20 | -0.03 |
| TPQNVI | 6 | 671.35 | -0.02 | $b_{11}$ ($2H^{+2}$) | 898.85 | -0.01 |
| YGYTPQNVI | 9 | 1054.51 | -0.01 | | | |
| WYGYTPQNVI | 10 | 1240.56 | -0.04 | | | |
| HWYGYTPQNVI | 11 | 1377.65 | -0.01 | | | |
| YHWYGYTPQNVI | 12 | 1540.70 | -0.02 | | | |

**Figure 3.5:** *Table of fragments identified in the ESI MS/MS of cf_K_GE11 (Fig. 3.4). Calculated m/z given as protonated ions, and calculated in GPMAW [59]. Where no measured mass is given, no corresponding molecular ion was found. The peptide fragmentation series are described in Methods, Section 2.8*

| GE11 Derivative | Ionisation | m/z$_{calc}$ | m/z$_{measured}$ | Deviation m/z |
|---|---|---|---|---|
| (d-Bu ester)-DOTA_K_GE11 | $H^+$ | 2167.1 | 2167.4 | 0.3 |
| (Bu ester)-DOTA_K_GE11 | $H^+$ | 2111.1 | 2111.5 | 0.4 |
| DOTA_K_GE11 | $Na^+$ | 2077.0 | 2077.3 | 0.3 |
| DOTA_K_GE11 | $H^+$ | 2055.0 | 2055.3 | 0.3 |
| DOTA_K_GE11$_{-N}$ | $H^+$ | 1941.0 | 1941.3 | 0.3 |
| DOTA_K_GE11$_{-N-K/Q}$ | $H^+$ | 1812.9 | 1813.3 | 0.4 |

**Table 3.2:** *Table of masses used throughout this Section, containing the calculated and measured m/z for the analysis of DOTA_K_GE11. Masses are calculated in GPMAW [59].*

to the $H^+$ and $Na^+$ ionisation of DOTA_K_GE11 respectively (Table 3.2). The fraction containing DOTA_K_GE11 constituted ∼11% of the signal at 280 nm (Fig. 3.6). In other investigated fractions, masses corresponding well to ionisations of DOTA_K_GE11$_{-N}$ (Fig. 3.9), (Bu ester)-DOTA_K_GE11 and DOTA_K_GE11$_{-N-K/Q}$ (Fig. 3.10) and (d-Bu ester)-DOTA_K_GE11 (Fig. 3.11) were identified (Table 3.2). The fraction containing DOTA_K_GE11 was purified by RP-HPLC, and an analytical RP-HPLC of the freeze dried sample (Fig. 3.7) was conducted where DOTA_K_GE11 now constitutes ∼96% of the signal detected at 280 nm.

## 3.2 Metal Complex Formation with DOTA_K_GE11

Theoretical MS spectra of gallium (Fig. 3.18) and europium (Fig. 3.19) DOTA_K_GE11 complexes were calculated using Bruker Daltronics IsotopePattern.

Ga-DOTA_K_GE11 complex formation at different temperatures for 8 min was conducted and the samples analysed by MALDI-TOF MS. At 40 °C (Fig. 3.12) single charged peaks were detected at m/z 2055.2 and 2121.2, corresponding well to DOTA_K_GE11 and Ga-DOTA_K_GE11 respectively (Table 3.3). As the temperature was raised to 95 °C, the signal from DOTA_K_GE11 was no longer detected (Fig. 3.13). The isotopic pattern of Ga-DOTA_K_GE11 is comparable to the theoretical spectrum (Fig. 3.18).

DOTA_K_GE11 was run concurrently in both buffers as references, and seems stable for the investigated temperatures (25, 40, 95 °C). DOTA_K_GE11 in water buffer at 95 °C (Fig. 3.15), single charged peaks were detected at m/z 2055.1 and 2077.1 both corresponding to $H^+$ and $Na^+$ ionised DOTA_K_GE11 respectively. The DOTA_K_GE11 in acetic acid / sodium acetate buffer at 95 °C sample (Fig. 3.14) has single charged peaks at m/z 2054.8 and 2086.8 corresponds to DOTA_K_GE11 (Table 3.1) and an unknown substance at m/z +32 with an isotopic pattern similar to that of DOTA_K_GE11. Also the isotopic pattern of DOTA_K_GE11 at m/z 2054.8 seems different in water buffer than acetic acid / sodium acetate buffer, which was found for all investigated temperatures.

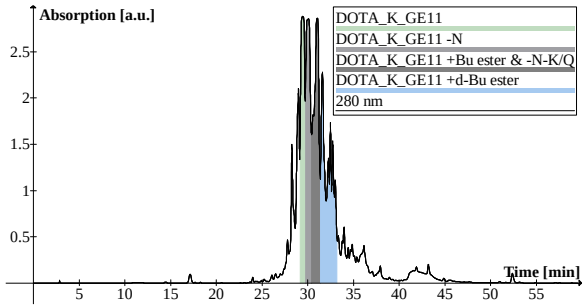


**Figure 3.6:** *RP-HPLC chromatogram of the DOTA_K_GE11 synthesis product. The analytical program was used, 100% ACN as gradient and 0.1% TFA in $H_2O$ as solvent. Four fractions were analysed. The fraction marked DOTA_K_GE11 (∼ 11%) was purified by a multistep gradient.*

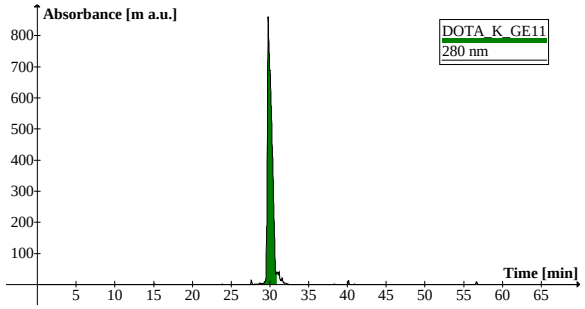


**Figure 3.7:** *RP-HPLC chromatogram of the RP-HPLC purified fraction DOTA_K_GE11 (Fig. 3.6). The analytical program was used, 100% ACN as gradient and 0.1% TFA as solvent. The RP-HPLC purified fraction (∼96%) was analysed by MS (Fig. 3.8).*

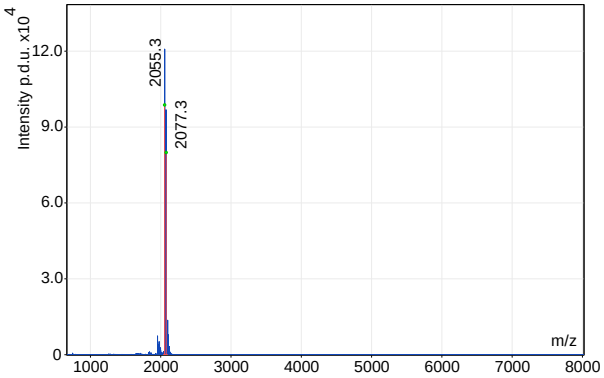


**Figure 3.8:** *MALDI-TOF spectrum of the purified DOTA_K_GE11 RP-HPLC fraction (Fig. 3.7). Single charged peaks at m/z 2055.3 and 2077.3, corresponding well to [DOTA_K_GE11 + H/Na]$^+$ = m/z 2055.0 and 2077.0 respectively.*

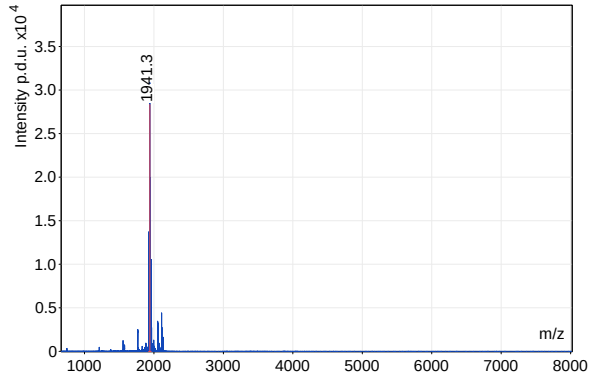


**Figure 3.9:** *MALDI-TOF spectrum of the 2$^{nd}$ DOTA_K_GE11 fraction (Fig. 3.6). Single charged peaks at m/z 1941.3, corresponding well to [DOTA_K_GE11$_{-N}$ + H]$^+$ = m/z 1941.0.*

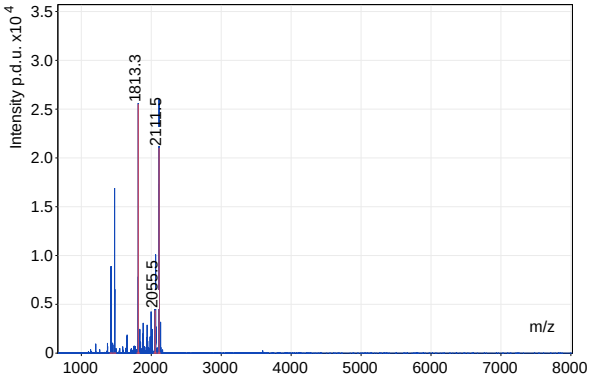


**Figure 3.10:** *MALDI-TOF spectrum of the 3$^{rd}$ DOTA_K_GE11 RP-HPLC fraction (Fig. 3.6). Major identified single charged peaks at m/z 2111.5, 2055.5 and 1813.3, corresponding well to [(Bu ester)-DOTA_K_GE11 + H]$^+$ = m/z 2111.1, [DOTA_K_GE11 + H]$^+$ = m/z 2055.0 and [DOTA_K_GE11$_{-N-K/Q}$ + H]$^+$ = m/z 1812.9 respectively.*

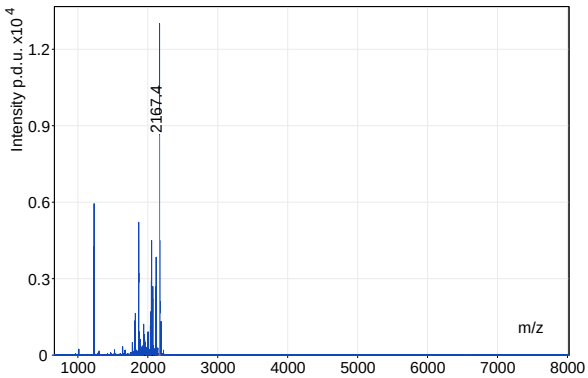


**Figure 3.11:** *MALDI-TOF spectrum of the 4$^{th}$ DOTA_K_GE11 RP-HPLC fraction (Fig. 3.6). Major identified single charged peak at m/z 2167.4, corresponding well to [(d-Bu ester)-DOTA_K_GE11 + H]$^+$ = m/z 2167.1.*

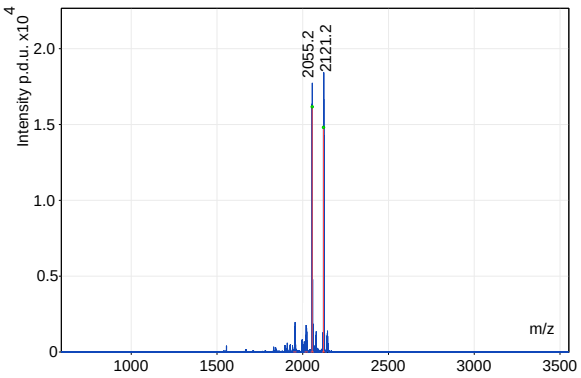


**Figure 3.12:** *MALDI-TOF MS spectrum of Ga-DOTA_K_GE11 at 40 °C for 8 min. Single charged peaks detected at m/z 2055.2 and 2121.2, corresponding well to [DOTA_K_GE11 + H]$^+$ = m/z 2055.0 and [Ga-DOTA_K_GE11 + H]$^+$ = m/z 2120.9 respectively.*

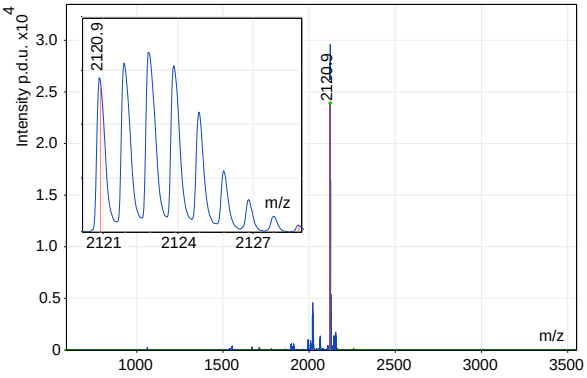


**Figure 3.13:** *MALDI-TOF MS spectrum of Ga-DOTA_K_GE11 at 95 °C for 8 min. Single charged peak detected at m/z 2120.9, corresponding well to [Ga-DOTA_K_GE11 + H]$^+$ = m/z 2120.9.*

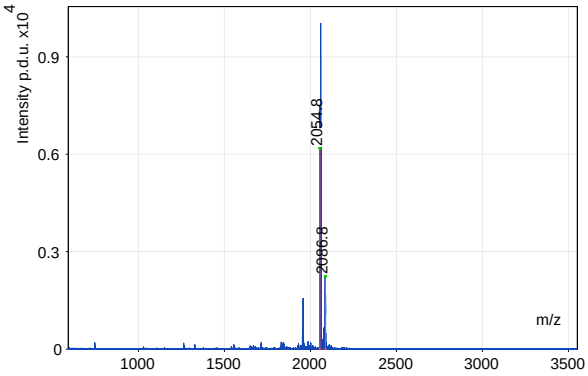


**Figure 3.14:** *MALDI-TOF MS spectrum reference of DOTA_K_GE11 in buffer at 95 °C for 8 min. Single charged peaks detected at m/z 2054.8 and 2086.8, corresponding well to [DOTA_K_GE11 + H]$^+$ = m/z 2055.0 and an unknown substance at DOTA_K_GE11 + m/z 32.*

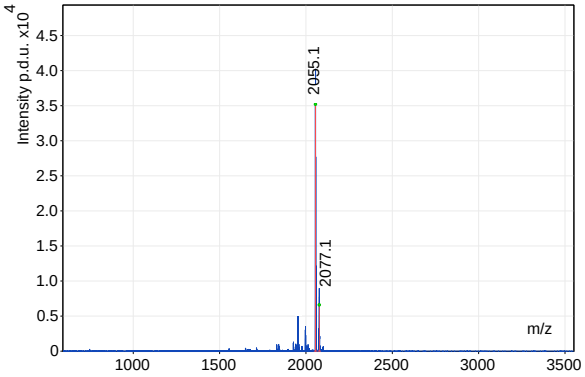


**Figure 3.15:** *MALDI-TOF MS spectrum reference of DOTA_K_GE11 in $H_2O$ at 95 °C for 8 min. Single charged peaks detected at m/z 2055.1 and 2077.1, corresponding well to [DOTA_K_GE11 + H / Na]$^+$ = m/z 2055.0 / 2077.0.*

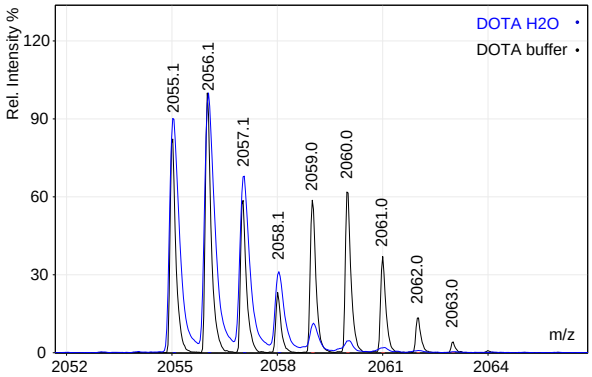


**Figure 3.16:** *MALDI-TOF MS spectrum comparison of Ga-DOTA_K_GE11 in water buffer and buffer at 40 °C for 8 min. There is a m/z +4 mass shift, resulting in a dublet of the expected isotopic pattern. The signals at m/z 2055.1 and 2059.0 corresponding well to DOTA_K_GE11 and DOTA_K_GE11 m/z +4 respectively.*

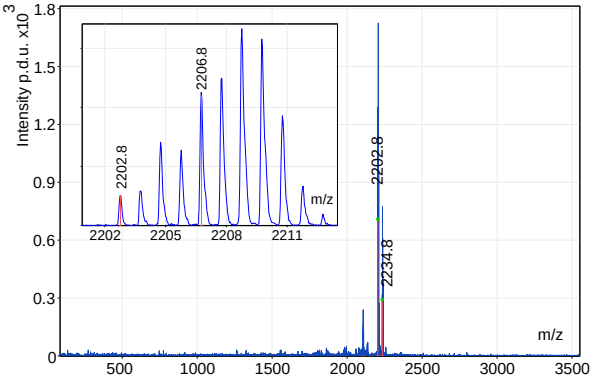


**Figure 3.17:** *MALDI-TOF MS spectrum of Eu-DOTA_K_GE11 at 40 °C for 8 min. Single charged peaks detected at m/z 2202.8 and 2234.8, corresponding well to [Eu-DOTA_K_GE11 + H]$^+$ = m/z 2202.9 and an unidentified substance at m/z +32. The dublet isotopic distribution at m/z 2202.8 is shown.*

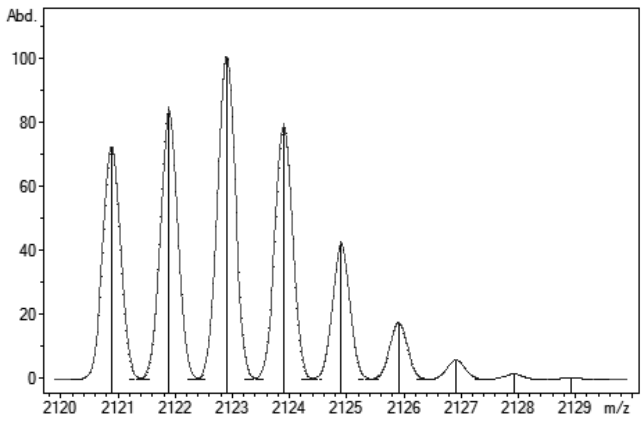


**Figure 3.18:** *Theoretical MS spectrum of the protonated Ga-DOTA_K_GE11 complex (Ga $C_{97}$ $H_{133}$ $N_{23}$ $O_{27}$). Created with Bruker Daltronics IsotopePattern.*

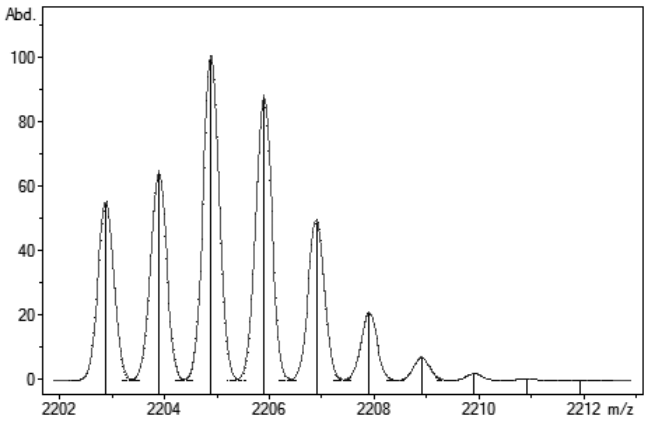


**Figure 3.19:** *Theoretical MS spectrum of the protonated Eu-DOTA_K_GE11 complex (Eu $C_{97}$ $H_{133}$ $N_{23}$ $O_{27}$). Created with Bruker Daltronics IsotopePattern.*

| GE11 Derivative | Ionisation | $m/z_{calc}$ | $m/z_{measured}$ | Deviation m/z |
|---|---|---|---|---|
| Eu-DOTA_K_GE11 | $H^+$ | 2202.9 | 2202.8 | -0.1 |
| Ga-DOTA_K_GE11 | $H^+$ | 2120.9 | 2121.2/2120.9 | 0.3/0 |
| DOTA_K_GE11 | $Na^+$ | 2077.0 | 2077.1 | 0.1 |
| DOTA_K_GE11 | $H^+$ | 2055.0 | 2055.1 | 0.1 |

**Table 3.3:** *Table of masses used in this section. Calculated and measured m/z for the analysis of the complex formations. Calculations: [DOTA_K_GE11 + $H^+_{ionisation}$ - $3H_{chelation}$ + Eu / Ga] = m/z 2202.9 / 2120.9. Masses calculated in GPMAW V9.02 [59] and Bruker Daltonics IsotopePattern V1.2.*

For the Eu-DOTA_K_GE11 complex formation, no difference between 40 °C and 95 °C was detected, therefore, 40 °C is presented (Fig. 3.17). Single charged peaks are detected at m/z 2202.8 and 2234.8, where the first corresponds to Eu-DOTA_K_GE11 and the latter to Eu-DOTA_K_GE11 m/z +32. Also here the isotopic distribution at m/z 2202.8 seems to have a m/z +4 version (at m/z 2206.8) when comparing to the theoretical spectrum (Fig. 3.19). No peak is seen for DOTA_K_-GE11. The Eu-DOTA_K_GE11 complex was analysed by fluorescence spectroscopy by excitation of europium and indirect excitation by exciting tryptophan at 270 nm [52], but no emission from europium could be detected.

## 3.3 Fluorescence Spectroscopy Analysis of cf_K_GE11

For the fluorescence spectroscopy analysis, water was analysed prior to each experiment as a reference, showing insignificant emission compared to cf_K_GE11 and cf samples. An emission scan was performed with $\lambda_{exc}$ = 492 nm (Fig. 3.20) specified by the producer *Sigma-Aldrich*, and the maximum emission was found at 517 nm for cf_K_GE11 and 511 nm for cf. An excitation scan was performed where emission at 517 and 511 nm was monitored for cf_K_GE11 and cf respectively (Fig. 3.21). cf_K_GE11 had maximum emission at 517 nm with $\lambda_{exc}$ = 491 nm with minor emission peaks at excitation 482, 469 and 450 nm. cf was found to have maximum emission at 511 nm with $\lambda_{exc}$ = 469 nm, with minor emission peaks at excitation 481, 450 and 491 nm.

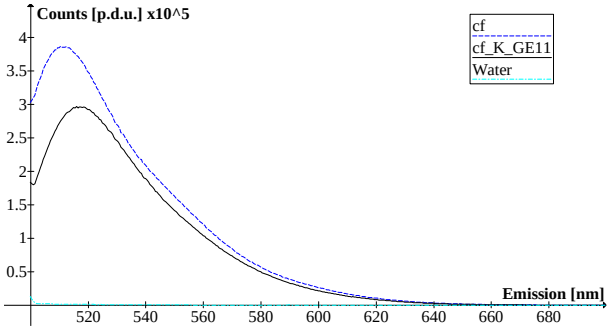


**Figure 3.20:** *Fluorescence spectroscopy emission scan performed on cf and cf_K_GE11, excited at 468 nm. The maximum emission for cf_K_GE11 was at 517 nm, and for cf at 511 nm.*

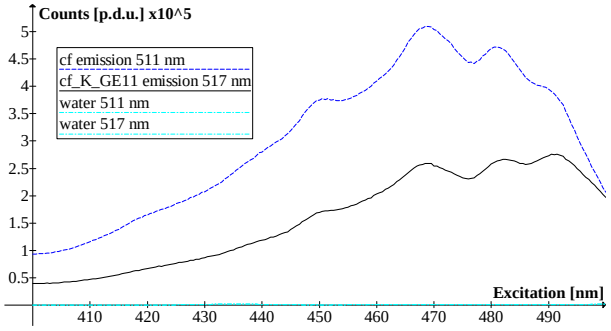


**Figure 3.21:** *Fluorescence spectroscopy excitation scan performed on cf and cf_K_GE11. Maximum emission at 517 nm for cf_K_GE11 with excitation at 491 nm, with minor peaks when exciting at 482, 469 and 450 nm. For cf, maximum emission at 511 nm was for excitation at 469 nm, with minor emission peaks when exciting at 481, 450 and 491 nm.*

## 3.4 Cultivation of Cells

The doubling times for the four cell lines, NR6, NR6W, NR6wtEGFR and NR6M, were found based on the number of cells (Fig. 3.22). From the natural logarithm to the number of cells, a linear function was fitted, the slope of which equals the growth rate, k. The doubling time was then found as ln2/k (Table 3.4). The doubling times were determined for the cell lines in the following order, slowest to fastest: NR6 (which does not express the EGFR receptor), NR6wtEGFR (with low EGFR expression), NR6W (with EGFR overexpression), and NR6M (expressing the ligand independent EGFRvIII), which is the expected when the cells are expressing the receptor as stated.

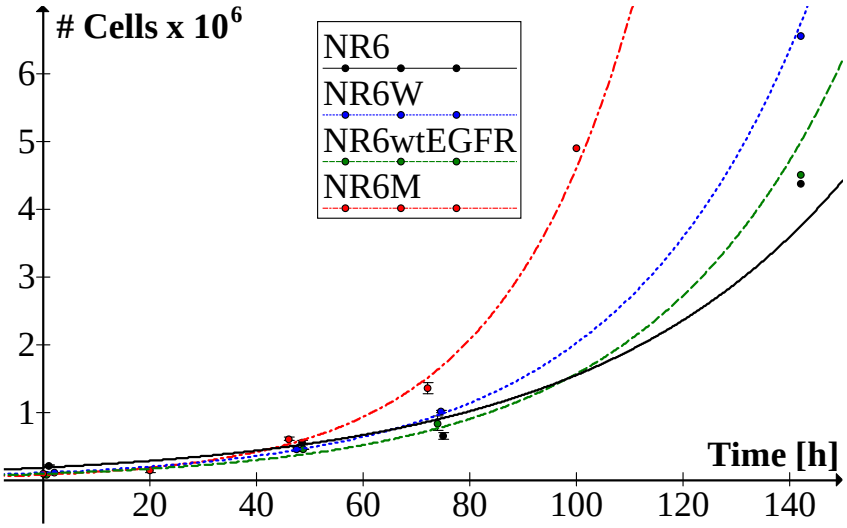


**Figure 3.22:** *Growth curves for the four cell lines; NR6 with no EGFR expression, NR6W overexpressing EGFR, NR6wtEGFR wild type expression of EGFR and NR6M expressing EGFRvIII, with an exponential fit. From the natural logarithm to the number of cells, a linear function was fitted, the slope of which equals the growth rate k.*

| Cell line | Slope | $R^2$ of fit | Doubling time |
|---|---|---|---|
| NR6 | 0.0209 | 0.9678 | 33.1 h |
| NR6wtEGFR | 0.0274 | 0.9911 | 25.3 h |
| NR6W | 0.0286 | 0.9996 | 24.3 h |
| NR6M | 0.0384 | 0.9784 | 17.4 h |

**Table 3.4:** *Calculated doubling time of the cell lines. The doubling time is calculated as ln2/k (Fig. 3.22).*

# 3.5 Verification of EGFR and EGFRvIII Expression

## 3.5.1 Western Blot

The western blot was performed using an anti-human EGFR and EGFRvIII antibody cocktail (host: mouse) with expected protein bands at 170 kDa and 145 kDa respectively to verify the receptor expression, and anti-mouse α-Tubulin mAb (host: mouse) as a positive control with an expected band at ∼ 55 kDa. As secondary antibody, Alexa Fluor 488 anti-Ms was used.

The western blot (Fig. 3.23) contained protein bands at ∼ 55 kDa for all four cell lines, corresponding well to α-tubulin, but no bands were observed at 170 kDa or 145 kDa indicating that the receptor is not present or that the antibody was incompatible with western blotting.

## 3.5.2 In-gel Digest

In-gel trypsin digest was performed on indicated spots (Fig. 3.24), peptides were extracted and analysed by LC-ESI MS/MS. A few peptide sequences were identified and searches were commenced in the NCBI and SwissProt databases, but no proteins could be identified. A 7.5% SDS-PAGE gel analysis of the cell lysate was conducted, but as no clear difference could be seen in the protein bands between the four cell lines, attempts to perform another in-gel digest were abandoned.

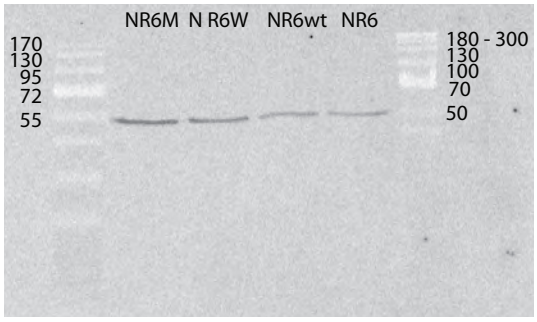


**Figure 3.23:** *Western blot of cell lysate with the anti-human EGFR and EGFRvIII antibody cocktail, expected protein bands at 170 kDa and 145 kDa respectively, and anti-mouse α-Tubulin antibody as a positive control with expected band at ∼ 55 kDa. Protein band at ∼ 55 kDa. Two different ladders were used.*

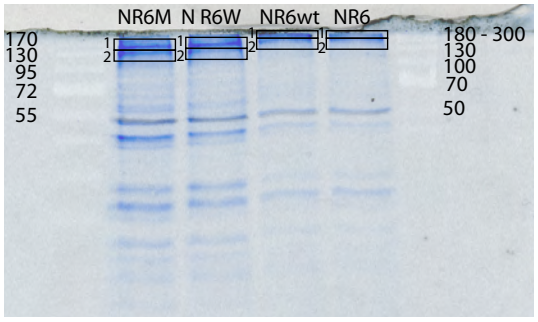


**Figure 3.24:** *Overlay of the 12% SDS-PAGE gel and western blot membrane to identify the two ladders on the gel. The indicated protein bands were analysed by MS/MS after an in-gel tryptic digest.*

## 3.5.3 Immunofluorescence

The intensity of the NR6 cell line (Fig. 3.25) is lower for the anti-EGFR and EGFRvIII antibody than the NR6wtEGFR- , NR6W- and NR6M cell lines. There is also a difference in the intensity between the NR6wtEGFR- and the NR6W cell

line (overexpression of EGFR), where the latter has the highest intensity. Finally there is a difference in the intensity between the NR6wtEGFR cells. The NR6M cell line has lower intensity from the staining of anti-EGFR and EGFRvIII antibody cocktail than the NR6W cells, but the overall intensity seems higher than for the NR6wtEGFR cells.

An antibody binding experiment was conducted using the antibody Mab806 which targets human EGFRvIII, but also has a lower affinity for human EGFR overexpression [40] (Fig. 3.26). Hoechst 33342 staining of the DNA was performed. The NR6- and NR6wtEGFR cell lines have comparable low intensities from the Mab806 antibody, which is significantly lower than the NR6W and NR6M cell lines. NR6M seems to have a higher intensity, and the intensity is unevenly distributed amongst the NR6M cells.

To investigate the cellular location of the receptor within the cells, fluorescence confocal laser scanning microscopy (CLSM) was performed on cells stained with the anti-human EGFR and EGFRvIII antibody cocktail (host: mouse) and anti-mouse α-Tubulin antibody (host: rabbit). As the goal was to investigate the cellular location of the receptor, the integration time and intensity was adjusted to give the brightest images. Therefore, the intensity is not comparable between the cell lines. Besides the intercellular frames (Fig. 3.28, 3.29 and 3.30), the frames were also combined into 3D images to more clearly illustrate the receptor distribution on the surface of the cells (Fig. 3.27). For the NR6W and NR6M cell lines (Fig. 3.29), the anti-human EGFR and EGFRvIII antibody cocktail bound on the surface of the entire cell (Fig. 3.27), with an overall distribution but also in more concentrated inclusions, which was expected. For NR6wtEGFR the same is valid, but also some signal is seen from within the cells. Images of NR6 were taken as a negative control where no signal from the anti-human EGFR and EGFRvIII antibody cocktail was seen (Appendix C).

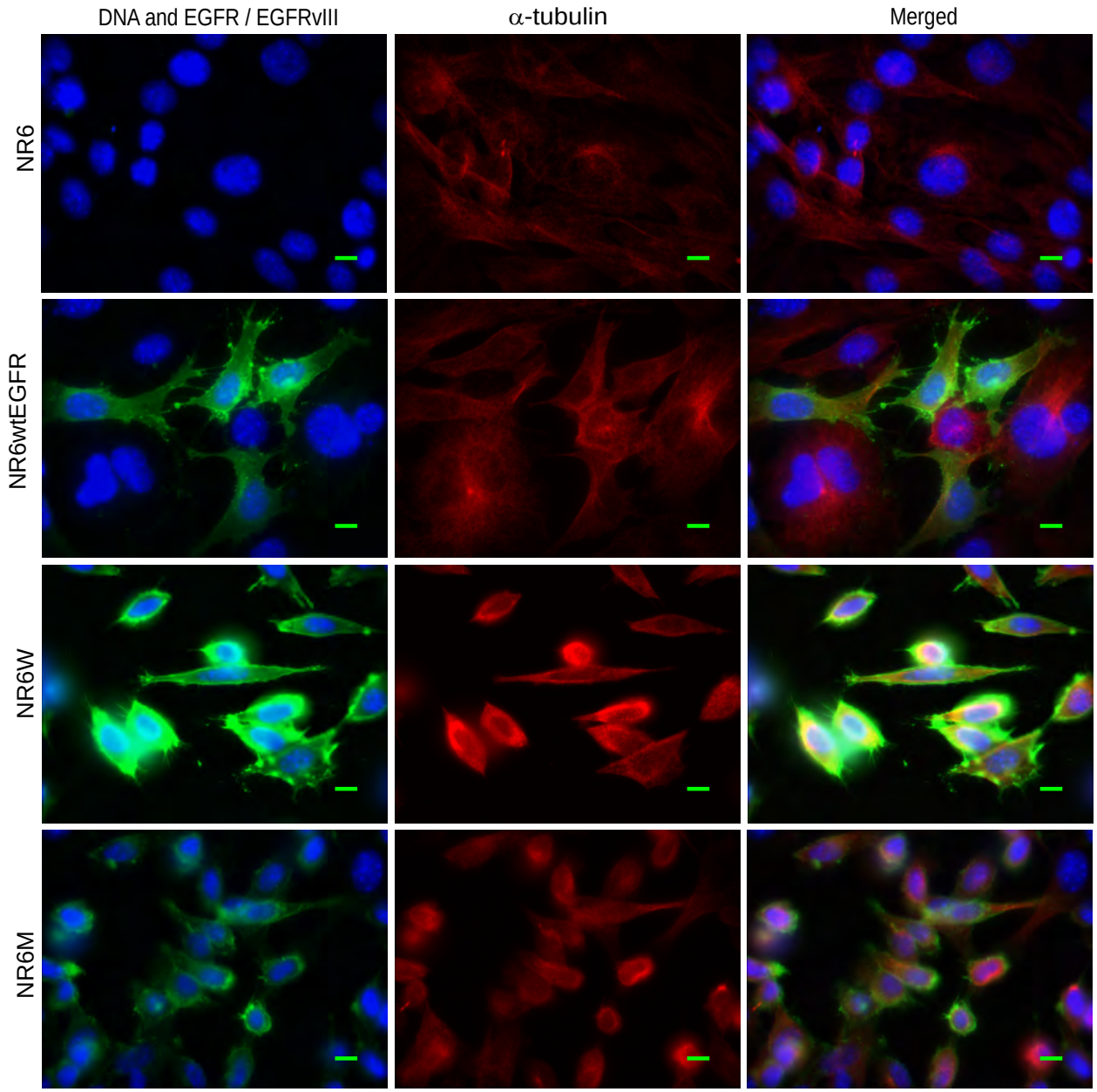


**Figure 3.25:** *Fluorescence microscopy images with 83x oil objective. Stained with anti-mouse α-tubulin antibody (red, 200 ms int.), anti-human EGFR and EGFRvIII antibody cocktail (green, 10 ms int.) and Hoechst 33342 (DNA) (blue, 5 ms int.). Bar is 10 µm. Image processed with ImageJ.*

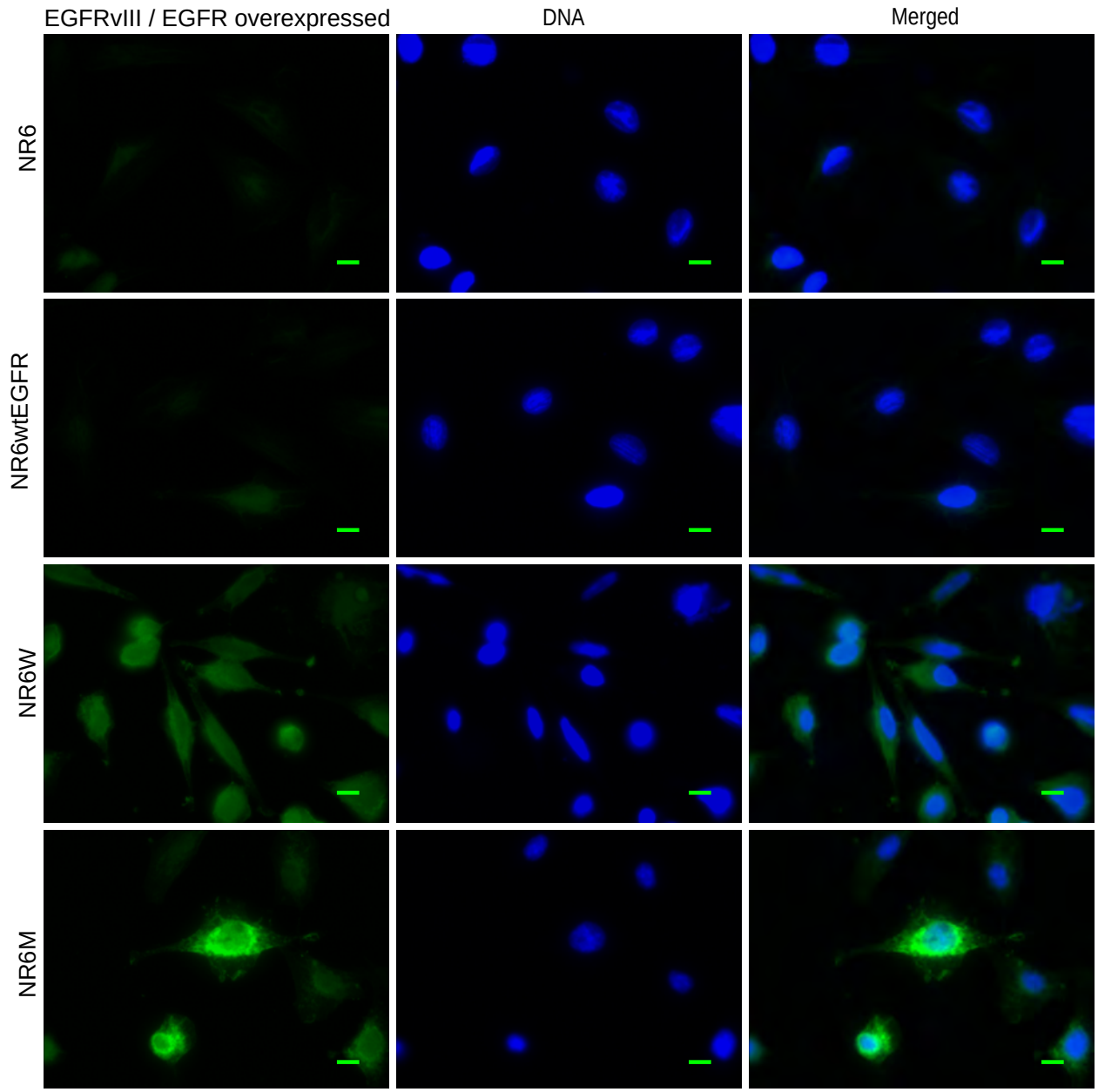


**Figure 3.26:** *Fluorescence microscopy images with 83x oil objective. Stained with Mab806 antibody (anti-human EGFRvIII / overexpressed EGFR) (green, 50 ms int.) and Hoechst 33342 (DNA) (blue, 5 ms int.). Bar is 10 µm. Image processed with ImageJ.*

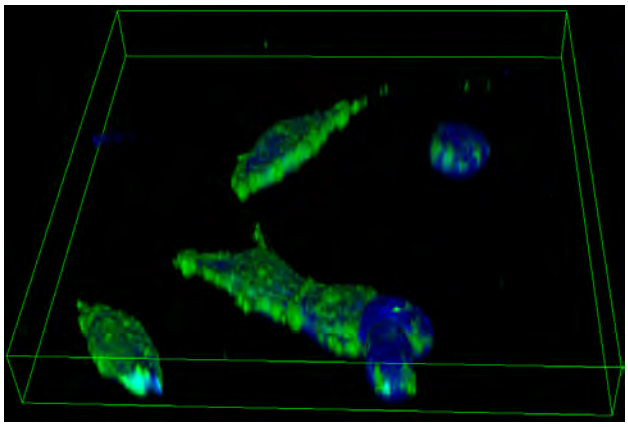

**(a)** *NR6wtEGFR, normal fibroblast cell expression of EGFR.*

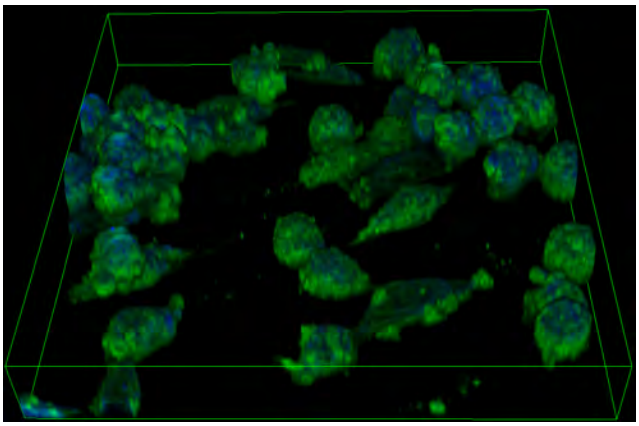

**(b)** *NR6W, overexpression of EGFR.*

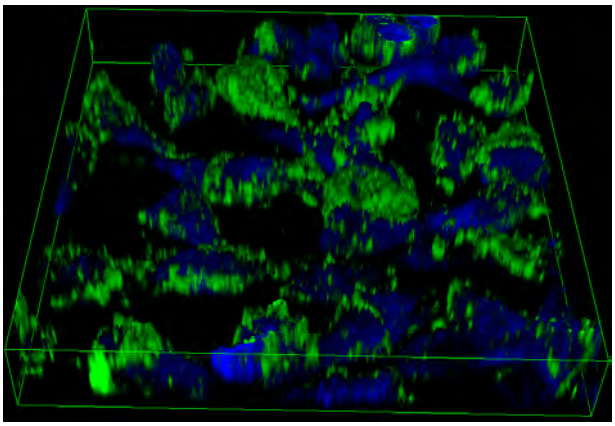

**(c)** *NR6M, expression of EGFRvIII.*

**Figure 3.27:** *3D images (146.25 µm x 146.25 µm, combined frames) from fluorescence CLSM of the cell lines, NR6wtEGFR, NR6W and NR6M. Staining of anti-mouse α-tubulin antibody (blue) and anti-human EGFR and EGFRvIII antibody cocktail (green). Image processed with ImageJ.*

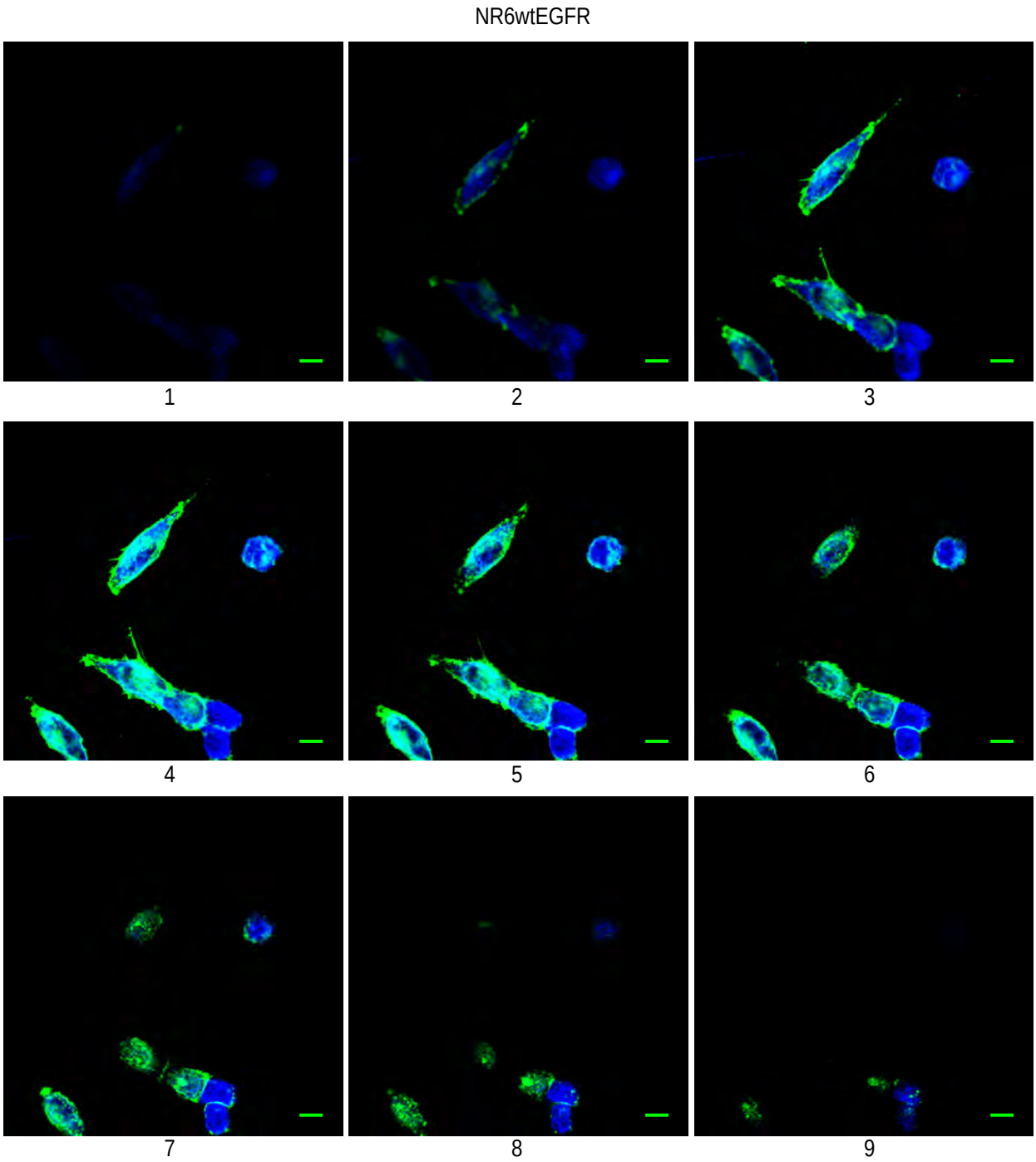


**Figure 3.28:** *Fluorescence CLSM frames of NR6wtEGFR cells, beginning from the microscope slide (1) and moving away in regular intervals as the numbers increase. Staining of anti-mouse α-tubulin antibody (blue) and anti-human EGFR and EGFRvIII antibody cocktail (green). Bar is 10 µm. Image processed with ImageJ.*

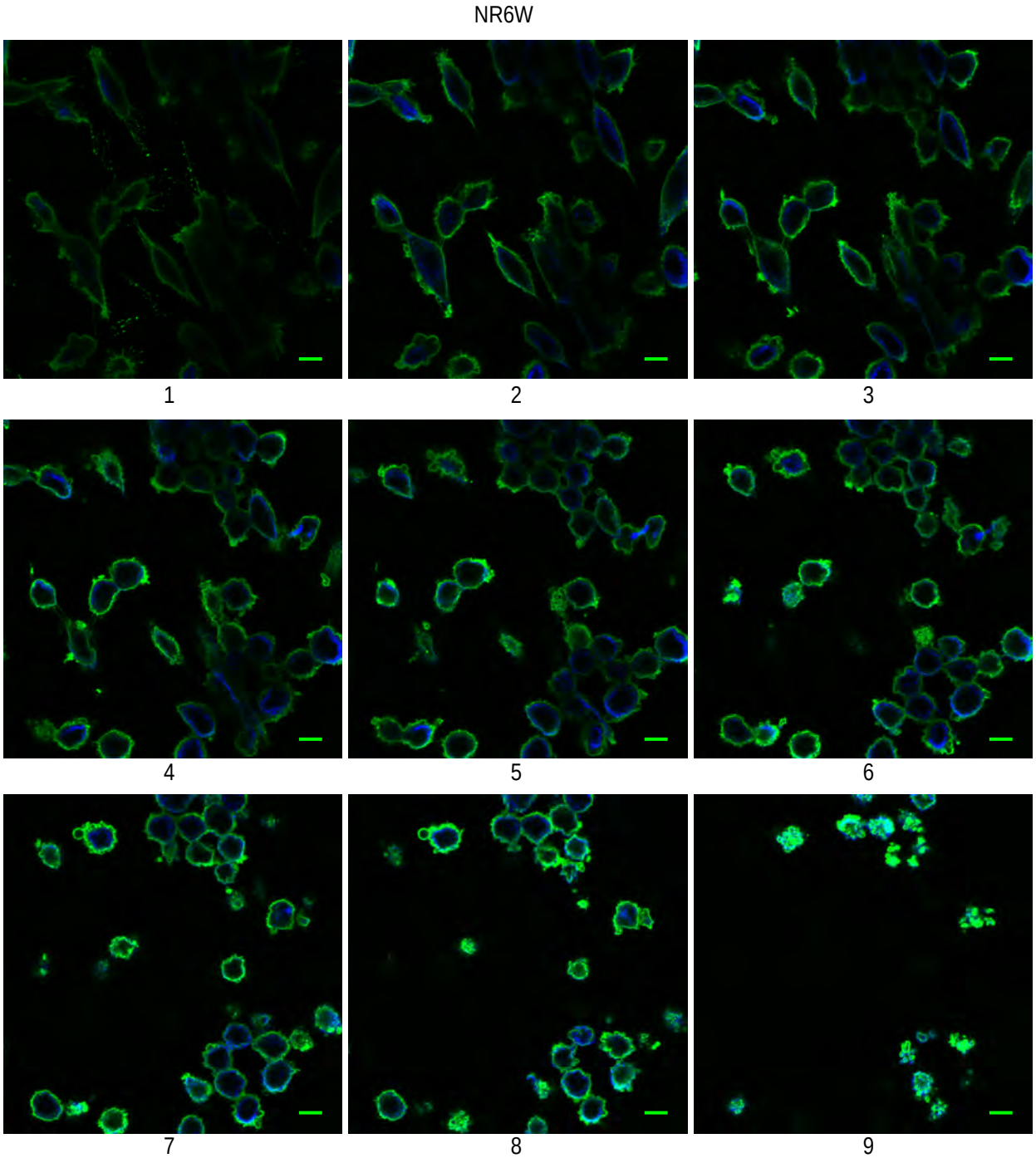


**Figure 3.29:** *Fluorescence CLSM frames of NR6W cells, beginning from the microscope slide (1) and moving away in regular intervals. Staining of anti-mouse α-tubulin antibody (blue) and anti-human EGFR and EGFRvIII antibody cocktail (green). Bar is 10 µm. Image processed with ImageJ.*

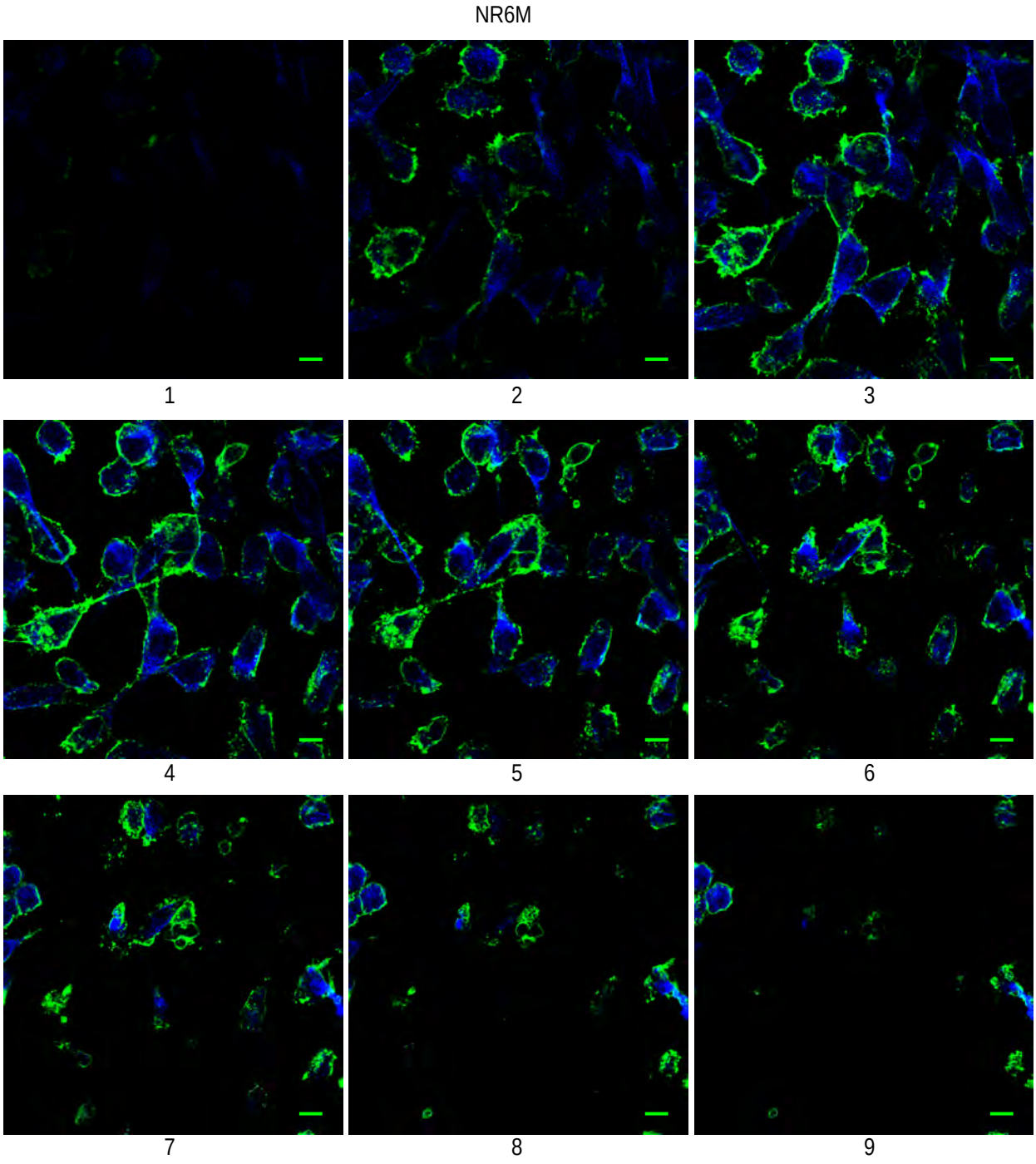


**Figure 3.30:** *Fluorescence CLSM frames of NR6M cells, beginning from the microscope slide (1) and moving away in regular intervals. Staining of anti-mouse α-tubulin antibody (blue) and anti-human EGFR and EGFRvIII antibody cocktail (green). Bar is 10 µm. Image processed with ImageJ.*

## 3.6 Targeting and Internalisation of cf_K_GE11 *in vitro*

### 3.6.1 Fluorescence Microscopy

The NR6 cells (Fig. 3.31) with no apparent EGFR expression had the lowest intensity from cf_K_GE11 of the four cell lines, where almost no fluorescent emission was detected. The NR6W cell line had a little higher intensity, and the highest intensity was seen from the NR6wtEGFR and NR6M cell lines. In all cases, the cf_K_GE11 emission appears be evenly distributed over the cells, but also concentrated in inclusions, and the intensity seems lower at the nucleus.

### 3.6.2 Fluorescence Confocal Laser Scanning Microscopy

The cells were analysed with fluorescence CLSM, to investigate if the signal originates from within the cells, but due to a low intensity and photo bleaching of cf_K_GE11, 3D images could not be successfully taken. However, a few low intensity images were obtained (Fig. 3.32), where inclusions of cf_K_GE11 is seen, mostly from the NR6wtEGFR and NR6M cells.

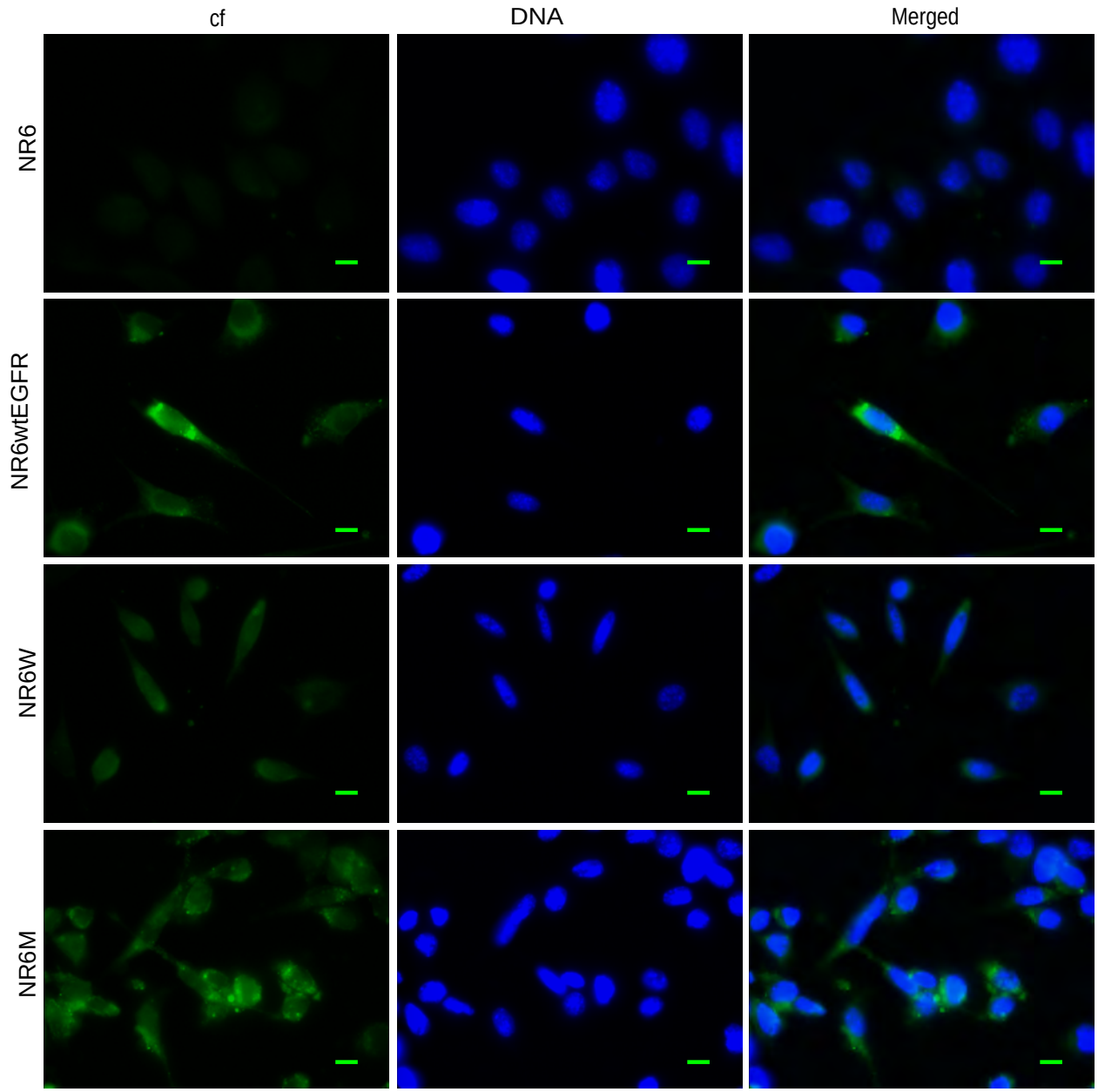


**Figure 3.31:** *Fluorescence microscopy images with 63x oil objective after overnight incubation in 5 µM cf_K_GE11 (green, 100 ms int.). Stained with Hoechst 33342 (DNA) (blue, 5 ms int.). Bar is 10 µm. Image processed with ImageJ.*

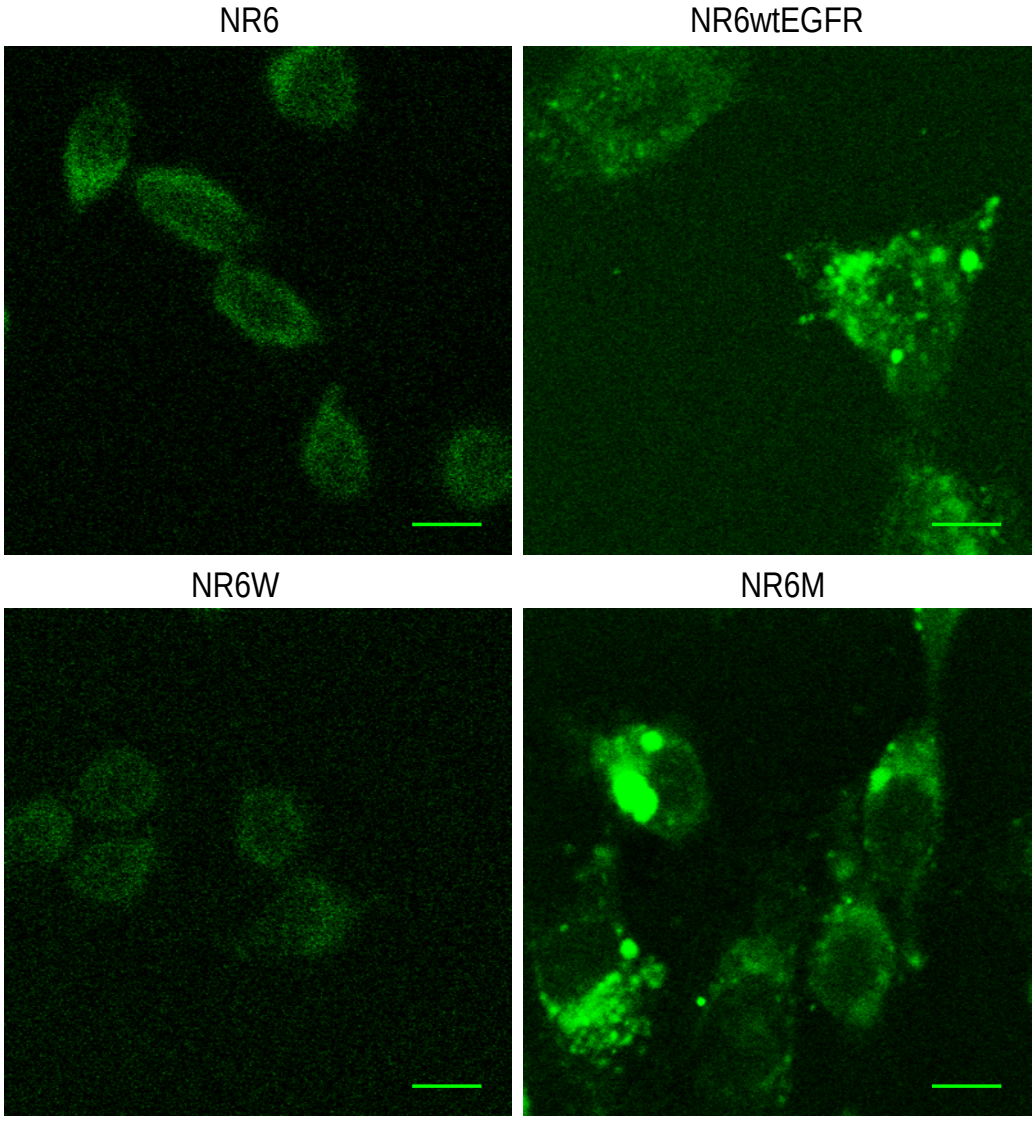


**Figure 3.32:** *Fluorescence CLSM images after overnight incubation in 5 µM cf_K_GE11. The intensity is not comparable between the images. Bar is 10 µm. Image processed with ImageJ.*

### 3.6.3 Flow Cytometry

Flow cytometry was used to evaluate the fluorescence intensity from a larger number of cells. After the samples were loaded, the intact cells (P1) were selected based on the forward scatter (FSC) which correlates with the size of the cells, and the side scatter (SSC) which correlates with the internal complexity of the cells. The measured average FITC fluorescence emission was calculated (Table 3.5). The cells (P1) were chosen so the cell emission distribution was close to a Gaussian distribution (Fig. 3.33 and Fig 3.34), to ensure that a homogeneous selection of cells was made.

To investigate if the difference in cf_K_GE11 uptake could be explained by competitive binding with natural hormones present in the FBS used in the medium, the experiment was repeated where the cells were incubated in 0.5% FBS medium 24 h prior to the overnight incubation with cf_K_GE11 which also was done in 0.5% FBS medium. A trypsin free approach using only EDTA for detaching the cells was also attempted. This was performed to investigate the effect of the treatment with trypsin, as it properly removed the majority of the surface displayed receptors. However, all experiments confirmed the initial result: The highest intensity was from the NR6wtEGFR cells, followed by the NR6- and NR6W cells with comparable intensities and finally the NR6M cells with the lowest.

| Cell line | P1 Events # | P1 Parent % | P2 Parent % | P2 FITC Mean |
|---|---|---|---|---|
| NR6 | 17,313 | 57.7 | 98.8 | 70,089 |
| NR6W | 7,598 | 25.3 | 98.2 | 70,678 |
| NR6wtEGFR | 21,443 | 71.5 | 95.4 | 104,958 |
| NR6M | 4,324 | 33.5 | 98.1 | 44,288 |
| NR6 neg. | 17,807 | 59.4 | 99.5 | 7,345 |
| NR6W neg. | 5,102 | 22.2 | 99.0 | 5,364 |
| NR6wtEGFR neg. | 19,539 | 65.1 | 99.0 | 8,712 |
| NR6M neg. | 3,150 | 24.7 | 96.9 | 4,937 |

**Table 3.5:** *Summary of the flow cytometry data of cf_K_GE11 labelled cells (Fig. 3.33), and unlabelled cells as a negative control (Fig. 3.34). P1 is the initially selected cell population of the parent, and P2 is the population from the P1 population, selected for the calculations of the mean signals.*

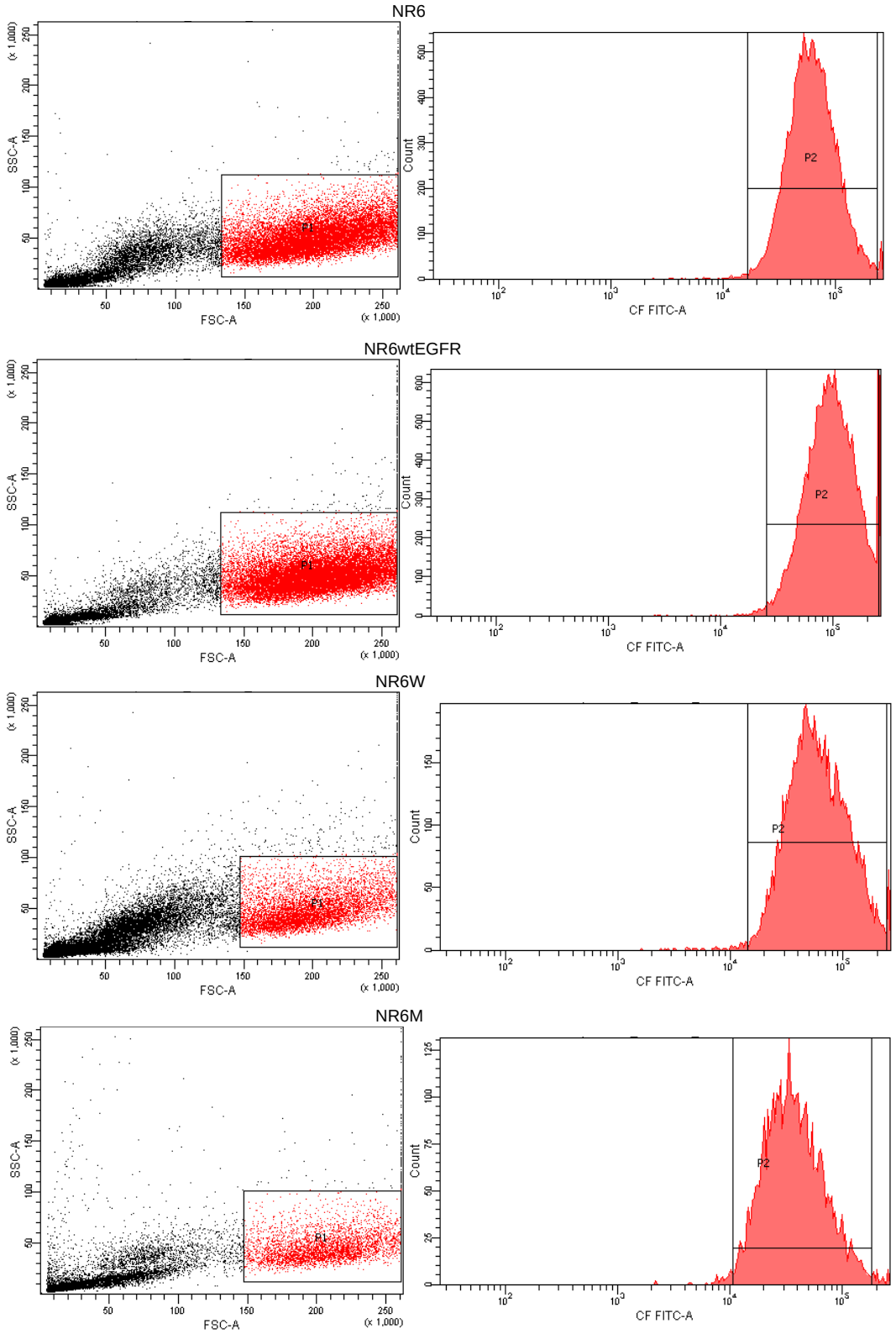


**Figure 3.33:** *Flow cytometry analysis of NR6, NR6wtEGFR, NR6W and NR6M cells after overnight incubation in medium with 5 µM cf_K_GE11. P1 defines the initially selected intact cells, and P2 the selected fluorescence emission used for the calculation of the average.*

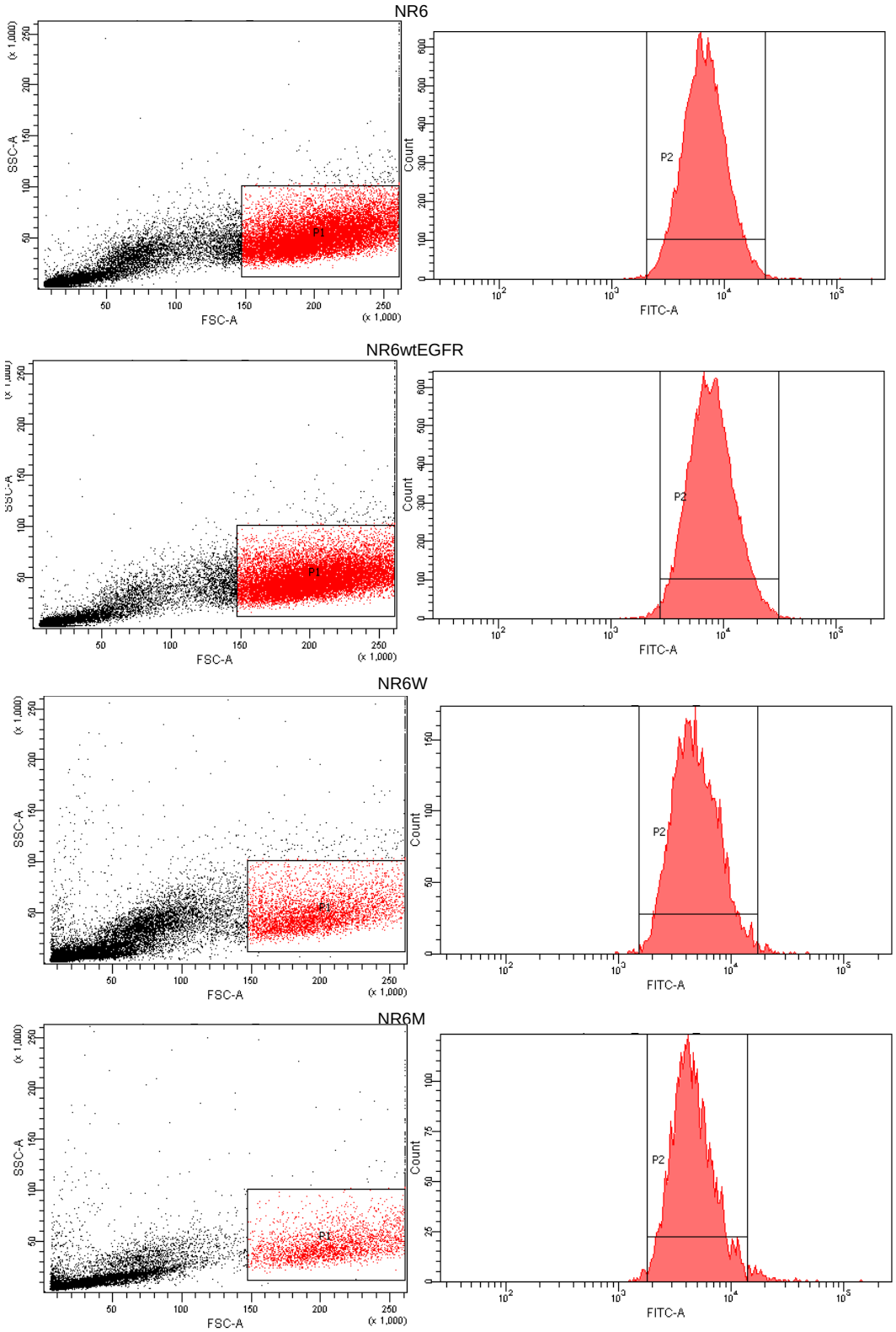


**Figure 3.34:** *Flow cytometry analysis of NR6, NR6wtEGFR, NR6W and NR6M cells to evaluate the autofluorescence. P1 defines the initially selected intact cells, and P2 the selected fluorescence emission used for the calculation of the average.*

# 4 Discussion

## 4.1 Synthesis and Purification of GE11 Derivatives

No apparent similarity was found between the AA sequences of EGF and GE11. However, the C-terminal Ile of GE11, could be comparable to the $Ile^{23}$ exposed on the surface of EGF which seems to bind to a hydrophobic pocket on the receptor [48]. Furthermore, GE11 has previously been modified at the N-terminus by [17] with a FITC label and retained affinity for EGFR. Therefore, the modifications to GE11 was in this project performed likewise at the amino N-terminus.

Labelling of GE11 was unsuccessfully attempted with ff. The work of [22, 53] have shown that binding to the free carboxyl-group of ff by peptides is unlikely. The reasons were found to be steric hindrance and an intramolecular bond which the carboxyl-group of ff forms to itself, predominantly below pH 3.5 or in organic solvents like DMF. This form of ff is termed the lactonic form, and is believed to be the reason for the unsuccessful labelling.

As the properties of ff matches the available equipment (in terms of fluorescence excitation, emission and intensity) and synthesis strategies, suitable fluorescein derivatives were identified. cf was chosen because of the compatibility with SPPS [53]. With cf, there are two possible sites of reaction: The 5(6) position, and like ff the 2 position. As the fluorophore mostly is in the lactonic state in organic solvents, the free carboxyl-group at position 2 (Fig. 1.2) is unreactive leaving only the 5(6) position reactive [22], which have been confirmed by the unsuccessful labelling of GE11 with ff. The labelling was successfully conducted using cf, verified by MS. However, unlabelled product was also detected on the RP-HPLC chromatogram, indicating that the protocol could be optimised. Attempts to purify the product by RP-HPLC were unsuccessful, and indications of peptide degradation were found, probably caused by the many freeze/unfreeze cycles and labelling attempts. A binding experiment was conducted on cells to investigate if the unspecific binding would be a problem or if the impurities could be washed away, but only unspecific binding was found and the cell lines could not be distinguished (data not shown). Therefore, another synthesis was performed with an optimised protocol based on the synthesis of cf_GE11.

Lysine was added to the N-terminus of GE11, which provided two amino groups for labelling, if solid phase labelling with cf or conjugation with the metal chelator DOTA proved difficult, and to make the peptide more hydrophilic. Furthermore, the cf labelling time was increased to 24 h and a final piperidine deprotection step was performed to remove excess cf molecules [22]. As the deprotection step was performed, the waste changed from clear to a red colour confirming the removal of non N-terminus bound cf. The correct weight of the cf labelled peptide was verified by MALDI-TOF MS. On an ESI MS/MS spectrum of the cf_K_GE11, overlapping fragmentation series were identified corresponding to cf_K_GE11, confirming the the correct sequence of cf_K_GE11, and N-terminus positioning of the cf label.

No unlabelled product was found using the improved protocol for peptide labelling, and no excess cf was detected in the final product by ESI MS. Therefore, the performed washing steps seems sufficient. The fluorescence spectroscopy investigation of cf_K_GE11 confirmed the fluorescence properties of the labelled peptide. The difference in fluorescence properties from cf_K_GE11 to free cf could originate from impurities in the sample or changed conformation of cf when attached to a peptide. However, the fluorescence from cf_K_GE11 matched the emission and excitation maxima given by the vendor. Therefore, the fluorescence properties of cf after conjugation to a peptide were as expected, and the fluorescence ability of cf_K_GE11 was verified.

In the calculations of the yield, absorption at 280 nm (mainly tryptophan) was used, thus peptides where the coupling of tryptophan had failed was not detected. However, absorption at 214 nm (mainly the peptide bond) correlated well with absorption at 280 nm, and the ESI MS spectrum of the crude cf_K_GE11 synthesis product revealed a seemingly high purity, so the deviation from the real yield is expected to be low.

The synthesis of DOTA_K_GE11 had a yield of only $\sim$11%, mainly due to the incomplete deprotection of the DOTA (t-Bu ester). Problems related to the unreliable deprotection of DOTA (t-Bu ester) and subsequent purification problems have been reported by [24, 61]. By using a longer TFA mediated deprotection time than 4 h, a higher yield could possibly be achieved and also heating during the synthesis. However, a too long deprotection time could result in peptide decomposition so perhaps another approach than TFA mediated cleavage should be utilised as proposed by [61]. The truncated peptides observed, such as the DOTA_K_GE11$_{-N}$ and DOTA_K_GE11$_{-N-K/Q}$ which was not observed in the cf_K_GE11 synthesis product, most likely originates from a machine malfunction which paused the program. These two issues made the RP-HPLC purification of DOTA_K_GE11 necessary, and the purification proved effective as a $\sim$96% pure product was achieved.

In summary, the improved synthesis protocol of cf_K_GE11, utilising double coupling at several positions and increasing the coupling time from 20 min to 60 min, increased the yield from $\sim$43% of GE11 (prior to fluorescent labelling) to $\sim$70% of cf_K_GE11 (post cf labelling), confirming the importance of long coupling times and double coupling of certain AAs in SPPS. Heating the RV during the synthesis, could possibly improve the yield further if needed. The fluorescence of cf_K_GE11 is comparable to that of cf, with only minor changes, verifying the preserved fluorescence properties of the fluorescently labelled peptide.

## 4.2 Metal Complex Formation with DOTA_K_GE11

If DOTA_K_GE11 is to be used in diagnostic PET/CT scans, it is vital that a complex with a metal such as $^{68}$Ga can be formed. Based on MALDI-TOF MS results, it was found that the Ga-DOTA_K_GE11 complex was formed at 40 °C, but first at 95 °C was DOTA_K_GE11 without a metal no longer detected. MALDI-TOF MS is not a quantitative method, but nonetheless, the result indicates the need for high temperature during complex formation with gallium, when the formation time is kept at 8 min. A low chelation time is essential in hospital protocols when working with metals such as $^{68}$Ga, with a relatively short half-life. The difference between the radioactive $^{68}$Ga and the used stable isotopes $^{69/71}$Ga is believed to be neglectable in the chelation. It is, therefore, assessed that the complex also can be formed with $^{68}$Ga. Inspired by [26], a 20% molar excess of $GaCl_3$ to DOTA_K_GE11 was chosen which seemed sufficient as the complex was formed for all detectable DOTA_K_GE11 at 95 °C.

The formation of the complex was also investigated using europium as metal, to see if Eu-DOTA_K_GE11 complex could be formed. The Eu-DOTA_K_GE11 complex would be fluorescent, enabling fluorescence studies of tissue samples. Another possibility is to study the formation of the metal-DOTA complex, as the fluorescence intensity is expected to increase as the complex is formed. In turn, this presents a way of optimising the labelling protocol by monitoring the fluorescence signal using different protocols. To allow for detection of the complex formation, water was used as buffer to ensure quenching of free europium would take place. Upon MALDI-TOF MS analysis, only the Eu-DOTA_K_GE11 complex was detected for all investigated temperatures and not DOTA_K_GE11 without a metal, indicating faster Eu complex formation under these conditions, compared with the Ga-DOTA_K_GE11 complex This observation is consistent with that made by [35], where it has been demonstrated that the formation of the Eu DOTA complex is faster at pH 5.5 than 2.5-3 (water pH 5.87, buffer pH 3.89). However, the buffer aids to the solubility of the gallium. Likewise, a 20% molar excess of $EuCl_3$ to DOTA_K_GE11 was chosen which seemed sufficient as the complex was formed, and DOTA_K_GE11 without a metal was not detected.

Besides the MS signal for the protonated Eu-DOTA_K_GE11, an isotopic distribution matching the expected was also found at m/z +4 and m/z +32. The m/z +4 and +32 isotope patterns is also seen for the protonated DOTA_K_GE11 in the acetic acid / sodium acetate buffer, but not in the DOTA_K_GE11 water reference. The observed masses fits to what is seen by [62] for the oxidation of tryptophan, which results in +4, +16 and +32 Da modifications to the peptide (Fig. 4.1). Upon investigation, a low intensity signal is also present at m/z +32 for the Ga-DOTA_K_GE11 samples. Due to problems with the matrix crystal formation, probably caused by the presence of salts, these samples were purified by an Empore C18 nanocolumn prior to analysis. This change in protocol from the other samples might explain why the oxidised tryptophan is not detected with as high counts in

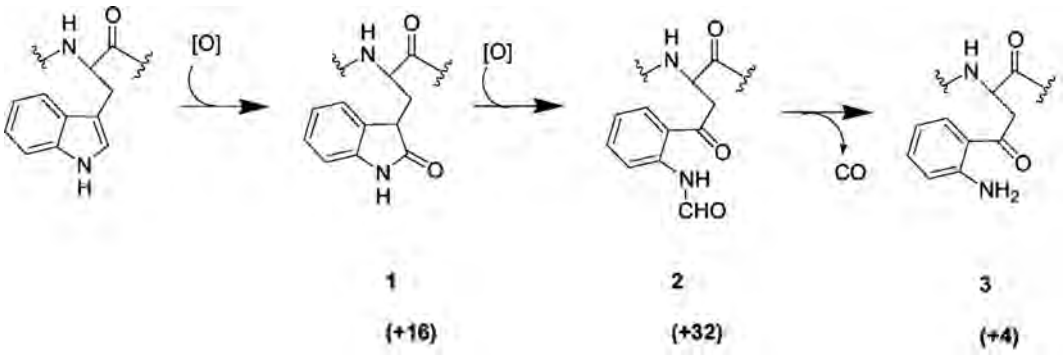


**Figure 4.1:** *Products of the oxidation of tryptophan in proteins and peptides, and the resulting increase in mass. [62]*

these samples.

As MALDI-TOF MS confirmed the formation of the Eu-DOTA_K_GE11 complex, fluorescence spectroscopy analysis was performed. However, fluorescence could not be detected from the Eu-DOTA_K_GE11 complex (data not shown), a possible explanation being the high degree of fluorescence from the DOTA_K_GE11 molecule. Indirect excitation was then attempted using tryptophan, which has an emission wavelength close to the excitation of europium. However, still no emission from europium was detected. The experiment could be redone using laser equipment with a more direct excitation of europium, or time gated fluorescence techniques as performed by [26].

In summary, DOTA_K_GE11 is capable of forming a complex with stable gallium, and thereby most likely able to be labelled with $^{68}$Ga and detected in PET/CT systems. Therefore, if the affinity of the peptide for EGFR and/or EGFRvIII can be verified, the transition to a radioactive drug seems highly feasible. DOTA_K_GE11 is also capable of forming complexes with europium, however, fluorescence spectroscopy investigations proved unsuccessful at verifying the europium fluorescence, most likely due to emission from DOTA_K_GE11.

## 4.3 Cultivation of Cells

The doubling time for the four cell lines was found to evaluate the state of the cells after several years at -135 °C, and in the used environment. Comparing measured doubling times for the cell lines ((Table 3.4)) with the doubling times published by [56] (NR6: 53.0 h, NR6W: 26.4 h, NR6M: 15.4 h), the numbers correlate well except for the NR6 cell line. The measured -20.1 h difference in doubling time most likely originates from different compositions of the growth medium, as all cell lines, except NR6M are seen to have a slightly faster doubling time. The DMEM/high medium used in this project had a high concentration of glucose, vitamins and AAs. However, no information regarding the medium used by the other group could be

found [56]. Another option is a cell line cross contamination. However, the shape of the cells differs between the cell lines and was analysed continuously in a light microscope throughout the entire growth period. Also, the experiment was conducted twice using different freezing stocks and as doublets, and in the case of a cell line contamination the doubling time of NR6 should be increasing throughout the experiment, which was not the case. The small effect of EGFR overexpression is also demonstrated as NR6W only has a slightly higher growth rate than NR6wtEGFR. Finally, the experiment demonstrates the preserved function of the human EGFR and EGFRvIII in the mouse cells.

## 4.4 Verification of EGFR and EGFRvIII Expression

For verification of the receptor expression, a western blot was performed. Applicability for the anti-human EGFR and EGFRvIII antibody cocktail for western blotting is unknown (information from vendor). However, the western blot only detected a protein band corresponding to the α-Tubulin and no protein band at 170 kDa or 145 kDa. The western blot was, therefore, successful but also showed that the anti-human EGFR and EGFRvIII antibody cocktail was not compatible with this technique, or that the receptor expression was not present, which would contradict what was indicated by the growth rate result. Therefore, an in-gel tryptic digest was attempted to verify the presence of protein by MS/MS. However, only a few peptides were found and not enough to yield a protein result, most likely caused by low protein concentration, as most were transferred during blotting. The cell lysate was subsequently separated by size, using a 7.5% SDS-PAGE gel, but no clear difference in the bands could be detected so the MS/MS protein identification was abandoned.

As no antibodies compatible with western blotting could be obtained, within the project period, the expression verification was done using antibodies and the binding analysed with fluorescence microscopy and fluorescence CLSM. The fluorescence microscopy images of the NR6 cell line, stained with anti-human EGFR and EGFRvIII antibody cocktail and Mab806 antibody (anti-EGFRvIII antibody, with a low affinity for EGFR overexpression also [40]) indicated that the NR6 cell line had the least expression of both receptors, as only a very low intensity was detected. In comparison, NR6wtEGFR had somewhat higher intensity from the anti-human EGFR and EGFRvIII antibody cocktail, but comparable to the NR6 cell line with the Mab806 antibody. This indicates that the NR6wtEGFR has some expression of EGFR. The NR6W cell line had the highest intensity from the anti-human EGFR and EGFRvIII antibody cocktail of the four cell lines, and also bound the Mab806 antibody, indicating that the NR6W overexpresses EGFR. The NR6M cell line had the highest intensity from the Mab806 and also bound the anti-human EGFR and EGFRvIII antibody cocktail but to a lower degree than the NR6W cells, indicating that the expression is of the EGFRvIII. For the NR6wtEGFR cell line with anti-

human EGFR and EGFRvIII antibody cocktail staining, and NR6M with Mab806 antibody staining it seems that the antibody binding and, thus, receptor expression is unevenly distributed between the cells. This could be due to cell line cross contaminations even though great care was taken to avoid this, or it can be a naturally occurring difference in expression pattern. The observed was consistent throughout the samples so if the change in expression level is caused by a cross contamination it would originate from an early stage of growth or a large contamination, as the increase in cell passage number was kept below 10 and $\sim$1 mio cells were transferred in each sub cultivation. The different expression between the cells was first observed using the anti-human EGFR and EGFRvIII antibody. To ensure that the issue was not a cell line contamination, new frozen stocks of all cell lines were started from the earliest achievable stock, but the pattern was found again using the Mab806 antibody. Thus, a cell line cross contamination would have to originate prior to this project, and also affect the growth rate experiment, where a clear difference between the cells was seen. Therefore, the most likely explanation seems to be that the cells have different expression profiles of the receptor.

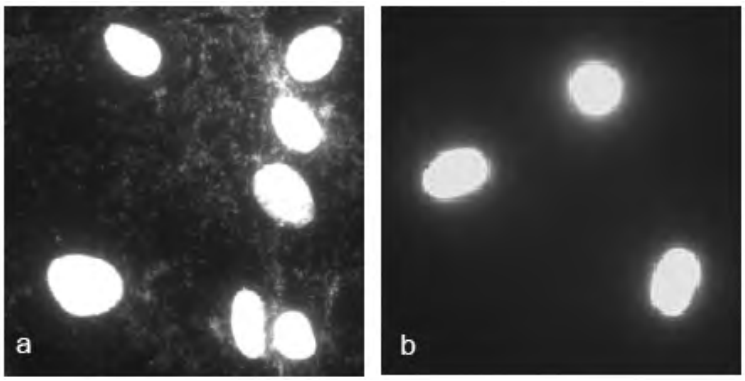


**Figure 4.2:** *Fluorescence image of fibroblast cell lines stained with Hoechst 33258 before (a) and after ciprofloxacin treatment of cultured skin fibroblasts (b). [63]*

Another plausible explanation is an infection of the cell lines, e.g. by mycoplasma (Fig. 4.2). The mycoplasmas are parasites, usually attached to the extracellular surface of the cells, but can also penetrate the membrane. It is the smallest self-replicating organism known to exist, and due to lack of rigid cell wall, they constitute a distinct class within the prokaryotes. Mycoplasma contaminations represents a frequent problem when studying cultured cells, where they are estimated to be in 5-35% of cultures. The contamination is difficult to detect, as the cells usually grow well and appear normal. In addition, mycoplasma infections are highly contagious and can rapidly spread through the cell stocks, the effect of which changes between inhibition of cell proliferation, induction of apoptosis and malignant transformation. The biological activity of mycoplasmas may also incorrectly be interpreted as originating from the host cells. [63]

The growth rate was comparable to what was measured by others, but the infection of mycoplasma does not always alter this. Therefore, an infection is also a plausible explanation for the observed difference in receptor expression. The cells were not mycoplasma tested in this project, but have been previously. However, as the cells were grown with other cell lines, it cannot be dismissed that an infection was present.

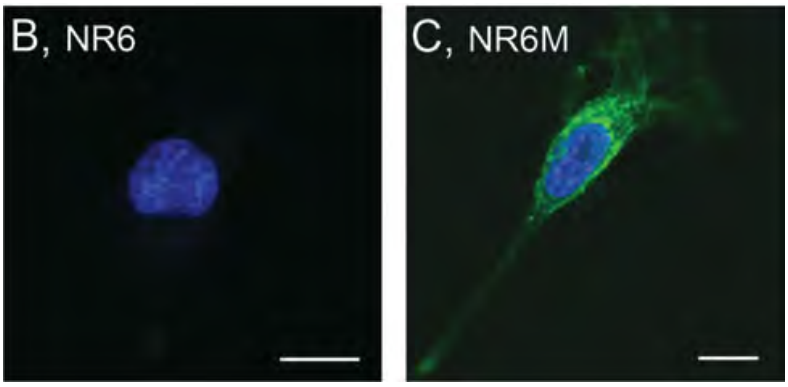


**Figure 4.3:** *Confocal images of (B) NR6 and (C) NR6M cells, incubated with the antibody fab-488 (green) against an extracellular epitope of EGFRvIII and To-Pro-3 for nuclei staining (blue) and cells. NR6M cells show staining with fab-488. Bar size 10 µm [41]*

The fluorescence CLSM revealed that the majority of the receptors are located on the surface of the cells, mainly in inclusions, distributed over the entire cells. This is in agreement with what [41] have found for NR6 and NR6M (Fig. 4.3), indicating the expected placement of the receptor. Some anti-human EGFR and EGFRvIII antibody cocktail staining is also detected within the cells, mainly for the NR6wtEGFR cell line, but it cannot be concluded if the signal originates from internalised EGFR or is caused by a membrane collapse due to the cell preparation.

In summary, the immunofluorescence experiment indicated that NR6 expressed neither EGFR nor EGFRvIII, and the NR6wtEGFR cell line expressed some EGFR. NR6W bound the anti-human EGFR and EGFRvIII antibody cocktail and the Mab806 antibody, but the intensity of the latter was the lowest of the two, indicating that the expression is that of EGFR overexpression. However, it cannot be dismissed that the cell line also is expressing EGFRvIII. For the NR6M cells, Mab806 bound the strongest and the anti-human EGFR and EGFRvIII antibody cocktail to some degree, indicating that the expression was that of EGFRvIII. However, it cannot be concluded if also EGFR was expressed.

The fluorescence CLSM images indicate that the receptor, for the most part, is located on the surface of the cells, with an overall distribution but also in inclusions, as expected. A difference in expression was detected between the cells, which could indicate a cell infection, likely mycoplasma, however as the cells were not tested during the project period, this remains a hypothesis.

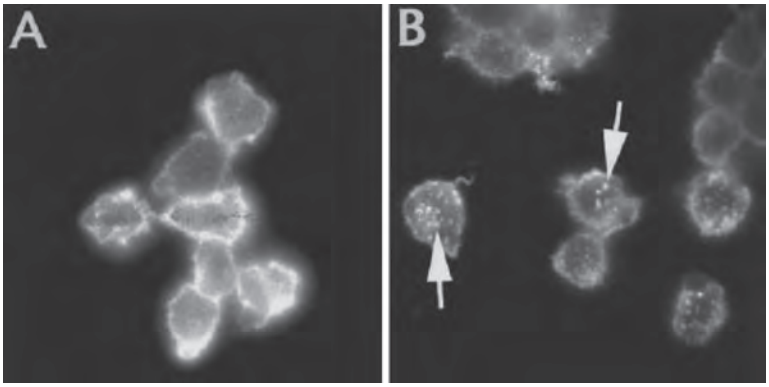


**Figure 4.4:** *Immunofluorescence microscopy detection of anti-EGFRvIII Mab internalisation. Cells incubated with anti-EGFRvIII antibody (A) Incubated with secondary antibody. (B) Incubated with secondary antibody after blocking of surface-associated primary antibody showing the internalised EGFRvIII. [64]*

As the amount of EGFR expression cannot be precisely verified, a western blot of equal concentrations of cell lysate should be conducted. By integrating the intensity of the protein bands, the amount of expressed protein could be assessed and the expression pattern of NR6wtEGFR and NR6W could be further verified. Finally, the expression of the four cell lines should be verified by tryptic digesting and ESI MS/MS to ensure the expression is solely that of EGFR or EGFRvIII, which also has not been verified. A high enough protein concentration could be assured by performing an immunoprecipitation of the cell lysate using an appropriate antibody.

## 4.5 Targeting and Internalisation of cf_K_GE11 *in vitro*

The internalisation of FITC-GE11 has been verified by others using confocal microscopy (Fig. 4.5), where internalisation and concentration into inclusions was seen [17]. EGFRvIII and EGFR are known to be internalised (Fig. 4.4), but EGFRvIII at a much lower rate than EGFR, and the internalised EGFRvIII was for the most part found in recycling compartments and not lysosomes [41]. cf_K_GE11 was therefore expected to be internalised and concentrated in inclusions (Fig. 4.5), possibly in lysosomes for EGFR [17] or recycling compartments for EGFRvIII but at a lower degree [41].

The fluorescence microscopy images of NR6 cells treated with cf_K_GE11 had the lowest intensity of the four cell lines. This indicates that unspecific binding was not an issue, and that the obtained purity of cf_K_GE11 and number of used washing steps were sufficient. However, the intensity from the NR6W cells seems less than that of NR6wtEGFR and NR6M cells. This contradicts that the staining and thus internalisation correlates with the degree of receptor expression. It has

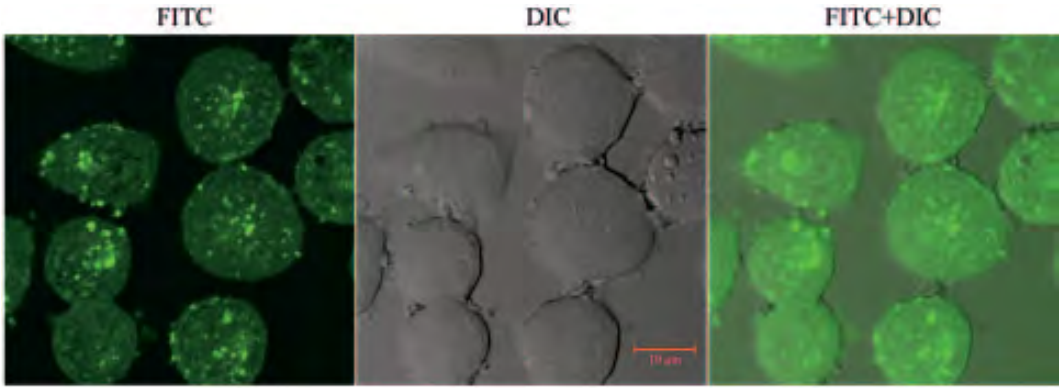


**Figure 4.5:** *FITC visualization and differential interference contrast (DIC) confocal microscope image of internalisation of 5 μM FITC-GE11 in SMMC-7721 cells after 16 h incubation. [17]*

been reported by [40] that the conformation of a small part of the EGFR is changed upon overexpression. Nonetheless, the staining of the NR6W cells is almost comparable to the observed for the NR6, which indicates that the cf_K_GE11 is not internalised by EGFR. The intensity from the NR6M cells seems comparable to the NR6wtEGFR cells, which is the highest of the four cell lines. Generally, the overall intensity is lower in the nucleus, indicating that cf_K_GE11 is indeed internalised and that the signal is not that of unspecific binding. However, from the fluorescence microscopy analysis it could not be concluded if cf_K_GE11 was taken up. Therefore, fluorescence CLSM was performed on the cell lines. to verify that the signal originated from within the cells. The fluorescence CLSM confirmed the fluorescence microscope images, and the detected inclusions were detected. However, due to photobleaching stacked images could not be obtained, and only a few images were obtained. Therefore, if the focal plane was within the cells is unknown.

To evaluate a larger number of cells, flow cytometry analysis of cells in solution was performed. When comparing the emission of the negative control (unstained cells) to the emission of the cells incubated in medium containing cf_K_GE11, the intensity of the latter is higher by a factor of at least eight for all cell lines (Table 3.5). The degree of autofluorescence from the cells is, therefore, concluded to be neglectable in comparison to the cf_K_GE11 signal. The cf_K_GE11 treated NR6 cells were expected to represent the background intensity, but the high intensity from these cells indicates a high degree of unspecific binding, even though the samples were washed a total of six times prior to measurements. Consistent with the fluorescence microscopy images, the intensity from the NR6 cells was comparable to that of the NR6W cells, and the cells with the highest intensity was the NR6wtEGFR, questioning if the cf_K_GE11 is internalised by EGFR. However, the high degree of staining of the NR6M cells detected with the fluorescence- microscopy and CLSM was not confirmed, but the cell line was found by flow cytometry to have the lowest intensity of the four cell lines.

It was demonstrated that the difference in intensity was not caused by competitive binding by hormones present in the FBS, nor the trypsin treatment for detaching the cells. The cells in the chamber slides used for fluorescence microscopy and fluorescence CLSM were washed 6 times with PBS and fixed by 4% formaldehyde, whereas the cells used for flow cytometry were detached, washed by centrifugation three times, and left overnight at 4 °C in a 1.35% formaldehyde fixing solution. Therefore, the preparation of the cells was different, as was the two techniques in method of detecting fluorescence intensity. The signal from within the cells might have a different effect on the end result, whether if the fluorescence microscopy and flow cytometry results are directly comparable is unknown. Another explanation is that the cells have different sizes, leading to differences in the intensity from unspecific binding as a large cell will have more space for unspecific bound peptide and thus give a stronger emission signal. This is indicated in the autofluorescence from the cells, which correlates well with the measured emission, for all cell lines except for NR6W which should be lower than measured. Differences in size was, however, not indicated by the FSC or observed during cell counting using a haemocytometer. The emission from an area containing cell fragments was investigated, where a much higher intensity was found. In flow cytometry the selection of the intact cells used to calculate the mean is therefore very important, and a potential source of error. A staining which has intracellular targets could therefore be performed, along with DNA staining to ensure that only intact cells were selected for the analysis. The effect of more washing steps could also be investigated along with incubation of cf_K_GE11 with different concentrations than the used 5 $\mu$M, which was found to work by [17]. Finally, a blocking experiment where unlabelled K_GE11 or EGF is added along with cf_K_GE11 could be conducted to investigate if the internalisation is by an EGF target.

In summary, based on fluorescence microscopy, fluorescence CLSM and flow cytometry it seems that the *in vitro* EGFR overexpression or EGFRvIII targeting ability of cf_K_GE11 is poor, and mostly unspecific binding was detected. The inconsistent results raise a question if the cells were subject to an infection of some kind, e.g. by mycoplasmas, but as the cells were not tested this remains unknown.

The affinity and internalisation of FITC-GE11 has been verified on SMMC-7721 cells by [17]. As GE11 has not been tested previously using the NR6 cell line some unknown factor may be present in the model system, but as the antibodies bound to the receptor seemingly without problems, this indicates that the issue is not the receptor but the peptide. The lack of affinity could therefore originate from the introduction of the lysine residue at the N-terminus of GE11. Lysine is a hydrophilic residue and is placed in a hydrophobic region. Therefore the introduction of the AA may have altered the affinity of the peptide toward the EGFR. To evaluate the effect of the added lysine residue to the N-terminus of GE11, the hydrophilicity was calculated using the Innovagen peptide property calculator [65] for GE11 (Fig. 4.4) and K_GE11 (Fig. 4.7), respectively. It was concluded that the charge of the GE11 peptide at neutral pH, where the experiment was conducted, is 0.1 for GE11 and

1.1 for K_GE11. As the FITC label (used for FITC-GE11) also is classified as being hydrophobic, the insertion of the lysine residue seems to have changed the hydrophilicity of the peptide somewhat. Therefore, it is a plausible explanation for the lack of affinity, and what was seen for the most part was unspecific binding.

To investigate, a new experiment could be conducted using GE11 labelled with cf, and test the peptide on the NR6 cell line. The cell lines could also be tested to evaluate if the results are effected of a mycoplasma infection. However, further experiments using cf_K_GE11 seems not to be necessary, as the affinity for EGFR or EGFRvIII most likely is low. New projects could, therefore, investigate GE11 or other peptides e.g. with affinity for the cancer-specific EGFRvIII receptor [49].

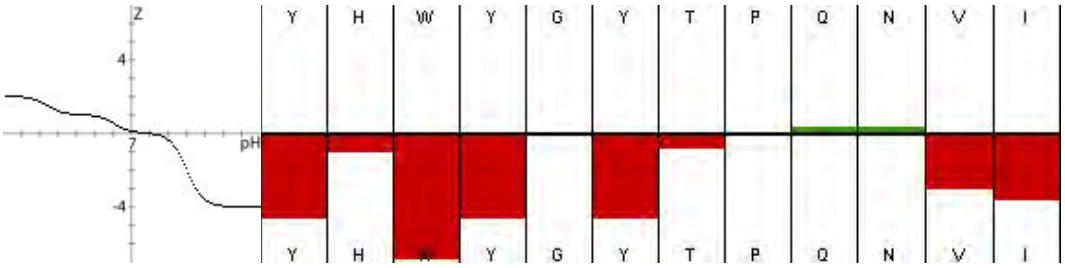


**Figure 4.6:** *Hydrophilicity overview of the AAs in GE11. Net charge at pH 7.0=0.1 and iso-electric point pI=7.6. Average hydrophilicity -1.2 and ratio hydrophilic residues / total number of residues 17%. [65]*

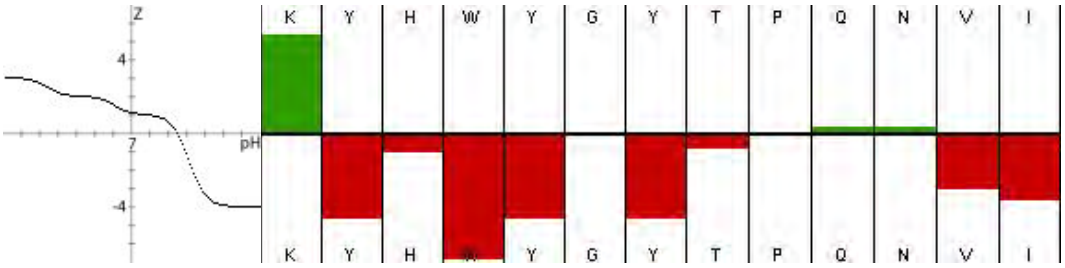


**Figure 4.7:** *Hydrophilicity overview of the AAs in K_GE11. Net charge at pH 7.0:1.1, and iso-electric point pI=9.4. Average hydrophilicity: -0.9. Ratio of hydrophilic residues / total number of residues: 23%. [65]*

# 5 Conclusion

The synthesis protocol was optimised and the peptides cf_K_GE11 and DOTA_K_-GE11 were synthesised to 70% and 96% purity, respectively. An efficient method of fluorescent peptide labelling was employed using cf, and the fluorescence properties were verified by fluorescence spectroscopy. Gallium and europium were successfully chelated in the purified DOTA_K_GE11 and verified by MS, demonstrating the potential of labelling the DOTA_K_GE11 peptide with a radionuclide.

The expression patterns of the NR6, NR6wtEGFR, NR6w and NR6M cell lines were partly verified using two different antibodies analysed with fluorescence microscopy and fluorescence CLSM. However, attempts to verify the expression by western blot and MS/MS verification of digested protein were unsuccessful, most likely due to incompatible antibodies and a low protein concentration.

Using fluorescence microscopy, fluorescence CLSM and flow cytometry, it was found that the *in vitro* EGFR overexpression and EGFRvIII targeting ability of cf_K_GE11 was poor. The most likely cause was found to be the addition of the hydrophilic AA Lys to the N-terminus. Therefore, the novel $^{68}$Ga-DOTA_K_GE11 was not tested using the mouse model, and the *in vivo* targeting ability remains unknown.

New projects could investigate GE11 or other peptides further with DOTA e.g. with affinity for the cancer-specific EFGRvIII receptor [49]. Also the potential of europium labelling and time gated fluorescence verification of receptor expression in tissue slides could be investigated to continue the development of probes in the diagnostics and therapy of cancer.

# Bibliography


[1] "Imaging service - stanford hospital & clinics." Webpage - http://stanfordhospital.org/clinicsmedServices/medicalServices/imaging /services_petct.html, June 2011. STANFORD Hospital & Clinics.

[2] D. Peer, J. M. Karp, S. Hong, O. C. Farokhzad, R. Margalit, and R. Langer, "Nanocarriers as an emerging platform for cancer therapy," *Nature Nanotechnology*, vol. 2, pp. 751–760, 2007.

[3] M. Gabriel, A. Oberauer, G. Dobrozemsky, C. Decristoforo, D. Putzer, D. Kendler, C. Uprimny, P. Kovacs, R. Bale, and I. J. Virgolini, "$^{68}$ga-dota-tyr$^{3}$-octreotide pet for assessing response to somatostatin-receptor-mediated radionuclide therapy," *The Journal of Nuclear Medicine*, vol. 50, pp. 1427–1434, September 2009.

[4] D. Wild, J. S. Schmitt, M. Ginj, H. R. Mäcke, B. F. Bernard, E. Krenning, M. de Jong, S. Wenger, and J. Reubi, "Dota-noc, a high-affinity ligand of somatostatin receptor subtypes 2, 3 and 5 for labelling with various radiometals," *European Journal of Nuclear Medicine and Molecular Imaging*, vol. 30, pp. 1338–1347, October 2003.

[5] H. R. Macke, M. Hofmann, and U. Haberkorn, "$^{68}$ga-labeled peptides in tumor imaging," *The Journal of Nuclear Medicine*, vol. 46, pp. 172S–178S, January 2005.

[6] V. Rufini, M. L. Calcagni, and R. P. Baum, "Imaging of neuroendocrine tumors," *Seminars in Nuclear Medicine*, vol. 36, pp. 228–247, July 2006.

[7] I. Velikyan, *Synthesis, Characterisation and Application of $^{68}$Ga-labelled Macromolecules*. PhD thesis, Uppsala University - Department of Chemistry, 2005. Webpage - http://urn.kb.se/resolve?urn=urn:nbn:se:uu:diva-5876.

[8] J. C. Reubi, H. R. Mäcke, and E. P. Krenning, "Candidates for peptide receptor radiotherapy today and in the future," *The Journal of Nuclear Medicine*, vol. 46, pp. 67S–75S, 2005.

[9] A. Rahmim and H. Zaidi, "Pet versus spect: strengths, limitations and challenges," *Nuclear Medicine Communications*, vol. 29, pp. 193–207, 2008.

[10] M. W. Pedersen, M. Meltorn, L. Damstrup, and H. Poulsen, "The type iii epidermal growth factor receptor mutation," *The Annals of Oncology*, vol. 12, pp. 745–760, 2001.

[11] R. I. Nicholson, J. M. W. Gee, and M. E. Harper, "Egfr and cancer prognosis," *European Journal of Cancer*, vol. 37, pp. S9–S15, 2001.

[12] B. R. Voldborg, L. Damstrup, M. Spang-Thomsen, and H. S. Poulsen, "Epidermal growth factor receptor (egfr) and egfr mutations, function and possible

role in clinical trials," *The Annals of Oncology*, vol. 8, no. 12, pp. 1197–1206, 1997.

[13] A. J. Fischman, J. W. Babich, and H. W. Strauss, "A ticket to ride: Peptide radiopharmaceuticals," *The Journal of Nuclear Medicine*, vol. 34, pp. 2253–2263, 1993.

[14] F. Alexis, J.-W. Rhee, J. P. Richie, A. F. Radovic-Moreno, R. Langer, and O. C. Farokhzad, "New frontiers in nanotechnology for cancer treatment," *Urologic Oncology*, vol. 26, pp. 74–85, 2008.

[15] H. Lodish, A. Berk, C. A. Kaiser, M. Krieger, M. P. Scorr, A. Bretscher, and H. Ploegh, *Molecular Cell Biology*, vol. f. Sara Tenney, 6th ed., 2004.

[16] J. M. Berg, J. L. Tymoczko, and L. Stryer, *Biochemistry*. W. H. Freeman and Company New York, 6th ed., 2007.

[17] Z. Li, R. Zahao, X. Wu, Y. Sun, M. Yao, J. Li, Y. Xu, and J. Gu, "Identification and characterization of a novel peptide ligand of epidermal growth factor receptor for targeted delivery of therapeutics," *The FASEB Journal*, vol. 19, pp. 1978–1985, December 2005.

[18] L. M. D. León-Rodríguez and Z. Kovacs, "The synthesis and chelation chemistry of dota-peptide conjugates," *Bioconjugate Chemistry*, vol. 19, pp. 391–402, February 2008.

[19] S. Song, D. Liu, J. Peng, Y. Sun, Z. Li, J. Gu, and Y. Xu, "Peptide ligand-mediated liposome distribution and targeting to egfr expressing tumor in vivo," *International Journal of Pharmaceutics*, vol. 363, pp. 155–161, 2008.

[20] S. Song, D. Liu, J. Peng, H. Deng, Y. Guo, L. X. Xu, A. D. Miller, and Y. Xu, "Novel peptide ligand directs liposomes toward egf-r high-expressing cancer cells in vitro and in vivo," *The FASEB Journal*, vol. 5, pp. 1396–1404, 2009.

[21] J. Fernández-Carneado and E. Giralt, "An efficient method for the solid-phase synthesis of fluorescently labelled peptides," *Tetrahedron Letters*, vol. 45, pp. 6079–6081, 2004.

[22] R. Fischer, O. Mader, G. Jung, and R. Brock, "Extending the applicability of carboxyfluorescein in solid-phase synthesis," *Bioconjugate Chemistry*, vol. 14, pp. 653–660, 2003.

[23] L. Song, E. J. Hennink, I. T. Young, and H. J. Tanke, "Photobleaching kinetics of fluorescein in quantitative fluorescence microscopy," *Biophysical Journal*, vol. 68, pp. 2588–2600, 1995.

[24] J. K. Sosabowski and S. J. Mather, "Conjugation of dota-like chelating agents to peptides and radiolabeling with trivalent metallic isotopes," *Nature Protocols*, vol. 1, pp. 972–976, 2006.

[25] L. L. Chappell, B. E. Rogers, M. B. Khazaeli, M. S. Mayo, D. J. Buchsbaum, and M. W. Brechbiel, "Improved synthesis of the bifunctional chelating agent 1,4,7,10-tetraaza-n-(1-carboxy-3-(4-nitrophenyl)propyl)-n',n'',n'''-tris(acetic acid)cyclododecane (pa-dota)," *Bioorganic & Medicinal Chemistry*, vol. 7, pp. 2313–2320, 1999.

[26] P. Táborský, I. Svobodová, Z. Hnatejko, , P. Lubal, S. Lis, M. Försterová, P. Hermann, I. Lukeš, and J. Havel, "Spectroscopic characterization of eu(iii) complexes with new monophosphorus acid derivatives of $h_4$dota," *Journal of Fluorescence*, vol. 15, pp. 507–512, 2005.

[27] N. Viola-Villegas and R. P. Doyle, "The coordination chemistry of 1,4,7,10-tetraazacyclododecane-n,n',n'',n'''-tetraacetic acid ($h_4$dota): Structural overview and analyses on structure-stability relationships," *Coordination Chemistry Reviews*, vol. 253, pp. 1906–1925, 2009.

[28] S. Liu, "Bifunctional coupling agents for radiolabeling of biomolecules and target-specific delivery of metallic radionuclides," *Advanced Drug Delivery Reviews*, vol. 60, pp. 1347–1370, September 208.

[29] K. P. Zhernosekov, D. V. Filosofov, R. P. Baum, P. Aschoff, H. Bihl, A. A. Razbash, M. Jahn, M. Jennewein, and F. Rösch, "Processing of generator-produced $^{68}$ga for medical applications," *The Journal of Nuclear Medicine*, vol. 48, pp. 1741–1748, October 2007.

[30] L. G. Luyt and J. A. Katzenellenbogen, "A trithiolate tripodal bifunctional ligand for the radiolabeling of peptides with gallium(iii)," *Bioconjugate Chemistry*, vol. 13, pp. 1140–1145, August 2002.

[31] W. A. P. Breeman and A. M. Verbruggen, "The 68ge/68ga generator has high potential, but when can we use 68ga-labelled tracers in clinical routine?," *European Journal of Nuclear Medicine and Molecular Imaging*, vol. 34, pp. 978–981, 2007.

[32] R. P. Baum, V. Prasad, M. Hommann, and D. Hörsch, "Receptor pet/ct imaging of neuroendocrine tumors," *Recent Results in Cancer Research*, vol. 170, pp. 225–242, 2008.

[33] S. Ekambaram, "Effect of host-structure on the charge of europium ion," *Journal of Alloys and Compounds*, vol. 390, pp. L1–L3, 2005.

[34] C. R. D. Silva, J. Vagner, R. J. G. R. Lynch and, and V. J. Hruby, "Optimization of time-resolved fluorescence assay for detection of eu-dota-labeled ligand-receptor interactions," *Analytical Chemistry*, vol. 398, pp. 15–23, March 2010.

[35] P. Táborský, I. Svobodová, P. Lubal, Z. Hnatejko, S. Lis, and P. Hermann, "Formation and dissociation kinetics of eu(iii) complexes with $h_5$do3ap and similar dota-like ligands," *Polyhedron*, vol. 26, pp. 4119–4130, 2007.

[36] S. Ahmed, A. S. Mathews, N. Byeon, A. Lavasanifar, and K. Kaur, "Peptide arrays for screening cancer specific peptides," *Analytical Chemistry*, vol. 82, pp. 7533–7541, 2010.

[37] J. F. Eary, "Pet imaging for planning cancer therapy," *The Journal of Nuclear Medicine*, vol. 42, pp. 770–771, May 2001.

[38] J. Boonstra, P. Rijken, B. Humbel, F. Cremers, A. Verkleij, and P. van Bergen en Henegouwen, "The epidermal growth factor," *Cell Biology International*, vol. 19, no. 5, pp. 413–430, 1995.

[39] M. W. Pedersen, V. Tkach, N. Pedersen, V. Berezin, and H. S. Poulsen, "Expression of a naturally occurring constitutively active variant of the epidermal growth factor receptor in mouse fibroblasts increases motility," *International Journal of Cancer*, vol. 108, pp. 643–653, February 2004.

[40] T. G. Johns, E. Stockert, G. Ritter, A. A. Jungbluth, H.-J. S. Huang, W. K. Cavenee, F. E. Smyth, C. M. Hall, N. Watson, E. C. Nice, W. J. Gullick, L. J. Old, A. W. Burgess, and A. M. Scott, "Novel monoclonal antibody specific for the de2-7 epidermal growth factor receptor (egfr) that also recognizes the egfr expressed in cells containing amplification of the egfr gene," *International Journal of Cancer*, vol. 98, pp. 398–408, 2002.

[41] M. V. Grandal, R. Zandi, M. W. Pedersen, B. M. Willumsen, B. van Deurs, and H. S. Poulsen, "Egfrviii escapes down-regulation due to impaired internalization and sorting to lysosomes," *Carcinogenesis*, vol. 28, pp. 1408–1417, 2007.

[42] J. L. Reiter, D. W. Threadgill, G. D. Eley, K. E. Strunk, A. J. Danielsen, C. S. Sinclair, R. S. Pearsall, P. J. Green, D. Yee, A. L. Lampland, S. Balasubramaniam, T. D. Crossley, T. R. Magnuson, C. D. James, and N. J. Maihle, "Comparative genomic sequence analysis and isolation of human and mouse alternative egfr transcripts encoding truncated receptor isoforms," *Genomics*, vol. 71, pp. 1–20, January 2001.

[43] D. Goodsell, "Rcsb protein data bank." Webpage - www.rcsb.org/pdb/static.do?p=education_discussion/molecule_of_the_month/pdb126_1.html, June 2010.

[44] M. W. Pedersen and H. S. Poulsen, "Mutationer i epidermal vækstfaktor- receptoren: struktur og tumorbiologisk relevans," *Ugeskrift for læger*, vol. 168, pp. 2354–2361, Juni 2006.

[45] A. Citri and Y. Yarden, "Egf-erbb signalling: towards the systems level," *Nature Reviews Molecular Cell Biology*, vol. 7, pp. 505–516, July 2006.

[46] "Uniprot." Webpage - www.uniprot.org, 2011.

[47] D. A. Engler, G. T. Montelione, and S. K. Niyogi, "Human epidermal growth factor: Distinct roles of tyrosine 37 and arginine 41 in receptor binding as determined by site-directed mutagenesis and nuclear magnetic resonance spectroscopy," *FEBS Letters*, vol. 271, pp. 47–50, October 1990.

[48] H. Koide, Y. Muto, H. Kasai, K. Kohri, K. Hoshi, S. Takahashi, K. Tsukumo, T. Sasaki, T. Oka, T. Miyake, T. Fuwa, D. Kohda, F. Inagaki, T. Miyazawa, and S. Yokoyama, "A site-directed mutagenesis study on the role of isoleucine-23 of human epidermal growth factor in the receptor binding," *Biochimica et Biophysica Acta*, vol. 1120, pp. 257–261, 1992.

[49] C. L. Denholt, P. R. Hansen, N. Pedersen, H. S. Poulsen, N. Gillings, and A. Kjær, "Identification of novel peptide ligands for the cancer-specific receptor mutation efgrviii using a mixture-based synthetic combinatorial library," *Biopolymers*, vol. 91, no. 3, pp. 201–206, 2009.

[50] Novabiochem, *Reagents for labeling & ligation*, 2010/2011. EMD, Peptide Synthesis.

[51] A. Aitken and M. Learmonth, *The Protein Protocols Handbook*. Humana Press, 1996. 1. Protein Determination by UV Absorption.

[52] T. E. Creighton, *Proteins: Structures and Molecular Properties*. W. H. Freeman and Company, 2nd ed., 1993.

[53] P. J. A. Weber, J. E. Bader, G. Folkers, and A. G. Beck-Sickinger, "A fast and inexpensive method for n-terminal fluorescein-labeling of peptides," *Bioorganic & Medicinal Chemistry Letters*, vol. 8, pp. 597–600, 1998.

[54] M. M. Martin and L. Lindqvist, "The ph dependence of fluorescein fluorescence," *Journal of Luminescence*, vol. 10, pp. 381–390, 1975.

[55] A. Wells, J. B. Welsh, C. S. Lazar, H. S. Wiley, G. N. Gill, and M. G. Rosenfeld, "Ligand-induced transformation by a noninternalizing epidermal growth factor receptor," *Science*, vol. 247, pp. 962–964, February 1990.

[56] S. K. Batra, S. Castelino-Prabhu, C. J. Wikstrand, X. Zhu, P. A. Humphrey, H. S. Friedman, and D. D. Bigner, "Epidermal growth factor ligand-independent, unregulated, cell-transforming potential of a naturally occurring

human mutant egfrviii gene," *Cell Growth & Differentiation*, vol. 6, pp. 1251–1259, 1995.

[57] M. Strohalm, D. Kavan, P. Novak, M. Volny, and V. Havlicek, "mmass 3: A cross-platform software environment for precise analysis of mass spectrometric data.," *Analytical Chemistry*, vol. 82, no. 11, pp. 4648–4651, 2010.

[58] M. Strohalm, M. Hassman, B. Kosata, and M. Kodicek, "mmass data miner: an open source alternative for mass spectrometric data analysis.," *Rapid Communications in Mass Spectrometry*, vol. 22, no. 6, pp. 905–908, 2008.

[59] "Gpmaw home." Webpage - http://www.gpmaw.com/, April 2011. Lighthouse data.

[60] R. P and F. J, "Proposal for a common nomenclature for sequence ions in mass spectra of peptides," *Biomedical Mass Spectrometry*, vol. 11, no. 11, p. 601, 1984.

[61] B. Wängler, C. Beck, U. Wagner-Utermann, E. Schirrmacher, C. Bauer, F. Rösch, R. Schirrmacher, and M. Eisenhut, "Application of tris-allyl-dota in the preparation of dota-peptide conjugates," *Tetrahedron Letters*, vol. 47, pp. 5985–5988, 2006.

[62] S. W. Taylor, E. Fahy, J. Murray, R. A. Capaldi, and S. S. Ghosh, "Oxidative post-translational modification of tryptophan residues in cardiac mitochondrial proteins," *The journal of Biological Chemistry*, vol. 278, pp. 19587–19590, May 2003.

[63] N. Darin, N. Kadhom, J. Briére, D. Chretien, C. M. Bébéar, A. Rötig, A. Munnich, and P. Rustin, "Mitochondrial activities in human cultured skin fibroblasts contaminated by mycoplasma hyorhinis," *BioMedCentral Biochemistry*, vol. 4, p. 15, November 2003.

[64] C. Wikstrand, C. Reist, G. Archer, M. Zalutsky, and D. Bigner, "The class iii variant of the epidermal growth factor receptor (egfrviii): characterization and utilization as an immunotherapeutic target," *Journal of NeuroVirology*, vol. 4, pp. 148–158, 1998.

[65] Innovagen, "Peptide property calculator." Webpage - http://www.innovagen.se/custom-peptide-synthesis/peptide-property-calculator/peptide-property-calculator.asp, May 2011.

# Appendices

# Materials

# A

All chemicals were of analytical grade and used without further purification.

| Product Name | Manufacturer |
|---|---|
| Anti-mouse α-tubulin rabbit antibody | Abcam, UK |
| Anti-mouse α-tubulin mouse antibody | Abcam, UK |
| Anti-human EGFR and EGFRvIII mouse antibody cocktail | Abcam, UK |
| Alexa fluor 488 goat anti-mouse antibody | Invitrogen, USA |
| Alexa fluor 647 goat anti-rabbit antibody | Invitrogen, USA |
| Dakocytomation | Dako, DK |
| DCM | Sigma-Aldrich, USA |
| DHB | Sigma Aldrich, USA |
| Diethyl ether | Sigma-Aldrich, USA |
| DIPEA | Advanced Chemtech, USA |
| DMEM/high | Invitrogen, USA |
| DMF | Applied Biosystems, Sweden |
| DMSO | Fisher Scientific, USA |
| EDT | Fisher Scientific, USA |
| EDTA | Invitrogen, USA |
| FBS | Invitrogen, USA |
| Fluorescein free acid | Fluka |
| Fmoc-glutamine-OH | Advanced Chemtech, USA |
| Fmoc-glycine-OH | Advanced Chemtech, USA |
| Fmoc-histidine-OH | Advanced Chemtech, USA |
| Fmoc-isoleucine-Wang Resin | Advanced Chemtech, USA |
| Fmoc-lysine-OH | Advanced Chemtech, USA |
| Fmoc-proline-OH | Advanced Chemtech, USA |
| Fmoc-tyrosine-OH | Advanced Chemtech, USA |
| Fmoc-tryptophan-OH | Advanced Chemtech, USA |
| Fmoc-threonine-OH | Advanced Chemtech, USA |
| Fmoc-valine-OH | Advanced Chemtech, USA |
| GE11 and related peptides | This work |
| Gentamicin | Invitrogen, USA |
| HBTU | Iris Biotech GmbH, Germany |
| HOBt | Advance ChemTech USA |
| Hoechst 33343 | Invitrogen, USA |
| Mab806 mouse antibody | Local stock |
| PBS | Invitrogen, USA |
| Penicillin/Streptomycin | Invitrogen, USA |
| Piperidine | Advanced Chemtech, USA |
| Protease inhibitor cocktail tablet | Roche, USA |
| SM0671, PageRuler prestained protein ladder | Fermentas, DE |
| SM1859, PageRuler prestained protein ladder | Fermentas, DE |
| TFA | Iris Biotech GmbH, DE |
| TIS | Sigma-Aldrich, USA |
| Trypan-blue | Invitrogen, USA |
| Trypsin | Invitrogen, USA |

**Table A.1:** *List of main antibodies, AAs, peptides and chemicals used in this work.*

| Device Name | Description | Manufacturer |
|---|---|---|
| Activo-P11 | Solid phase peptide synthesiser | ActivoTec, UK |
| Activotec | RV shaker | ActivoTec, UK |
| ALPHA 2-4 LD plus | Freeze dryer | Christ, DE |
| Axiovert 200M inverted microscope | Inverted fluorescence microscope | Zeiss, DE |
| Empore high performance extraction disk | C18 column material | Sigma-Aldrich, USA |
| FACSCanto | Flow cytometry device | BD, USA |
| Fluorescence Spectrophotometer | Fluorescence spectrophotometer | Photon Technology International, USA |
| Hybrid QTOF | Mass spectrometer | Bruker-Daltonics, DE |
| LSM510 meta | Confocal laser scanning microscope | Zeiss, DE |
| Manual Injection Valve | Injection for HPLC system | IDEX Health & Science, USA |
| Nanodrop Spectrophotometer ND-1000 | Spectrophotometer | Nanodrop, USA |
| pH meter 3510 | PH Meter | Jenway, UK |
| Reflex IV reflector TOF-MS | Reflector TOF-MS | Bruker-Daltonics, DE |
| Typhoon 8600 Variable Mode Imager | Typhoon scanner | Molecular Dynamics, SV |
| UltiMate 3000 Rapid Separation LC system | HPLC system | Dionex, USA |
| UltiMate nano-HPLC system | LC system for LC-ESI MS/MS | LC Packings, NL |

**Table A.2:** *List of main devices used in this project.*

# Synthesis of cf_GE11

# B

A theoretical yield of 0.20 mmol GE11 was synthesised using standard protocols on the Activo-P11 (*ActivoTec*) and solid phase labelling with ff. RP-HPLC was conducted on a saturated solution of ff GE11 labelling product, dissolved in 0.1% TFA in $H_2O$ at pH 1.87 (Fig. B.1).

Significant absorption at 280 nm was detected at retention time 26.5-29 min, where one peak with a shoulder was collected (Fig. B.1). The collected eluent was analysed by MALDI-TOF MS (Fig. B.2). For ff labelled GE11 [GE11 + ff - $H_2O$ + H / Na]$^+$ = m/z 1854.78 / 1876.76 is expected (Table B.1) so the RP-HPLC fraction appears to contain GE11 and GE11$_{-T_7}$ (GE11 lacking AA number 7, Thr), thus the synthesis of GE11 was successful, but the labelling with ff have been unsuccessful.

| GE11 Derivative | Ionisation | m/z$_{calc}$ | m/z$_{measured}$ | Difference m/z |
|---|---|---|---|---|
| ff_GE11 | $Na^+$ | 1876.76 | | |
| ff_GE11 | $H^+$ | 1854.78 | | |
| cf_GE11 | $H^+$ | 1898.77 | 1898.9 | 0.1 |
| cf_GE11$_{-T_7}$ | $H^+$ | 1797.73 | 1797.7 | 0 |
| GE11 | $H^+$ | 1540.72 | 1541.1 | 0.4 |
| GE11 | $Na^+$ | 1562.70 | 1563.2 | 0.5 |
| GE11$_{-T_7}$ | $H^+$ | 1440.68 | 1441.0 | 0.3 |
| GE11$_{-T_7}$ | $Na^+$ | 1461.66 | 1462.0 | 0.3 |

**Table B.1:** *Calculated and measured m/z for the MALDI-TOF MS analysis of GE11. m/z were calculated using Gpmaw [59].*

Therefore, a liquid phase labelling of GE11 with ff was attempted on the same

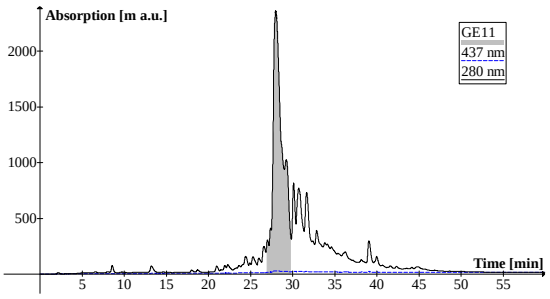


**Figure B.1:** *RP-HPLC chromatogram of the GE11 synthesis product after solid phase labelling with ff, using an analytical program with 100% ACN as gradient and 0.1% TFA in $H_2O$ as solvent. Eluent absorption at 280 nm and 437 nm was recorded to detect the precence of trypthophan and fluorescein respectively. The marked peak with retentiontime 26.5-29 min (∼43%) was analysed by MALDI-TOF. A baseline has been substracted.*

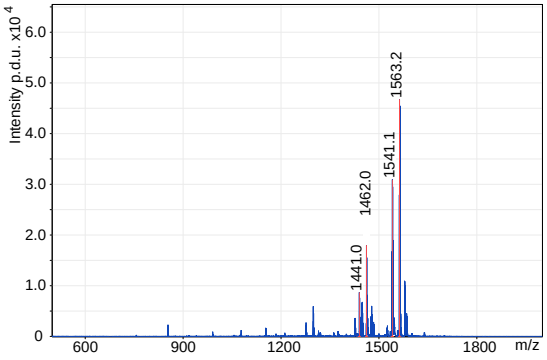


**Figure B.2:** *MALDI-TOF MS conducted on the collected GE11 RP-HPLC fraction (Fig. B.1). Single charged peaks at m/z 1541.1 / 1563.2 and m/z 1441.0 / 1462.0, corresponding well to [GE11 + H / Na]$^+$ = m/z 1540.72 / 1562.70 and [GE11$_{-T_7}$ + H / Na]$^+$ = m/z 1439.68 / 1461.66.*

product. A RP-HPLC analysis was conducted again (data not shown), but the chromatogram appeared largely unchanged and MALDI-TOF MS analysis of the fractions also appeared unchanged (data not shown). To ensure the labelled product was eluted from the RP-HPLC column, a MALDI-TOF MS analysis of the crude product was conducted (data not shown). The synthesis product was again found to contain GE11 and GE11$_{-T_7}$, among other impurities, so the solid- and liquid phase labelling protocols using ff have been unsuccessful.

The labelling of GE11 was then attempted with an isomeric mixture of the fluorescein derivative 5(6)carboxyfluorescein (cf), using the liquid phase protocol. After labelling using the liquid phase protocol, the product was purified by diethyl ether precipitation, and further purified by semi-preparative RP-HPLC (Fig. B.3). A gradient using the analytical program was initially run to determine the parameters for the purification program. When comparing the RP-HPLC chromatograms for ff labelling (Fig. B.1) and cf labelling (Fig. B.3) it is seen that absorption at 437 nm is much more predominant in the cf labelling, indicating that cf is present with the peptide. The eluent with retention time 15.5-16.5 min was collected and analysed by MALDI-TOF MS (Fig. B.4). The single charged peak at m/z 1898.9

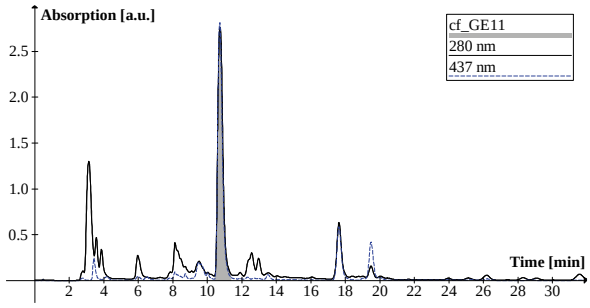


**Figure B.3:** *RP-HPLC chromatogram of cf_GE11. 100% ACN was used for the multistep gradient and 0.1% TFA as solvent. The marked peak with retentiontime 15.5-16.5 min was collected and analysed by MALDI-TOF MS. A baseline has been substracted.*

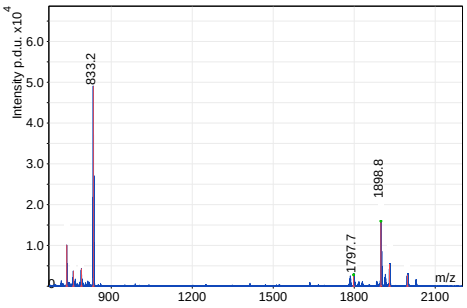


**Figure B.4:** *MALDI-TOF MS on the RP-HPLC fraction of cf_GE11. Single charged peaks at m/z 833.2, 1797.7 and 1898.9, the two latter corresponding to cf_GE11 and cf_GE11$_{-T_7}$. [$M_{cf\_GE11}$ + H]$^+$ = m/z 1898.77 and [cf_GE11 + H]$^+$ = m/z 1898.77, indicating a successful labelling of GE11.*

corresponds to cf_GE11, and the signal from GE11 is no longer found, both indicating that the labelling was a success (Table B.1). This conclusion is empowered by the single charged peak at m/z 1797.7, corresponding well to cf_GE11$_{-T_7}$, likewise the signal for GE11$_{-T_7}$ has disappeared. The unknown signal at m/z 833.2 was not seen prior to cf labelling. Therefore, to validate the cf_GE11 sequence and investigate the m/z 833.2 signal, ESI MS/MS analysis was performed.

For cf_GE11 the double charged cf_GE11 at m/z 950 was chosen as precursor (Fig. B.5). CID fragmentation was used, and the collision cell energy was raised from 0-35 eV. Peptides were identified corresponding to overlapping parts of the

a, b and y' peptide fragmentation series of cf_GE11, along with internal fragments (Table B.2). This verifies that cf_GE11 has been synthesised with the correct sequence, and that N-terminal cf labelling has been successful. Also m/z 833.2 was analysed by choosing the double charged m/z 417 as precursor (data not shown), but the only fragment that could be identified in the MS/MS was cf, leaving an unknown signal at (m/z 833.2 - cf) m/z 475.14, from where no AAs could be identified.

The MALDI-TOF MS spectrum of the RP-HPLC purified cf_GE11 (Fig. B.4) indicated the presence of several impurities and the presence of free cf. A LC-ESI MS/MS was conducted to further analyse the sample, which confirmed this (data not shown). However, to investigate if the impurities could be washed away, a binding experiment was conducted with cf_GE11 by preparing DMEM/high medium with 0, 5 and 50 $\mu$M cf_GE11. NR6 and NR6W cells were incubated in chamber slides with the fluorescent medium overnight, fixated, stained with Hoechst 33342 and mounted with Dakocytomation fluorescent mounting medium and a cover glass. The slides were sealed with nail polisher and the cells were analysed in fluorescence microscopes (data not shown) with a Hoechst- and a FITC filter, however, only the Hoechst staining was clearly visible. At integration time > 1s, only unspecific binding could be seen even after washing of the cells nine times with PBS for 5 min each.

It is assessed that the background originates from the seemingly large excess of cf most likely originating from the liquid labelling and other labelled impurities. The MS data also suggests that the peptide is breaking down, properly due to the many freeze/unfreeze cycles and labelling attempts. However, as the final labelling protocol with cf resulted in a labelled product, the reaction seems feasible. Therefore, a new synthesis was performed with an optimised protocol to get a more pure product, and possibly eliminate the need for RP-HPLC purification.

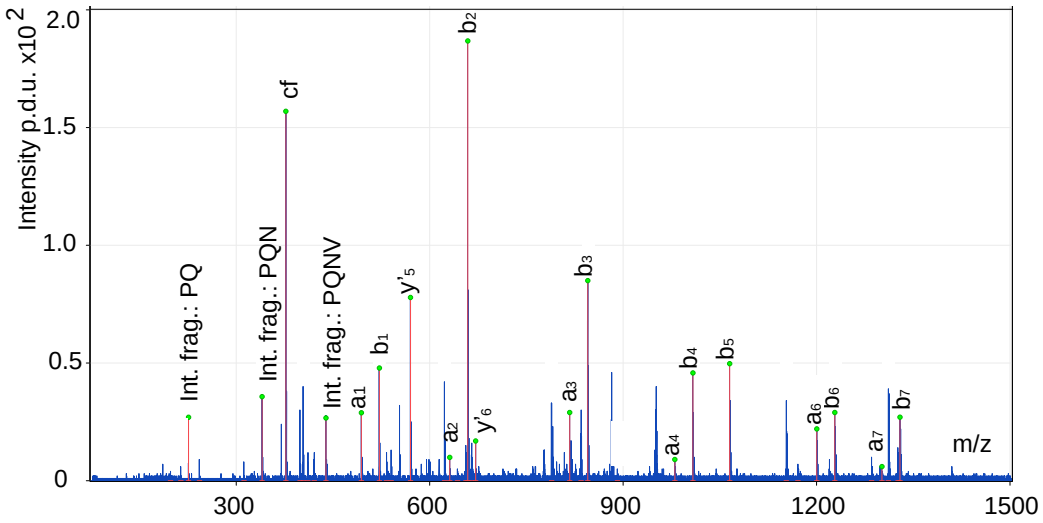


**Figure B.5:** *ESI MS/MS on the RP-HPLC fraction of cf_GE11, with precursor ion m/z 950 and the collision cell energy was raised 0-35 eV. Overlapping parts of the a, b and y' series of cf_GE11 were identified (Table B.2), confirming the sequence and successful cf labelling.*

| | | *a Series* | | *b Series* | |
|---|---|---|---|---|---|
| **Peptide** | **#** | **Meas. m/z** | **Deviation m/z** | **Meas. m/z** | **Deviation m/z** |
| cfY | 1 | 494.12 | 0 | 522.11 | -0.01 |
| cfYH | 2 | 631.18 | 0 | 659.17 | -0.01 |
| cfYHW | 3 | 817.25 | -0.01 | 845.24 | -0.02 |
| cfYHWY | 4 | 980.31 | -0.02 | 1008.31 | -0.01 |
| cfYHWYG | 5 | | | 1065.33 | -0.01 |
| cfYHWYGY | 6 | 1200.40 | -0.01 | 1228.39 | -0.02 |
| cfYHWYGYT | 7 | 1301.45 | -0.01 | 1329.44 | -0.01 |

| | | *y Series* | | *Other* | | |
|---|---|---|---|---|---|---|
| **Peptide** | **#** | **Meas. m/z** | **Deviation m/z** | **Peptide** | **Meas. m/z** | **Deviation m/z** |
| PQNVI | 5 | 570.32 | -0.01 | PQ | 226.12 | 0 |
| TPQNVI | 6 | 671.37 | 0 | PQN | 340.16 | 0 |

**Table B.2:** *Table of fragments identified in the ESI MS/MS of cf_GE11 (Fig. B.5). Calculated m/z given as protonated, and calculated using GPMAW [59]. Where no measured mass is given, non corresponding peak was found.*

# Confocal Laser Scanning Microscopy Negative Control

C

To investigate the placement of the receptor within the cells, fluorescence CLSM was performed. As a negative control, NR6 cells were analysed (Fig. C.1).

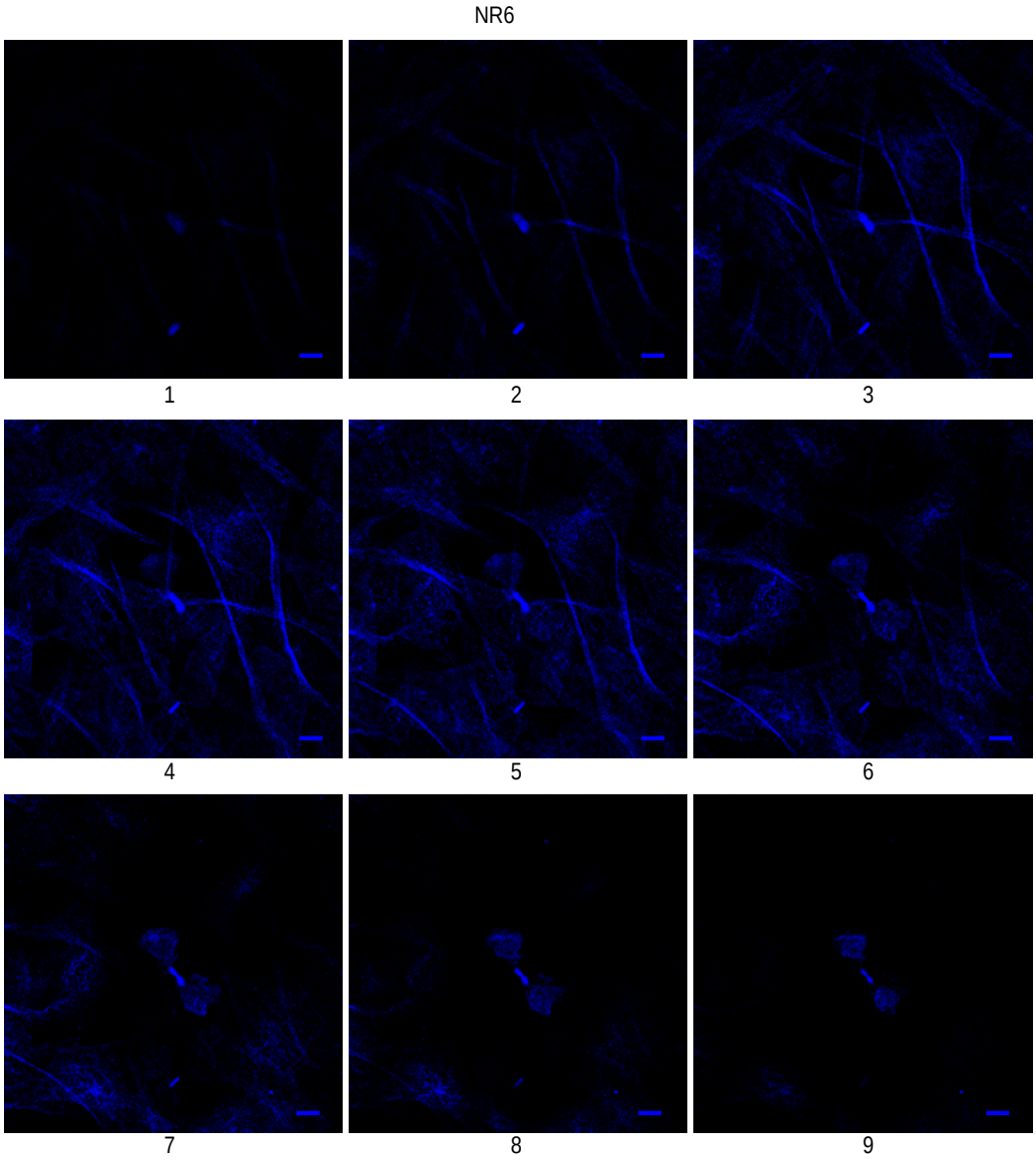


**Figure C.1:** *Fluorescence CLSM frames of NR6, beginning from the microscope slide (1) and moving away in regular intervals. Staining of anti-mouse α-tubulin antibody (blue) and anti-human EGFR and EGFRvIII antibody cocktail (green). Image processed with ImageJ.*